NAIST-IS-DD1821058

Doctoral Dissertation

K-Inverter Design for Inductive Power Transfer Systems with Multiple Receivers

Vo Quoc Trinh

March 15, 2021

Graduate School of Information Science
Nara Institute of Science and Technology

A Doctoral Dissertation
submitted to Graduate School of Information Science,
Nara Institute of Science and Technology
in partial fulfillment of the requirements for the degree of
Doctor of ENGINEERING

Vo Quoc Trinh

Thesis Committee:

Professor Minoru Okada
Professor Yuichi Hayashi
Associate Professor Takeshi Higashino
Assistant Professor Duong Quang Thang
Assistant Professor Chen Na

K-Inverter Design for Inductive Power Transfer Systems with Multiple Receivers*

Vo Quoc Trinh

Abstract

Inductive power transfer (IPT) is a non-radiative wireless power transfer technology which has been applied in many fields of life from medical treatment, kitchen equipment, portable electronic devices to transportation. In principle, IPT has utilized the coupling between two coils to transfer power. An inductive coupling is a K-inverter whose characteristic impedance represents the strength of the coupling link. In addition to inductive coupling, K-inverter can be created using passive elements consisting of inductors and capacitors. A K-inverter outputs a load-independent constant voltage when driven by a constant current and outputs a load-independent constant current when driven by a constant voltage. As a consequence, two K-inverters connected in cascade are able to output load-independent constant voltage if driven by a voltage source. Passive-element based K-inverter, known as CLC (capacitor-inductor-capacitor) or LCL (inductor-capacitor-inductor) topology, is usually employed in IPT systems to achieve constant load voltage. Constant load voltage is important because it guarantees stable working condition for load and enables load to consume power as expected by adjusting its resistance.

An advantage of IPT is to charge multiple receivers simultaneously. Recently, stabilizing multiple load voltages is still an attractive topic when rated voltages for receivers' loads and operating frequencies of receivers have diverged from application to application. More specifically, in addition to constant load voltages, different applications require differently rated voltages for their loads. In another

*Doctoral Dissertation, Graduate School of Information Science, Nara Institute of Science and Technology, March 15, 2021.

scenario, some receivers are located far from transmitter, leading to a deterioration of the system performance. Furthermore, besides the requirement of an individually rated voltage for load, each application may operate at an individual frequency. This work utilizes the properties of K-inverters to address the current challenges in multiple-receiver IPT systems. Firstly, multiple K-inverters are used inside charging platform to stabilize load voltages against load variations. Then, characteristic impedances of the K-inverters are adjusted so that the load voltages reach the rated values required by the users. Secondly, a cooperative IPT system where cooperative receiver can simultaneously draw power itself and transfer the rest of power to distant receiver is proposed. K-inverter-based compensation is employed for cooperative receiver to realize cooperative characteristic while still stabilizing two load voltages against load variations. Finally, a multiple-frequency IPT system where multiple sources operating at multiple frequencies share a common transmitting resonator to deliver power to multiple receivers is proposed. Each pair of source and corresponding receiver operates at an individual operating frequency. K-inverters are combined with band-reject filters to separate power link of each pair of source-corresponding receiver and stabilize load voltages. As a result, each pair of source and corresponding receiver is considered as independently operating at their individual frequency. Therefore, a full voltage control for each load can be achieved without affecting the operation of other pairs of source-corresponding receiver.

The findings in this dissertation highlight that it is completely feasible to use K-inverters and compensation circuits to stabilize load voltages in multiple-receiver IPT systems under single or multiple operating frequencies.

Keywords:

inductive power transfer, load-independent voltage, multiple-receiver, cooperative transmission, multiple-frequency

Contents

List of Figures

List of Tables

Chapter 1

Introduction

1.1. Wireless Power Transfer and Classification

Wireless power transfer (WPT) has a very old origin with several evidences related to magnetic field. However, for early development of its theory, André-Marie Ampere should be mentioned as one of the pioneers researching on the theory of electromagnetics. His theory of electricity and magnetism published in 1827 [1] was a valuable achievement for the beginning of the general electromagnetic theory. Several years later, Micheal Faraday came up with electromagnetic induction and demonstrated it in a publication in 1831 [2]. At the same period of time, Joseph Henry also discovered similar phenomenon of electromagnetic induction. Lenz found that electromagnetic field would be in a direction that opposed any change in current [3]. Until 1865, by synthesizing and developing the achievements of the precedent scientists, the general electromagnetic theory was postulated by James Clerk Maxwell [4]. Today, the general electromagnetic theory is now preferred to as Maxwell's equations. Until early years of 20th century, wireless power transfer was realized by Nikola Tesla [5–7]. In his whole life, Nikola Tesla left us many works related to electromagnetic energy which were considered as the beginning form of wireless power transfer systems today [8]. The idea that electric energy could be transmitted through the air seemed to connect to his first recored coil, the system of power electric lamp using one wire. Fig. 1.1 describes the lamp which was powered using one filament and one leading-in wire.

For next tens of years, wireless power transfer has become a key factor in the

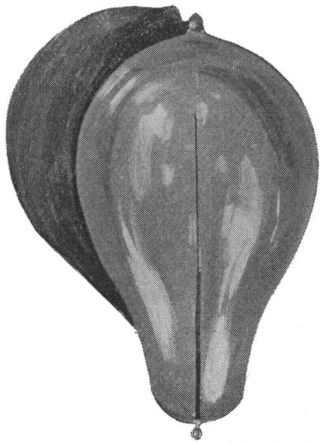

Figure 1.1. Lamp with single wire [9].

development of wireless communication. Until today, wireless power transfer technology has been applied in many fields of science and life. Wireless power transfer has been classified into two main categories including near-field and far-field wireless power transmission [10]. Far-field wireless power transmission, also known as radiative WPT, has two main technologies: microwave used mostly in wireless communication [11] and laser power beaming used in laser-based power transfer [12, 13]. In wireless communication systems, power transfer efficiency (PTE) is not one of the most important factors because the main purpose of using WPT in this kind of the systems is to exchange information successfully. The end-to-end PTE is from a fractional of percent to several percent only [11]. In wireless communication systems, the amount of power received by receivers is from hundreds of microwatts (µW) to a few milliwatts (mW) [14]. Another technology of far-field WPT is laser power beaming which is expected to be used for transferring power to unmanned aerial vehicles (UAV) [15]. As compared to microwave used in wireless communication, laser radiation has been more challenged because laser radiation could be dangerous and require light of sight transmission. In contrast, near-field WPT, also known as non-radiative WPT, has been found a use for powering or charging electronic devices. Main technologies in this category are inductive coupling, magnetic resonant coupling, capacitive coupling and magnetodynamic coupling. In near-field WPT, PTE is one of the most important

factors. Recently, RF-RF efficiency of up to over 90% can be achieved in near-field WPT. Accordingly, it has been primarily used for charging or powering systems in which transmitting/charging platforms usually deliver the amount of power of from several watts to kilowatts to loads.

1.2. Inductive Power Transfer

Inductive power transfer (IPT) is a WPT technology which uses coupling between two coils to transfer power over air. The illustration of IPT principle is described in Fig. 1.2. A transmitting coil is driven by an AC source to generate time-varying magnetic field. This variation of the magnetic field will induce a current at receiving coil according to the general electromagnetic theory discovered by James Clerk Maxwell. In the other word, an amount of power is transferred from the transmitting coil across the air to the receiving coil.

As mentioned above, inductive power transfer is a branch of wireless power transfer technologies. Therefore, IPT is not a recently discovered concept. It was discovered more than a century ago by Nikola Tesla [16]. Fig. 1.3 illustrates a very old IPT system which Tesla invented for electro-therapeutic purposes in 1898. He further found that power transfer capability of IPT system was enhanced when inductors were combined with resonant capacitors.

There have been many IPT systems developed from the day it has been firstly discovered. However, it has really been paid attention after the researchers from

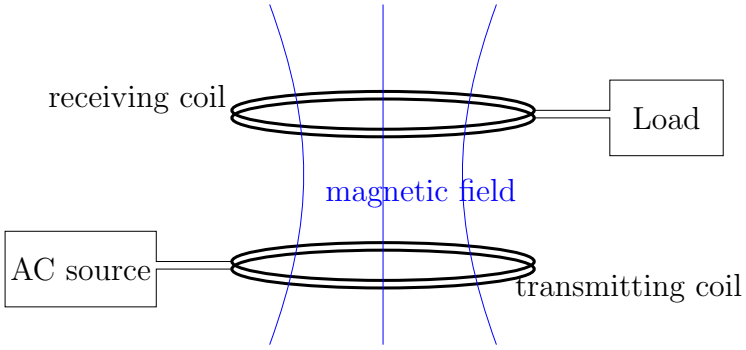

Figure 1.2. Illustration of the principle of IPT technology.

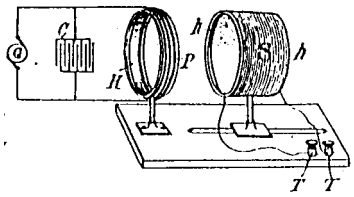

Figure 1.3. An early IPT system for electro-therapeutic purposes [16].

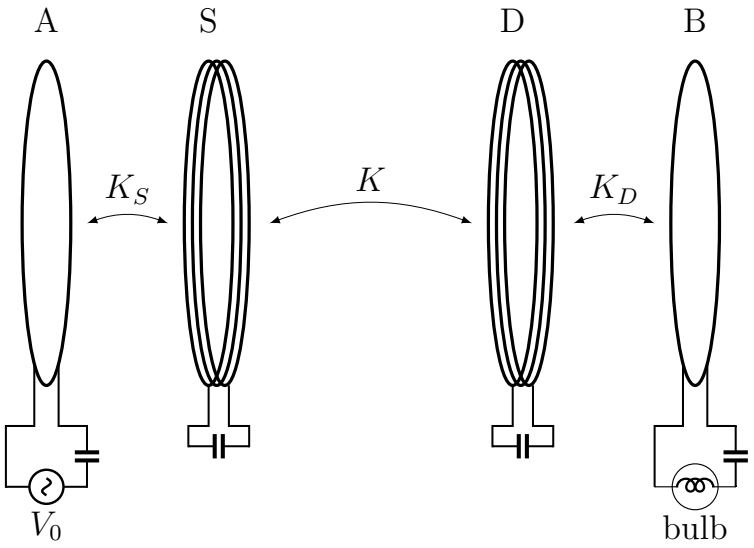

Figure 1.4. Illustration of IPT system used for powering a light-bulb in 2007.

Massachusetts Institute of Technology (MIT) published their work of using coupled magnetic resonances to transfer power wirelessly over 4 times of radius of transmitting coil [17]. Fig. 1.4 is the description of using IPT to powering a 60W bulb across 2m distance with the efficiency of up to 40%. Generally, there is no significant difference between the early IPT system and the today's ones.

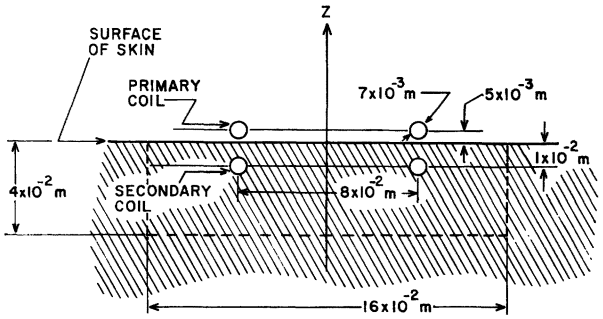

(a) Coil arangement

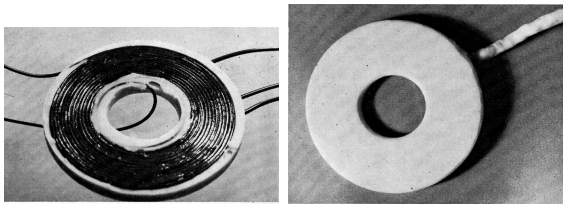

(b) Primary coil (c) Secondary coil

Figure 1.5. The coils and their arrangement in the investigation of power losses in tissue [25].

1.3. IPT's applications and future concerns

1.3.1 Applications

Due to inheriting the nature of wireless power transfer, IPT can transfer power without wires or cables. Since there is no physical connection between transmitter and receiver, IPT has been used to deal with the problems of transferring power, such as electrical isolation or freedom of receiver's movement [18]. Therefore, IPT's applications has spread in many fields of life from biomedical implants, mobile devices, electrical vehicles and trains [19–22].

For biomedical sector, IPT has been early used to transfer power to the coil which was implanted inside human body in 1960s [23, 24]. An experimental system was constructed to transfer power of 1kW across the skin of a dog in 1971 [25]. The coil arrangement used to investigate the inductive-type loss when transferring power through tissues was illustrated in Fig. 1.5. At that days semiconductor technology, however, was not flourished as today. Therefore, it was not possi-

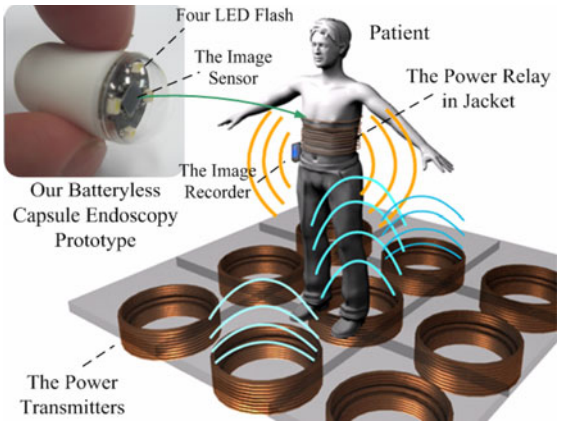

Figure 1.6. Two-hop inductive power transfer system to power capsule-size device placed inside human body [26].

ble to realize sufficiently small implantable systems to be suitable for biomedical applications. Fortunately, that semiconductor technology has dramatically advanced over years later brings about a significant decrease of components' size. That makes implantable devices more feasible in modern life. One evidence was a capsule-size device which was constructed to monitor inside body [26]. Fig. 1.6 shows the two-hop inductive power transfer system to power capsule-size device inside human body. In this system, power was transferred from the floor to capsule-size device over a distance of 1m with DC-to-DC efficiency of 3.04%. More surprisingly, an implantable device was designed to place inside human heart [27]. The experimental system in this research operated at the frequency of 13.56MHz and was able to deliver power to $5-80$mm with the efficiency of 56%. The other example of implantable devices is bionic eye which enables blind people to see again [28]. Fig. 1.7 is an illustration of a bionic eye used for blind people. The device attached on glass would take charge of transferring data to the bionic eye based on inductive link. Today, implantable devices are being paid more attention because these devices can help patients to feel more comfortable when they are examined. Many studies have been carried out to improve performance of IPT systems for implantable devices as well as to fulfill reliable interface between implantable devices and external devices [29–31].

Another application of IPT technology is to power electronic devices. A laptop

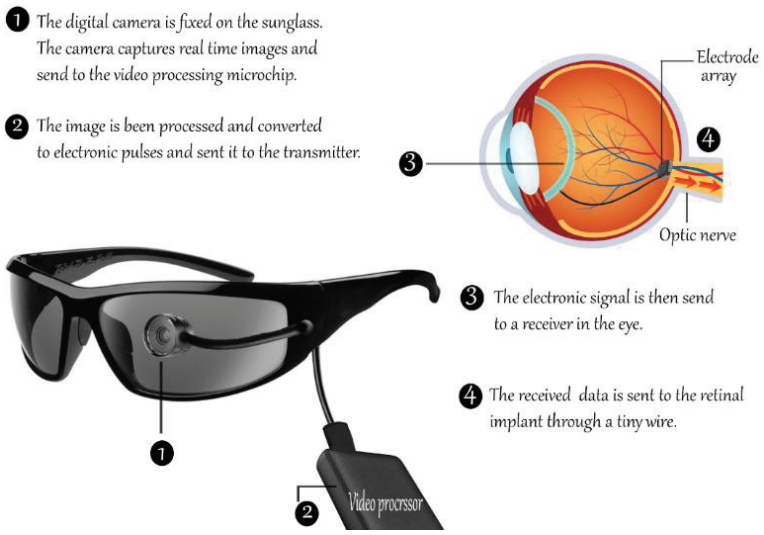

Figure 1.7. The operation of a bionic eye [28].

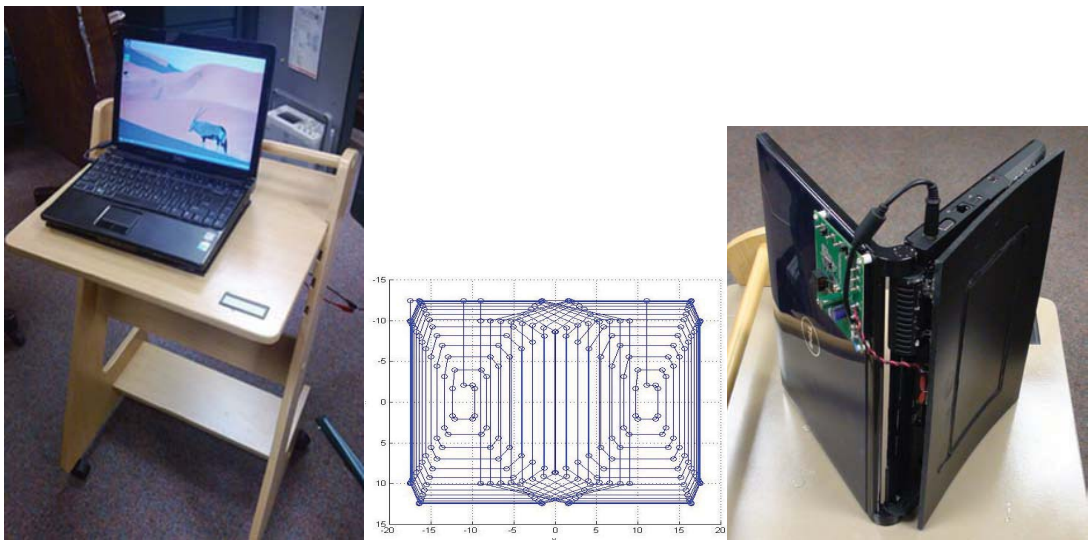

(a) Whole system (b) TX coil layout (c) Receiver

Figure 1.8. Prototype of powering laptop wirelessly [32].

was powered using IPT technology [32]. The prototype of IPT system which was able to supply power for battery-free laptop is illustrated in Fig. 1.8. The

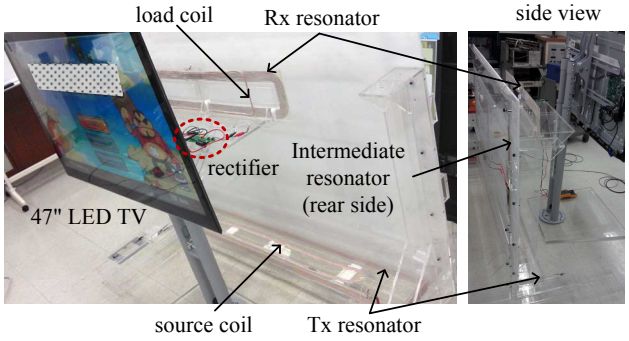

Figure 1.9. Powering an LED TV wirelessly [33].

transmitting coil had the size of 350mm $\times$ 250mm while the size of the receiving coil was 200mm $\times$ 120mm. The prototype could transfer the power of 32W to the laptop with the end-to-end efficiency of 60%. Similarly, IPT has been also used to power television [33, 34]. Fig. 1.9 shows the illustration of powering television wirelessly. This application using highly resonant technique could transfer the power of 150W to an LCD television.

A ubiquitous application of IPT technology today is to charge electronic devices [35]. Many kinds of electronic devices are often equipped a rechargeable battery, such as toothbrush, wearable devices, smart phone or electric vehicles. Therefore, IPT technology becomes suitable for battery-rechargeable electronic devices when it is more convenient than using wire or cable for charging. In order to forward to the convenience in charging, IPT-based charging platform for wearable devices was studied [36]. Specially, charging mobile phones using IPT technology has been extremely paid attention in recent years [37–39]. Besides using for small power charging with several watts, IPT technology has been utilized for high power charging, such as charging electric vehicles [40] where charging systems were required to operate with several tens to hundreds of kilowatts [41–43]. Fig. 1.10 is an example of charging a smart watch, smart phone with the power of 5W and electric vehicle charging system.

1.3.2 Future concerns

Although IPT's applications have continuously spread in many fields of science

(a) Charging a smart watch [36]

(b) Charging a mobile phone [44]

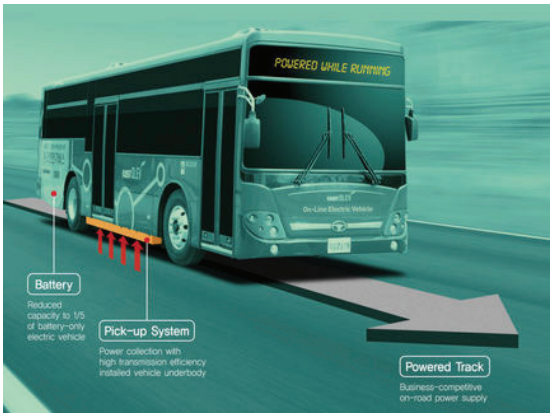

(c) EV charging system [45]

Figure 1.10. IPT applications in charging battery.

and daily life as mentioned above, some concerns still need to be addressed in future, including magnetic field exposure, energy security and transmission efficiency.

For the issue of magnetic field exposure, there are recently a few standards providing the guidelines to prevent human body from electromagnetic field exposure, consisting of the International Commission on Non-Ionizing Radiation Protection (ICNIRP) [46] or IEEE safety standards [47, 48]. There have been several studies investigating magnetic exposure caused by WPT systems on human body using human body model [49, 50]. Nevertheless, magnetic effect of IPT systems on sur-

rounding environment or real human body has not been investigated completely. Current IPT systems always leak magnetic flux into surrounding environment. Especially, magnetic flux leakage significantly increases when transmitting platforms operate without their receivers. For that reason, protecting human body as well as surrounding environment from magnetic field exposure is still a challenge for recent or future designs of IPT systems.

Another concern in future IPT systems is authority to use energy. Recently, there have been few studies focusing on energy security in IPT. They can temporarily be categorized into two main approaches, including physical security and communication-based security. In the first approach, the authors in [51, 52] adjusted operating frequencies according to the predefined regulation to deliver power authorized users. Unauthorized users would inefficiently pick up power because they had no knowledge of the regulation of operating frequencies. This kind of energy encryption is similar to frequency-hoping mechanism in wireless communication [53]. Other study utilized power beam formed by multiple transmitters to deliver power to receivers at certain positions only [54]. For the approach based on communication between transmitter and receiver, IPT systems will be equipped communication modules at both transmitter and receiver sides. The power transmission over power channel will be occurred once transmitter and receiver finish their authority process on communication channel. In general, the existing methods used to secure energy in IPT either required high complexity of users/receivers or protected energy from unauthorized users incompletely. Therefore, similar to electromagnetic field exposure, energy security is still a big challenge in IPT technology in future.

Finally, even though the theory of maximum achievable efficiency has almost completed in [55–60], transmission efficiency is still one of the biggest concerns in future IPT systems. Recently, IPT systems could achieve transmission efficiency of from several tens to over 90%. This number of transmission efficiency may be acceptable for low-power applications with several watts to hundreds of watts. However, it becomes a big problem for high-power IPT systems with a few kilowatts to several hundreds of kilowatts because power loss can cause the damage at transmitter side. The transmission efficiency limitation in recent IPT systems comes from the quality of the components used in the systems. In future, once

material technologies, specially semiconductor and superconductor, are advanced, the development of IPT technology will rapidly pushed forwards as cost reduces and performance is improved.

1.4. Motivation

Even though IPT was demonstrated hundred years ago, it has really flourished for last two decades with high attention in both industry and academia. For industry, IPT systems bring about the convenience in daily life with many applications mentioned above. For academia, the theory of maximum achievable efficiency of IPT systems has been quickly fulfilled for last decade. Once the theory of maximum achievable efficiency is mature, the stability of IPT systems become the key direction for the researches in near future. More specifically, in IPT systems, stable output voltages against load variations should be achieved to allow loads to consume the expected amount of power by adjusting their resistances. It leads to a better operation for the loads. Recently, constant load voltage against load variations in IPT systems with single transmitter and single receiver has been well studied. In such IPT systems, a famous topology, known as capacitor-inductor-capacitor (CLC), and/or relay are mostly used to realize the stability of output voltage for the load. It is, nevertheless, more challenged when IPT systems are scaled up to multiple receivers. It is because the mentioned technologies has to encounter the problem coming from the couplings among receivers which will deteriorate the stability of the output voltages/currents. There have been a few studies focusing on stabilizing the load voltages in multiple-receiver IPT systems. However, stabilizing multiple load voltages in multiple-receiver IPT systems is still an attractive topic when rated voltage for each load and and operating frequencies have diverged from application to application. In practice, for different applications, each receiver often requires individually rated voltage for its load. Therefore, multiple-receiver IPT systems, whose advantage is to charge multiple users simultaneously, should be advanced to be able to deliver individually rated voltage to each receiver. In other scenario, charging platform needs to deliver power to several receivers which are located far from it. In these cases, instead of using additional supporters to help to deliver power to distant receivers, it is more

convenient if some receivers can change to cooperative mode to relay power to distant receivers while still drawing power itself. Last but not least, one growing problem in IPT's applications is the divergence of operating frequencies. It means that each application requires not only an individually rated voltage for its load but also an individual operating frequency. In this scenario, a new type of multiple-receiver IPT system should be proposed to charge each receiver with individually rated voltage under its operating frequency.

1.5. Contributions

In order to address the above mentioned challenges, this dissertation proposed multiple-receiver IPT systems which could simultaneously stabilize the load voltages against load variations under different requirements. The contributions of this dissertation were as follows.

1. Firstly, charging platform consisting of one source resonator and multiple transmitting resonators was used to deliver and control load voltages for multiple receivers [P.W1], [P.J1]. This structure was equivalent to the structure of multiple K-inverters formed by the couplings between the source resonator and the transmitting resonators. Therefore, the currents flowing in the transmitting resonators were fixed because multiple K-inverters were driven by a source voltage. These stable currents, in turn, induced constant voltages to the loads regardless of load variations. Moreover, once load voltages were stabilized, the rated load voltages could be achieved by changing the characteristic impedances of the K-inverters, in the other word, by adjusting the arrangement of the transmitting resonators inside charging platform.

2. Secondly, a cooperative IPT system where cooperative receiver could simultaneously play two roles, including supporting transmitter to deliver power to a distant receiver and drawing power itself, was proposed [P.C1], [P.C2], [P.C3]. K-inverter was applied for cooperative receiver to realize cooperative characteristic while still stabilizing the load voltages.

3. Finally, multiple-frequency charging IPT systems were proposed to stabilize load voltages for multiple receivers operating at different frequencies [P.W2], [P.C4]. In these systems, multiple sources shared a common transmitting coil to deliver power to corresponding receivers. Each pair of source and corresponding receiver operated at an individual frequency. K-inveters were combined with band-reject filters to separate the power link of each pair of source and corresponding receiver while still stabilizing load voltage for each receiver. Consequently, even though using a common transmitting coil, each pair of source and corresponding receiver was considered as operating independently. Each load voltage could be controlled by adjusting the corresponding source voltage without affecting the operation of other pairs of source and corresponding receiver.

1.6. Design methodology

In practice, the process of producing any system should be followed a certain design methodology to achieve as good performance as possible and reduce system production time. The following design process can be applied for producing the proposed systems. The main steps are as follows. Firstly, an IPT system is theoretically proposed to satisfy the requirements. Then, theoretical analysis should be verified by simulations (based on LTSpice and/or WIPL software). This step can help to save the time of examining the developing theory. Next, we construct the proposed system based on theoretical analysis. Here, Vector Network Analyzer (VNA) machine or LCR-meter machine can be used to support construction process. Finally, the performance of the prototype/product should be examined by measures from oscilloscope machine or equivalent machines.

In these steps, constructing coupling networks and compensation networks is the most important for the proposed systems to operate as desired. This step can be divided into sub-steps as follows.

- Transmitting and receiving coils should be designed first because they depend on the requirements of size and operating frequency. The coils should be made from low-loss materials such as litz wire.

- Then, the couplings between them or Z-parameters should be measured using VNA or LCR-meter machines.

- After obtaining the measured couplings, compensation networks, consisting of capacitors and inductors, are calculated to meet the needs of the receivers. In particular, in the proposed systems, the main relationship among the compensatory components is resonance. The capacitors or the inductors can be selected first if it is difficult for adjusting their value. Then, the other components are constructed based on the resonant relationships.

However, there are some additional issues which we should pay attention when deploying the proposed systems in practical environment.

- The first is noise caused by other systems. As described above, the principle of IPT system is electromagnetic field variation. Therefore, it can be totally affected by the energy of electromagnetic field caused by other systems. For wireless communication systems, power received at users is just from hundreds of microwatts to tens of milliwatts only. That amount of power is negligibly small to power of from a few watts to hundreds of kilowatts received by users in the proposed IPT systems. As a result, electromagnetic noise caused by wireless communication systems totally has no effect on the operation of the proposed IPT systems. In contrast, interference should be taken into account when the proposed systems are deployed nearby other IPT systems. It is because the coils in proposed systems may be coupled to the coils of nearby IPT systems, leading to power exchange among them. For that reason, there should be isolation mechanism between the IPT systems to guarantee the stability of the proposed systems and nearby IPT systems.

- The second is quality factor of the components used in the proposed systems. In theoretical analysis, quality factor of the components in compensation networks is often omitted for simplicity. However, in practice, quality factor of compensatory components as well as of coils is the most important factor because it significantly contributes to transmission efficiency. As a consequence, the coils and the compensatory components of the proposed

systems should be high-quality ones if the proposed systems is expected to attain high efficiency. Recently, quality factor of coils or compensatory components is limited by material technologies. In future, the development of material technologies, semiconductor and/or superconductor, is expected to create nearly ideal components.

- The third is design margins for the proposed systems. Mostly, the compensatory components in the proposed systems are designed depending on resonant relationship. In practice, we will never attain the perfect match of resonance between inductor and capacitor. In the other word, there cannot be a capacitor whose capacitance completely cancels out inductance of an inductor or vice versa. Consequently, there always exits an imaginary part of total impedance after inductor and capacitor are constructed with resonant relationship. Basically, the performance of the proposed systems is better as imaginary part of total impedances in resonant relationships is closer to zero. Therefore, the quality of resonant design is decided depending on the requirements of quality of the proposed system and recent material technologies. Recently, imaginary part of total impedance under 1Ω or around 0.5Ω can be acceptable for resonant designs in either experiments or industry. These values are also considered as the design margin of resonance for the proposed systems. The other margin is quality factor of the coils as well as the compensatory components. In practice, once quality factor of the coils and the compensatory components is over 200, the proposed systems can achieve transmission efficiency of over 90% which is acceptable for low-power charging applications. Accordingly, quality factor of 200 can be considered as another margin design for the proposed systems.

1.7. Dissertation outline

The rest of the dissertation is organized as follows

Chapter 2 of the dissertation presents an overview of IPT systems. A typical single-input single-output (SISO) IPT system, consisting of equivalent AC source, compensation networks, coupling network and equivalent load, is analyzed. Then, theoretical analysis on load voltage stability in conventional single-

input single-output (SISO) and single-input multiple-output (SIMO) IPT systems is presented. This chapter also describes K-inverter and how it can help to stabilize load voltages against load variations in SISO and SIMO IPT systems.

In Chapter 3 proposes an IPT system using multiple K-inverters to control load voltages for multiple receivers [P.W1], [P.J1]. This chapter also explains how structure of multiple K-inverters can help to stabilize and adjust load voltages against load variations by theoretical analysis. Then this chapter presents simulation and experimental results to verify the feasibility of the proposed system.

Chapter 4 focuses on developing a cooperative IPT system where cooperative receiver can simultaneously support transmitter to deliver power to a distant receiver and draw power itself [P.C1], [P.C2], [P.C3]. In this chapter, it is proved that adding K-inverter to cooperative receiver can realize cooperative characteristic while still stabilizing two load voltages against load variations. This chapter also evaluates load voltage stability and RF-RF efficiency of the proposed cooperative IPT system and the one using two-coil repeater to do cooperative function under various coil arrangements.

In Chapter 5, multiple-frequency IPT system with one transmitter and multiple receivers is proposed [P.W2], [P.C4]. In this system, multiple sources operating at different frequencies share the same transmitting coil to deliver power to corresponding receivers. This chapter illustrates how novel K-inverters separate power of each operating frequency used by one source and corresponding receiver and stabilize load voltages against load variations. In this chapter, it is illustrated that any load voltage control performed from one pair of source and corresponding receiver will not affect the operation of the other pairs of source and corresponding receiver.

Chapter 6 summarizes the dissertation.

Chapter 2

IPT system models with K-inverter

2.1. Introduction

Recently, a typical IPT system included the main blocks as described in Fig. 2.1 [10, 22]. At transmitter side, an DC source supplies power for an inverter while clock generator took charge of generating operating frequency for the system. The combination of the DC source and clock generator at the inverter yielded a high-power AC signal which was used to drive transmitting coil. At receiving side, induced voltage was rectified to become DC voltage. Then, this voltage was regulated to the level matched the requirement of the load. Finally, the regulated voltage was delivered to the load.

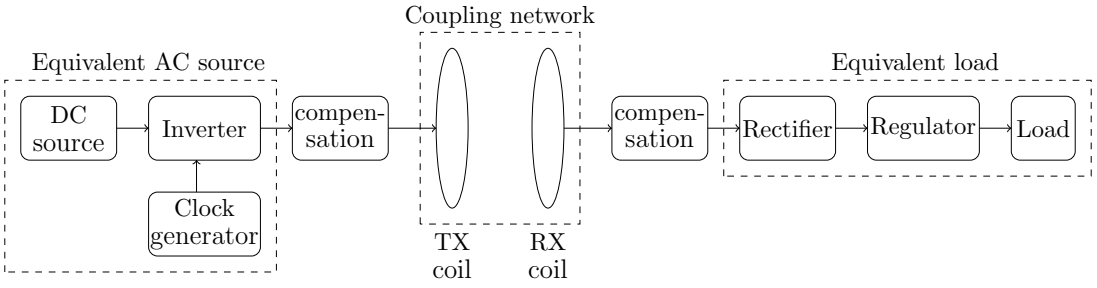

Figure 2.1. Typical IPT system.

In order to improve the performance of IPT system, several parts of IPT systems have been studied, such as coil design/analysis [61–66], inverter design [67–69], rectifier design [70, 71]. However, this work in this dissertation concentrates on proposing compensation networks to realize the desired functions in IPT systems. Therefore, for the sake of simplicity in theoretical analysis, the combination of DC source, inverter and clock generator is considered as equivalent AC source V_0 while the combination of rectifier, regulator and load is considered as equivalent load R. As a result, the equivalent IPT system is modeled as in Fig. 2.2.

In Fig. 2.2, the inductor with the self-inductance L_0 denotes for TX coil while the inductor with the self-inductance L_1 is for RX coil. The mutual inductance between TX coil and RX coil is denoted by M.

The RF-RF efficiency is defined by

$$\eta = \frac{P_{\text{out}}}{P_{\text{in}}}, \tag{2.1}$$

where P_{in} is the power supplied by AC source V_0 and P_{out} is the power consumed by the load R.

After the work of MIT's scientists was published, IPT technology has been increasingly concerned from academia. Recently, IPT systems can be classified into four types, including single-input single-output (SISO) IPT systems, multiple-input single-output (MISO) IPT systems, single-input multiple-output (SIMO)

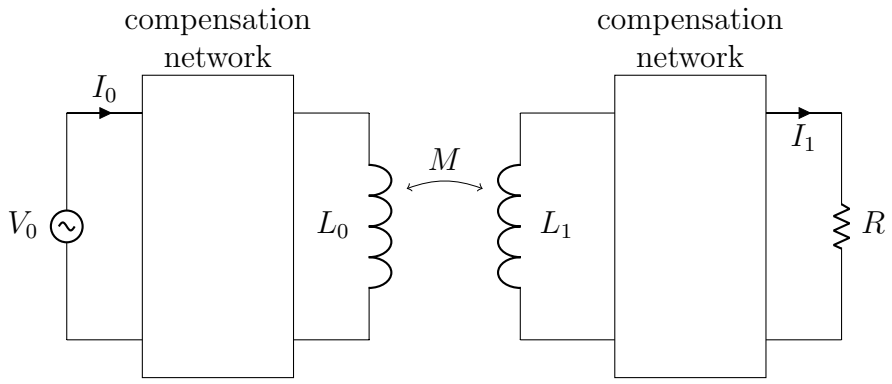

Figure 2.2. Equivalent IPT system.

IPT systems and multiple-input multiple-output (MIMO) IPT systems. The theory of maximum achievable efficiency of these IPT systems has been quickly fulfilled in about one decade only. Initially, the maximum achievable efficiency in single-input single-output (SISO) was formulated by considering the coupling network as a black box with known scattering-parameter matrix or Z-parameter matrix [55, 56, 72].

For IPT systems using multiple transmitters to deliver power to single receiver, the operation behaviors have been investigated in many studies [73–79]. Then the limitation of RF-RF transferable efficiency was addressed in [57, 80, 81]. These studies illustrated that the MAE in MISO IPT systems could be obtained once the cross couplings among the transmitting coils were mitigated and the source voltages were adjusted to optimal values. As a results, the MAE would be characterized by an overall kQ-product where k denoted for coupling coefficient and Q was quality factor of the coils. Quality factor of an inductor L at operating frequency f with internal resistance r is defined by

$$Q_L = \frac{2\pi f L}{r} \tag{2.2}$$

Similarly, quality factor of an capacitor C at operating frequency f with internal resistance r is defined by

$$Q_C = \frac{1}{2\pi f C r} \tag{2.3}$$

In compared with SISO and MISO IPT systems which can deliver power to one receiver only, SIMO IPT systems which used one transmitter to transfer power to multiple receivers simultaneously. This kind of the IPT systems has been also investigated in many studies [82–91]. It was discovered that in SIMO IPT systems with given loads once the cross couplings among receivers were eliminated the system could attain highest efficiency [58, 59, 92].

Finally, due to the advantage of using low-power source to charge for larger-power devices, multiple-input multiple-output (MIMO) IPT systems have also received the attention from scientists [93–98]. The study in [60] unified the theory of maximum achievable efficiency for single-input single-output (SISO), single-input multiple-output (SIMO), multiple-input single-output (MISO) or multiple-input multiple-output (MIMO) IPT systems.

That the theory of maximum achievable efficiency was completely investigated brought about the benchmark or criterion to evaluate the operation of IPT systems. In order to realize IPT systems for applications, scientists have now concentrated on the designs which are able to stabilize the operation of IPT systems. In IPT systems, output voltage, output current or output power were often stabilized to match the requirements of the loads. In this dissertation, stabilizing output voltage is focused on because it can be applied in many applications.

Throughout this dissertation, it is assumed that all the passive components are linear and that the IPT system is operating in a steady state without switching harmonics.

2.2. K-inverter

Generally, immittance inverter has played a very important role in wireless communication and power systems. Immittance inverter has been divided into two types, including admittance inverter and impedance inverter [99]. A lossless admittance inverter is a two-port network in which the admittance Y_2 is connected to one port, the other port will see an transformed admittance

$$Y_1 = \frac{J^2}{Y_2}, \tag{2.4}$$

where J is real and the characteristic admittance of the inverter, called J-inverter. A J-inverter can be implemented using L and C with π-shaped arrangements as in Fig. 2.3a and Fig. 2.3b. In contrast, for an ideal impedance inverter, if one port of an impedance inverter is connected with an impedance Z_2, the impedance Z_1 seen from other port will be

$$Z_1 = \frac{K^2}{Z_2}, \tag{2.5}$$

where K is real and the characteristic impedance of the inverter, called K-inverter. A K-inverter can be realized using inductors (L) and capacitors (C) with T-shaped arrangements as in Fig. 2.3c and Fig. 2.3d. Based on the characteristic of impedance transformation, K-inverter could be used to transform load impedance [99] or reduce impact of source internal resistance [17]. Another

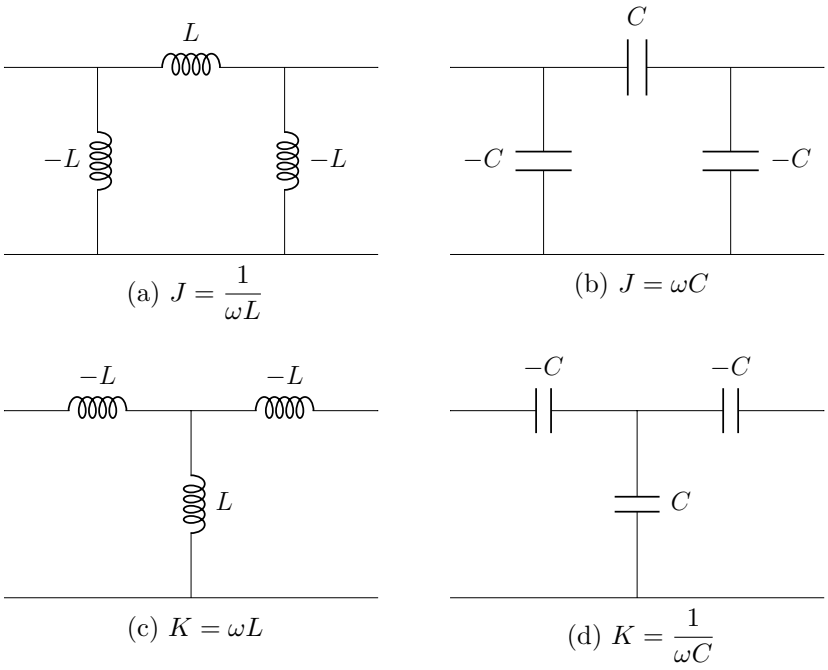

Figure 2.3. Admittance and impedance inverters.

important characteristic of K-inverter is that it can transform constant voltage to constant current and vice versa. It means that if one port of K-inverter is driven by a constant voltage, at the other port will output a constant current against load variations. Vice versa, if K-inverter is driven by a constant current, it will output a constant voltage against load variations. Correspondingly, if two K-inverters are connected in cascade, the characteristic of the input will be reserved at the output. It means a constant voltage or constant current going through two K-inverters connected in cascade is still a constant voltage or constant current against load variations.

For IPT systems, the coupling network between two coils can be modeled as T-model [100]. The illustration of T-model for the coupling network is shown in Fig. 2.4. Basically, the self-inductances L_0 and L_1 are often canceled out by series compensatory capacitors. Therefore, in comparison with the inverters described in Fig. 2.3c, it can be said that the coupling network between two coils in IPT system is a K-inverter when self-inductances of the coils are cancelled

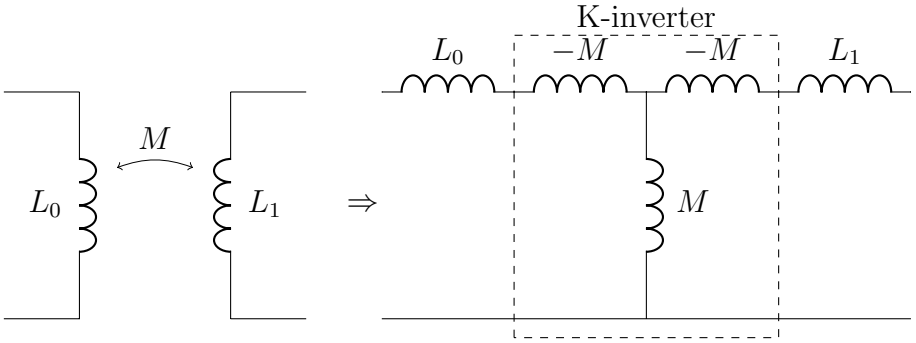

Figure 2.4. T-model for coupling network.

out using series resonant capacitors. Consequently, coupling network inherits the characteristics of K-inverters.

2.3. Constant load voltage in SISO IPT systems

2.3.1 Conventional SISO IPT system

For theoretical analysis, we considered a typical IPT system where transmitting coil and receiving coil were compensated by series capacitors as shown in Fig. 2.5. In this model, L_0 and L_1 denoted for the self-inductances of the transmitting coil and the receiving coil respectively. It was assumed that AC source supplies

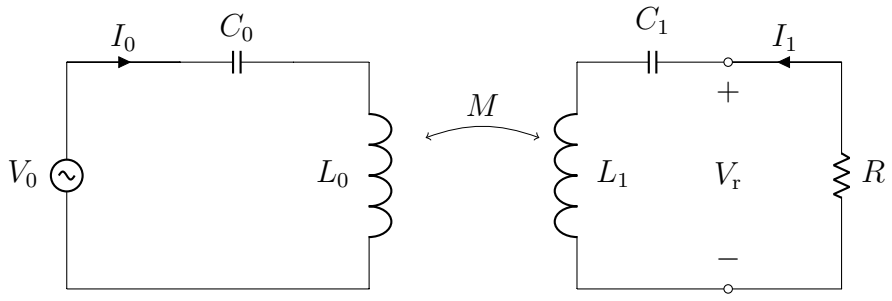

Figure 2.5. A conventional SISO IPT system with series compensations.

a constant voltage V_0 and operated at angular frequency ω

$$\omega = 2\pi f \tag{2.6}$$

where f was operating frequency. The currents flowing in the transmitting coil and the receiving coil were denoted by I_0 and I_1 respectively. The mutual inductance between two coils was M. For simplicity in theoretical analysis, we ignored the internal resistances of the coils in calculations. In the conventional IPT system, the resonant relationship among the components was given

$$\omega = 2\pi f = \frac{1}{\sqrt{L_0 C_0}} = \frac{1}{\sqrt{L_1 C_1}} \tag{2.7}$$

According to Kirchoff's laws, the relation between voltage-current was given

$$V_0 = \frac{1}{j\omega C} I_0 + j\omega L_0 I_0 + j\omega M I_1 \tag{2.8}$$

$$-RI_1 = j\omega M I_0 + j\omega L_1 I_1 + \frac{1}{j\omega C_1} I_1 \tag{2.9}$$

From (2.9), the current flowing in the receiving coil was derived

$$I_1 = \frac{-j\omega M}{R} I_0 \tag{2.10}$$

Therefore, substituting above equation into (2.8), we had the current flowing the transmitting coil

$$I_0 = \frac{R}{\omega^2 M^2} V_0 \tag{2.11}$$

Finally, the load voltage was given by

$$V_R = -RI_1 = R\frac{j\omega M}{R} I_0 = R\frac{j\omega M}{R}\frac{R}{\omega^2 M^2} V_0 = -\frac{R}{j\omega M} V_0 \tag{2.12}$$

Equation (2.12) indicated that in conventional IPT system, the load voltage depended on the load.

As mentioned above, the coupling network between two coils was considered as a K-inverter. Therefore, in order to stabilize the load voltage by a constant voltage source, another K-inverter should be added to form a network consisting of two K-inverters connected in cascade. Recently, two techniques, including CLC structure and relay-based structure, have been used as K-inverters.

2.3.2 CLC/LCL topology

In order to stabilize load voltage against load variations, a famous compensation network, called capacitor-inductor-capacitor (CLC) topology or inductor-capacitor-inductor (LCL), was applied into conventional IPT system. The behavior of CLC/LCL topology has been well explored in many studies [101–112]. Fig. 2.6 showed the application of CLC topology used to stabilize the load voltage in SISO IPT systems.

Here, inductor (L) and two capacitors (C) were combined in T-shape to form CLC compensation network. CLC topology and conventional series compensations were applied to stabilize the load voltage V_R. The constant load voltage was proved as follows. The resonant relation among compensatory components in the IPT system was given

$$\omega = 2\pi f = \frac{1}{\sqrt{LC}} = \frac{1}{\sqrt{L_0 C_0}} = \frac{1}{\sqrt{L_1 C_1}} \tag{2.13}$$

According to Kirschoff's laws, the relationship between voltages and currents in transmitter circuit was

$$V_0 = \frac{1}{j\omega C} I_0 + j\omega L I_L \tag{2.14}$$

$$I_0 = I_L + I_\mathrm{t} \tag{2.15}$$

From last three equations, the transmitting current I_t was derived

$$I_\mathrm{t} = -\frac{V_0}{j\omega L} \tag{2.16}$$

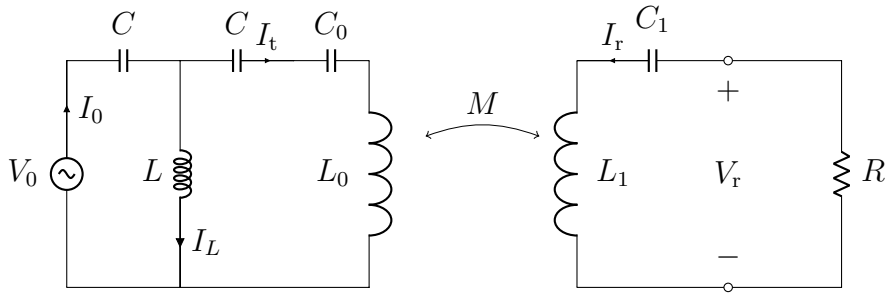

Figure 2.6. CLC topology for constant load voltage in SISO IPT system.

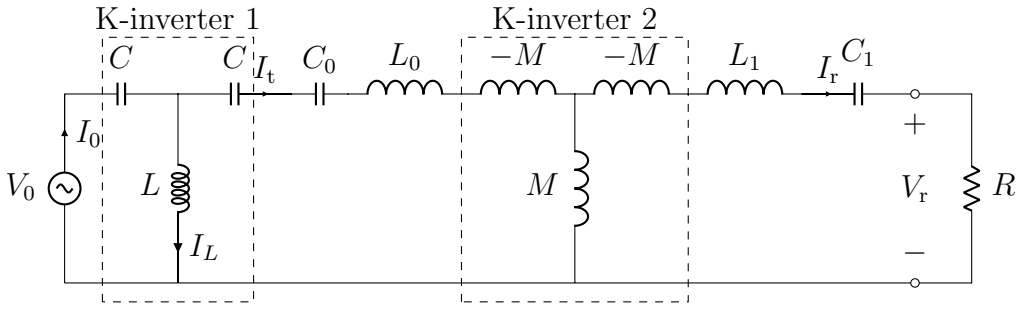

Figure 2.7. K-inverter based model for IPT system in Fig. 2.6.

(2.16) indicated that the transmitting current was kept constant regardless of the load variations. It was based on (2.10), the relation between the current flowing the receiving coil and source voltage was

$$I_{\mathrm{r}} = \frac{-j\omega M}{R}\left(-\frac{V_0}{j\omega L}\right) = \frac{M}{LR}V_0 \tag{2.17}$$

Therefore, the load voltage was derived by

$$V_R = -RI_{\mathrm{r}} = -\frac{M}{L}V_0 \tag{2.18}$$

Equation (2.18) showed that the load voltage was decided by the mutual inductance between two coils M, the compensatory inductance L in LCC topology and the source voltage V_0. It was obvious that the load voltage was independent of the load R.

According K-inverter based model, the equivalent circuit of the IPT system in Fig. 2.6 could be described as in Fig. 2.7. The theoretical analysis expressed above agreed with the properties of K-inverter. Specifically, constant source voltage inputted K-inverter 1, constant current I_{t} against load variations was achieved. Then, constant current I_{t} inputted K-inverter 2, constant voltage V_r against load variations was obtained again. It was confirmed that 2 K-inverters connected in cascade could help to deliver constant voltage from input to output.

2.3.3 Relay-based structure

Another way to keep load voltage stable against the load variations was to use a relay inserted between transmitter and receiver. Initially, the relay was employed

to support the transmitter to deliver power to a distant receiver. In addition, it was discovered that the relay could help to transform load impedance [17] or to reduce the impact of the source impedance [113]. Similar to CLC/CLC topology, relay-based structure has also played an important role in IPT systems. Many studies have been carried out to explore the advantage of relay-based structure as well as to investigate its further behaviors [114–129]. One important impact of relay-based structure was to boost and stabilize load voltage [105, 130, 131]. Fig. 2.8 was the description of a relay-based IPT system. Similar to the mentioned IPT systems, the power source operating at angular frequency ω supplied a constant voltage V_0. The transmitting coil, the relay coil and the receiving coil had the self-inductances L_0, L_1 and L_2 respectively. M_{01} was the mutual inductance between the transmitting coil and the relay coil. M_{12} was the mutual inductance between the relay coil and the receiving coil. In relay-based IPT system, since the mutual inductance between the transmitting coil and the receiving coil was negligibly small, it was ignored in theoretical analysis for simplicity. In the relay-based IPT system, the series compensation was used for transmitting coil, relay coil and receiving coil

$$\omega = 2\pi f = \frac{1}{\sqrt{L_0 C_0}} = \frac{1}{\sqrt{L_1 C_1}} = \frac{1}{\sqrt{L_2 C_2}} \tag{2.19}$$

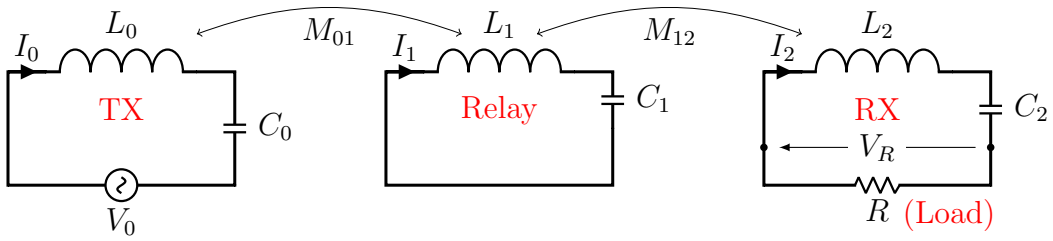

Figure 2.8. A relay-based IPT system.

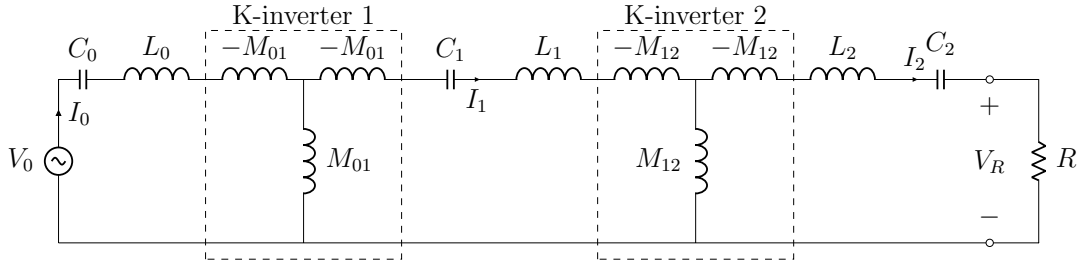

Figure 2.9. The equivalent circuit of the relay-based IPT system in Fig. 2.8.

According to Kirschoff's laws, the relation between voltage-current

$$V_0 = \frac{1}{j\omega C_0} I_0 + j\omega L_0 I_0 + j\omega M_{01} I_1 \tag{2.20}$$

$$0 = j\omega M_{01} I_0 + \frac{1}{j\omega C_1} I_1 + j\omega L_1 I_1 + j\omega M_{12} I_2 \tag{2.21}$$

$$-I_2 R = j\omega M_{12} I_1 + \frac{1}{j\omega C_2} I_2 + j\omega L_2 I_2 \tag{2.22}$$

Due to the resonant relationship in (2.26), the current flowing in the relay coil was derived from (2.20)

$$I_1 = \frac{V_0}{j\omega M_{01}} \tag{2.23}$$

Then substituting into (2.22) with the notice of the resonant relationship, the load voltage was derived

$$V_R = -RI_2 = -\frac{M_{12}}{M_{01}} V_0 \tag{2.24}$$

Equation (2.24) indicated that the load voltage was decided by the mutual inductances between two adjacent coils and the source voltage only. It agreed with the explanation using K-inverter based model. K-inverter model for the IPT system in Fig. 2.8 was illustrated in Fig. 2.9. According to the equivalent circuit in Fig. 2.9, since relay-based IPT system created 2 K-inverters connected in cascade, constant voltage could be delivered from input to output. Specifically, the constant voltage source V_0 inputting the K-inverter 1 created the constant current I_1 against load variations. The constant current I_1 going through the K-inverter 2 would gave constant voltage against load variations again.

2.4. Constant load voltages in SIMO IPT systems

2.4.1 Conventional SIMO IPT systems

One advantage of IPT systems is to simultaneously charging multiple receivers. In order to charge multiple receivers, SIMO IPT systems are often used than MIMO IPT systems because the charging platform of SIMO IPT systems is simpler and easier to be deployed. Fig. 2.10 shows the schematic description of a conventional SIMO IPT system with series compensation for every coils. This conventional IPT system model included one transmitter delivering power to N receivers. The transmitter and the receivers were equipped with one coil compensated by an self-resonant capacitor. V_0 denoted for the power supplier while V_i denoted for the i-th load voltage where $i \in \{1, 2, \ldots, N\}$. I_i was the current flowing the i-th coil. L_i was denoted for the self-inductance of the i-th coil. M_{0i} was the mutual inductance between the transmitting coil and the i-th coil. The cross couplings

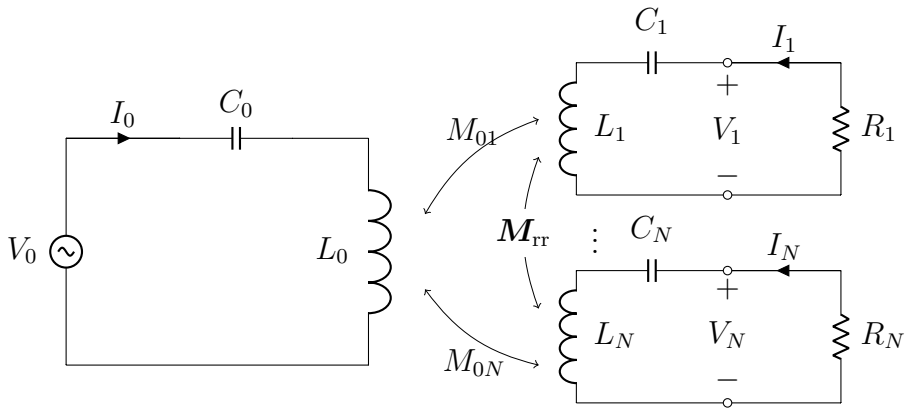

Figure 2.10. The model of a conventional single-transmitter multiple-receiver IPT systems using series compensation.

among the receiving coils was denoted by the matrix

$$\boldsymbol{M}_{\mathrm{rr}} = \begin{bmatrix} 0 & M_{12} & \dots & M_{1N} \\ M_{21} & 0 & \dots & M_{2N} \\ \vdots & \vdots & \ddots & \vdots \\ M_{N1} & M_{N2} & \dots & 0 \end{bmatrix} \tag{2.25}$$

It meant the resonant relation was given

$$\omega = 2\pi f = \frac{1}{\sqrt{L_0 C_0}} = \frac{1}{\sqrt{L_1 C_1}} = \cdots = \frac{1}{\sqrt{L_N C_N}} \tag{2.26}$$

It was noticed from the resonant condition in (2.26), the relation between voltage-current was

$$V_0 = j\omega \boldsymbol{M}_{0\mathrm{r}} \boldsymbol{I}_{\mathrm{r}} \tag{2.27}$$

$$-\boldsymbol{R}\boldsymbol{I}_{\mathrm{r}} = j\omega \boldsymbol{M}_{\mathrm{r}0} I_0 + j\omega \boldsymbol{M}_{\mathrm{rr}} \boldsymbol{I}_{\mathrm{r}} \tag{2.28}$$

where the coupling vector consisted of the mutual inductances between the transmitting coil and the receivers

$$\boldsymbol{M}_{0\mathrm{r}} = \boldsymbol{M}_{\mathrm{r}0}^{\mathrm{T}} = [M_{01}\ M_{02}\ \dots\ M_{0N}], \tag{2.29}$$

the receiving current vector was

$$\boldsymbol{I}_{\mathrm{r}} = [I_1\ I_2\ \dots\ I_N]^{\mathrm{T}} \tag{2.30}$$

and the matrix of loads was

$$\boldsymbol{R} = \begin{bmatrix} R_1 & 0 & \dots & 0 \\ 0 & R_2 & \dots & 0 \\ \vdots & \vdots & \ddots & \vdots \\ 0 & 0 & \dots & R_N \end{bmatrix} \tag{2.31}$$

From (2.28), we derived

$$\boldsymbol{I}_{\mathrm{r}} = -j\omega[\boldsymbol{R} + j\omega \boldsymbol{M}_{\mathrm{rr}}]^{-1} \boldsymbol{M}_{\mathrm{r}0} I_0 \tag{2.32}$$

Therefore, we had the relation between input voltage and input current

$$V_0 = \omega^2 \boldsymbol{M}_{0\mathrm{r}} [\boldsymbol{R} + j\omega \boldsymbol{M}_{\mathrm{rr}}]^{-1} \boldsymbol{M}_{\mathrm{r}0} I_0 \tag{2.33}$$

As a result, the load voltages were calculated as

$$\begin{aligned} \boldsymbol{V}_{\mathrm{r}} &= -\boldsymbol{R}\boldsymbol{I}_{\mathrm{r}} = j\omega\boldsymbol{R}[\boldsymbol{R} + j\omega\boldsymbol{M}_{\mathrm{rr}}]^{-1}\boldsymbol{M}_{\mathrm{r0}}I_0 \\ \text{or } \boldsymbol{V}_{\mathrm{r}} &= \frac{j\omega\boldsymbol{R}[\boldsymbol{R} + j\omega\boldsymbol{M}_{\mathrm{rr}}]^{-1}\boldsymbol{M}_{\mathrm{r0}}}{\omega^2\boldsymbol{M}_{\mathrm{0r}}[\boldsymbol{R} + j\omega\boldsymbol{M}_{\mathrm{rr}}]^{-1}\boldsymbol{M}_{\mathrm{r0}}}V_0 \end{aligned} \tag{2.34}$$

Equation (2.34) illustrated that the load voltages in the conventional SIMO IPT system depended on not only the loads but also the cross coupling among the receiving coils. Therefore, if there was no special designs for the conventional SIMO IPT systems, the load voltages would lose the stability against the load variations because of the cross couplings among the receiving coils.

2.4.2 Stabilizing load voltages in SIMO IPT systems

In order to keep the load voltages in SIMO IPT systems stable against the load, the authors in [132] proposed a method of adjusting the operating frequency to achieve stable point of the load voltages against the load variations. The mode system of the IPT system in [132] is described as in Fig. 2.11. In this system, it was assumed that there was no cross coupling among the receivers. Compensatory capacitors were initially designed to be resonant with corresponding coils at angular frequency ω_0. By adjusting the operating frequency, the system could attain the load-independent output voltages at the receivers. The load voltages

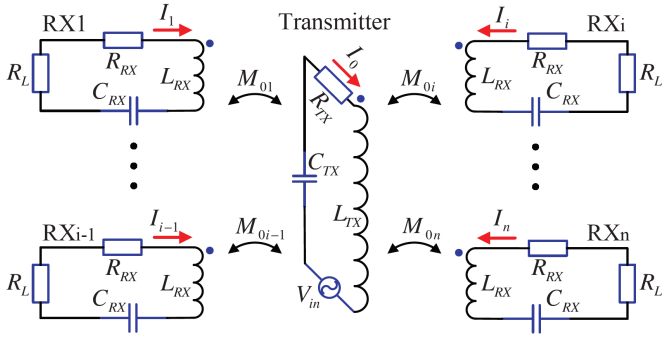

Figure 2.11. Illustration of the multiple-receiver IPT systems with load-independent output voltages in [132].

were given by [132]

$$V_L = \frac{k_{0i}\omega_n^2 V_{\text{in}}}{|\omega_n^2 - 1|}\sqrt{\frac{C_{\text{TX}}}{C_{\text{RX}}}} \tag{2.35}$$

where the normalized angular frequency

$$\omega_n = \frac{1}{\sqrt{1 \pm \sqrt{\sum_{i=1}^{n} k_{0i}^2}}} \tag{2.36}$$

The theoretical analysis was then confirm by the experiments. The experimental system and the results were shown in Fig. 2.12. The experimental results indicated that it was feasible to adjust the operating frequency to stabilize the load voltages against the load variations. Specifically, the load voltage of the third receiver was stable at two frequencies, 80.1kHz and 148.5kHz, when the set of coupling coefficients was as in Fig. 2.12b while at one frequency of 69.2kHz. However, in this system, the cross couplings among the receivers were not taken into account in theoretical analysis. The disadvantage of the method of adjusting operating frequency was not suitable for applications which required a certain operating frequency.

Another IPT system used to stabilize the load voltages for multiple receivers was proposed in [133]. In this system, a resonator was inserted between the transmitter and the receivers in conventional SIMO IPT system to stabilize the load voltages. The system model of this system was described as in Fig. 2.13. It was assumed that the couplings between the source coil and the receiving coils were negligibly small. The cross couplings could be compressed by using low operating frequency and the large loads. As a result, the load voltages were given by the formula below

$$|V_{L_i}| \approx \left|\frac{M_{T_i}}{M_{ST}} V_S\right| \tag{2.37}$$

The principle of the operation of the system was similar to that of SISO IPT system using LCC topology or relay-based structure. The current flowing in the transmitting coil TX was kept stable regardless of the loads. Then, it induced a constant voltage to each receiving coil. Because each receiver was a resonator, the constant induced voltage was delivered to corresponding load.

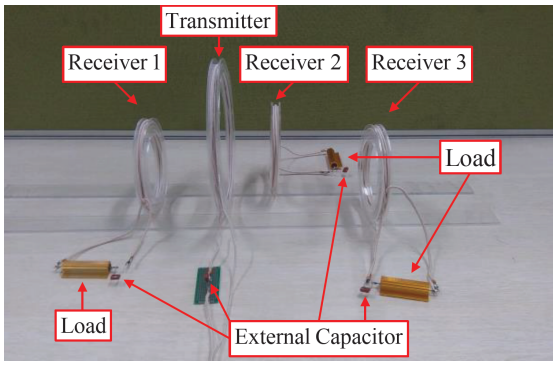

(a) Experimental system

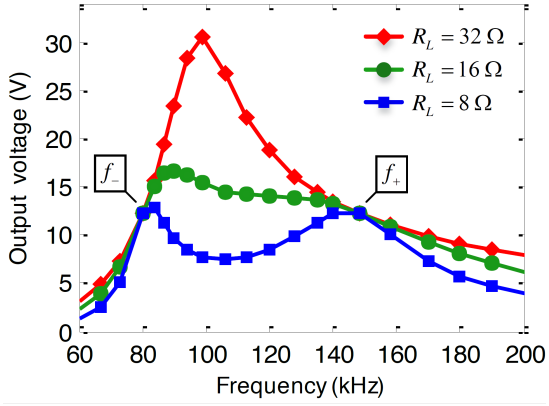

(b) $k_{01} = 0.1, k_{02} = 0.2, k_{03} = 0.5$

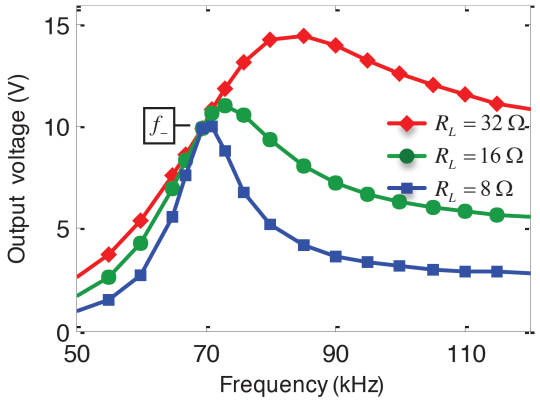

(c) $k_{01} = 0.4, k_{02} = 0.6, k_{03} = 0.8$

Figure 2.12. Experimental system and the results of the third output voltage for two settings of the system in [132].

The authors verified the theoretical analysis by experiments as in Fig. 2.14 The experimental results showed that when any receiver moved out or joined the charging system, the output voltages of the other receivers were unchanged. It confirmed that each load was isolated from the others. However, in this system, the load voltages were not controlled separately because the couplings among the transmitting coil and the receiving coils were fixed. Therefore, it would be difficult to apply for charging multiple receivers where each receiver required a rated voltage for its load.

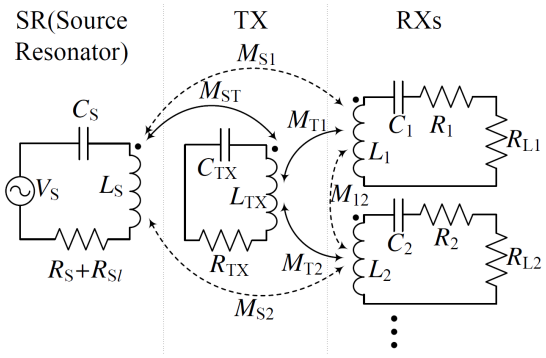

Figure 2.13. Illustration of stabilizing the multiple load voltages using resonator in [133].

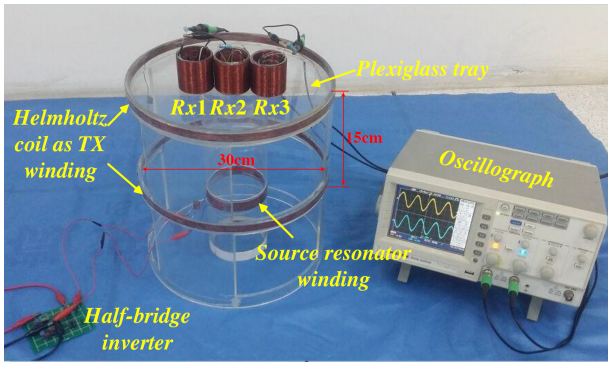

Figure 2.14. Experimental system to illustrate the load-isolation output voltages in [133].

2.5. Conclusion

This chapter showed the details and the importance of K-inverter in stabilizing load voltage in SISO IPT systems. Several studies of stabilizing load voltages in multiple-receiver IPT systems were mentioned in this chapter. However, the recent studies could not be applied for the scenarios in which each application required a rated voltage for its load or some receivers were located far from transmitter or different applications could operate at different frequencies. These challenges will be addressed in next three chapters.

Chapter 3

Load voltage stabilization and adjustment in SIMO IPT system using multiple K-inverters

3.1. Introduction

In this chapter, SIMO IPT system using multiple K-inverters, equivalent to multiple transmitting resonators, to control the load voltages from the transmitter side was proposed. As mentioned above, in the conventional SIMO IPT systems, load voltages depended on the cross couplings among the receivers and the loads. Several IPT systems have been proposed to stabilizing the load voltages for multiple receivers [132, 133]. However, these works cannot satisfy additional requirement where each receiver requires a differently rated voltage. In order to address this challenge, this chapter proposed the IPT system using multiple resonators to stabilize and adjust load voltages to differently rated voltages [P.W1], [P.J1].

3.2. System model

3.2.1 System description

The system using multiple resonators to control load voltages is described as in Fig. 3.1. At the side of charging platform, the source is the output of an inverter which supplies a constant voltage V_0. Inverter operates at frequency f with a corresponding angular frequency $\omega = 2\pi f$. The source drives the source resonator to deliver power to M transmitting resonators inside the charging platform. Then, the power from the source resonator is divided into sub-streams to deliver to N receivers. At the receiver side, each receiver is equipped a resonator and requires a rated voltage for its load. It is noted that in this system, N receivers are N independent users. This design objective here is control the load voltages to match rated voltages for the loads. By using the proposed system, this task can be done by adjusting the arrangement of the transmitting coils inside the charging platform. For the sake of simplicity, the mechanical part taking charge of adjusting the arrangement of the transmitting coils is omitted.

In the model, k and l are used to index the resonators where $k, l \in \{0, 1, \ldots, M, M+1, \ldots, M+N\}$. The source resonator is indexed 0 while the numbers from 1 to M are used for M transmitting resonators and the numbers from $M+1$ to $M+N$ are indexed fro N receivers. The loads of N receivers are assumed to be the resistances and denoted by R_{M+1}, R_{M+2}, $\ldots$, R_{M+N}. The self inductance, internal resistance and resonant capacitance of the k-th resonator are denoted by L_k, r_k and C_k, respectively. For all $k \in \{0, \ldots, M+N\}$, the self inductance L_k and capacitance C_k of the k-th resonator satisfy the resonance condition

$$\omega^2 L_k C_k = 1. \tag{3.1}$$

L_{kl} denotes for the mutual inductance between the k-th resonator and the l-th resonator, where $k \neq l$. In Fig. 3.1, V_k denotes for the complex phasor of voltage of the k-th resonator while I_k is for the complex phasor of current flowing it.

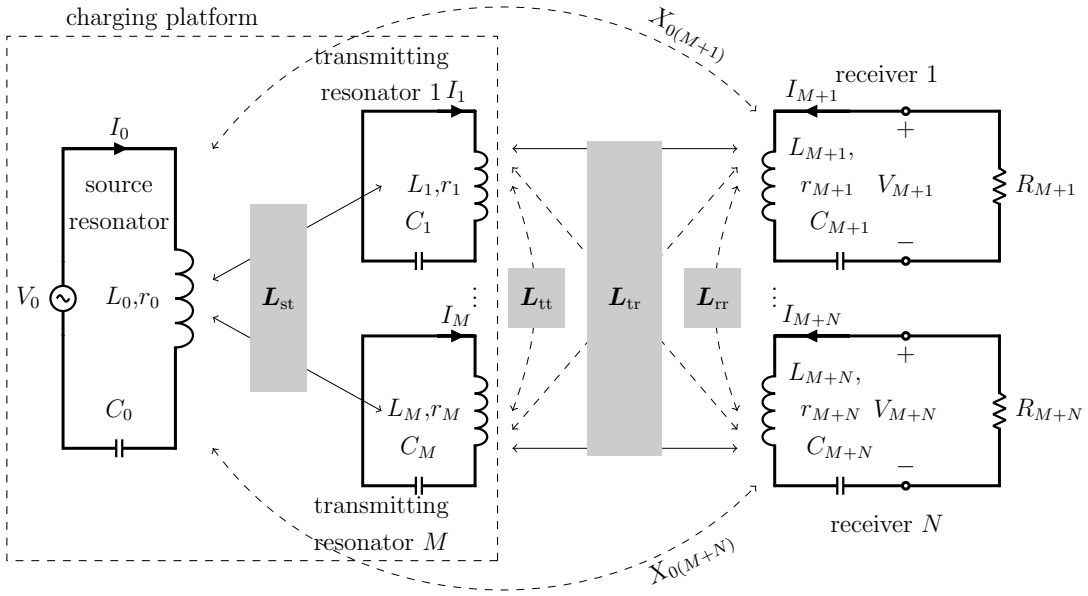

Figure 3.1. Multiple-resonator-based IPT system

3.2.2 Stability of output voltages

The relation between voltages and currents in the system is given by

$$\begin{bmatrix} V_0 \\ \mathbf{0} \\ \boldsymbol{V}_{\rm r} \end{bmatrix} = \begin{bmatrix} r_0 & j\omega\boldsymbol{L}_{\rm st} & j\omega\boldsymbol{L}_{\rm sr} \\ j\omega\boldsymbol{L}_{\rm ts} & \boldsymbol{r}_{\rm t} + j\omega\boldsymbol{L}_{\rm tt} & j\omega\boldsymbol{L}_{\rm tr} \\ j\omega\boldsymbol{L}_{\rm rs} & j\omega\boldsymbol{L}_{\rm rt} & \boldsymbol{r}_{\rm r} + j\omega\boldsymbol{L}_{\rm rr} \end{bmatrix} \begin{bmatrix} I_0 \\ \boldsymbol{I}_{\rm t} \\ \boldsymbol{I}_{\rm r} \end{bmatrix}. \tag{3.2}$$

In (3.2), vector $\mathbf{0}$ is the zero column vector of size M; the vector of the load voltages is $\boldsymbol{V}_{\rm r} = [V_{M+1}\ V_{M+2}\ \cdots\ V_{M+N}]^{\rm T}$; the vector of currents in the transmitting resonators is $\boldsymbol{I}_{\rm t} = [I_1\ I_2\ \cdots\ I_M]^{\rm T}$. The diagonal matrix $\boldsymbol{r}_{\rm t}$ consists of the internal resistances of the transmitting coils while the diagonal matrix $\boldsymbol{r}_{\rm t}$ consists of those of the receiving coils. $\boldsymbol{L}_{\rm st} = [L_{01}\ L_{02}\ \cdots\ L_{0M}]$ is the mutual inductance vector between the source coil and the transmitting ones, $\boldsymbol{L}_{\rm sr} = [L_{0(M+1)}\ L_{0(M+2)} \cdots L_{0(M+N)}]$ is that between the source coil and the receiving ones. And, $\boldsymbol{L}_{\rm tr}$ is the mutual inductance matrix between the transmitting

coils and receiving coils, which is expressed by

$$\boldsymbol{L}_{\mathrm{tr}} = \begin{bmatrix} L_{1(M+1)} & L_{1(M+2)} & \cdots & L_{1(M+N)} \\ L_{2(M+1)} & L_{2(M+2)} & \cdots & L_{2(M+N)} \\ \vdots & \vdots & \ddots & \vdots \\ L_{M(M+1)} & L_{M(M+2)} & \cdots & L_{M(M+N)} \end{bmatrix}. \tag{3.3}$$

Because of the reciprocity of the network, $\boldsymbol{L}_{\mathrm{st}}^{\mathrm{T}} = \boldsymbol{L}_{\mathrm{ts}}$, $\boldsymbol{L}_{\mathrm{sr}}^{\mathrm{T}} = \boldsymbol{L}_{\mathrm{rs}}$ and $\boldsymbol{L}_{\mathrm{tr}}^{\mathrm{T}} = \boldsymbol{L}_{\mathrm{rt}}$. The matrix $\boldsymbol{L}_{\mathrm{tt}}$ whose elements are the mutual inductances among the transmitting coils is

$$\boldsymbol{L}_{\mathrm{tt}} = \begin{bmatrix} 0 & L_{12} & \cdots & L_{1M} \\ L_{21} & 0 & \cdots & L_{2M} \\ \vdots & \vdots & \ddots & \vdots \\ L_{M1} & L_{M2} & \cdots & 0 \end{bmatrix}, \tag{3.4}$$

and the matrix $\boldsymbol{L}_{\mathrm{rr}}$ whose elements are the mutual inductances among the receiving coils is

$$\boldsymbol{L}_{\mathrm{rr}} = \begin{bmatrix} 0 & \cdots & L_{(M+1)(M+N)} \\ \vdots & \ddots & \vdots \\ L_{(M+N)(M+1)} & \cdots & 0 \end{bmatrix}. \tag{3.5}$$

For the load side, the relation between the load voltages and the load currents is expressed by

$$\boldsymbol{V}_{\mathrm{r}} = -\boldsymbol{R}_l \boldsymbol{I}_{\mathrm{r}}, \tag{3.6}$$

where $\boldsymbol{R}_l = \mathrm{diag}(R_{M+1}, R_{M+2}, \cdots, R_{M+N})$ is the diagonal matrix whose the diagonal entries are the load resistances. Let

$$\tilde{\boldsymbol{Z}}_{\mathrm{tt}} = \boldsymbol{r}_{\mathrm{t}} + j\omega \boldsymbol{L}_{\mathrm{tt}}, \tag{3.7}$$

and

$$\tilde{\boldsymbol{Z}}_{\mathrm{rr}} = \boldsymbol{r}_{\mathrm{r}} + j\omega \boldsymbol{L}_{\mathrm{rr}}. \tag{3.8}$$

From (3.6) and (3.2), the transmitting currents are derived in term of the input current as follows

$$\boldsymbol{I}_{\mathrm{r}} = -j[\boldsymbol{R}_l + \tilde{\boldsymbol{Z}}_{\mathrm{rr}}]^{-1}[\omega \boldsymbol{L}_{\mathrm{rs}} I_0 + \omega \boldsymbol{L}_{\mathrm{rt}} \boldsymbol{I}_{\mathrm{t}}]. \tag{3.9}$$

Combining (3.9) and the second row of (3.2), we have the relation between the transmitting currents and the input current

$$\boldsymbol{I}_{\mathrm{t}} = -[\tilde{\boldsymbol{Z}}_{\mathrm{tt}} + \omega^2 \boldsymbol{L}_{\mathrm{tr}}[\boldsymbol{R}_l + \tilde{\boldsymbol{Z}}_{\mathrm{rr}}]^{-1}\boldsymbol{L}_{\mathrm{rt}}]^{-1} \times [j\omega \boldsymbol{L}_{\mathrm{ts}} + \omega^2 \boldsymbol{L}_{\mathrm{tr}}[\boldsymbol{R}_{\mathrm{l}} + \tilde{\boldsymbol{Z}}_{\mathrm{rr}}]^{-1}\boldsymbol{L}_{\mathrm{rs}}]I_0. \quad (3.10)$$

Therefore, based on (3.2), (3.9) and (3.10), the relation between the output voltages and the input currents is obtained

$$\boldsymbol{V}_{\mathrm{r}} = [\boldsymbol{A} - \boldsymbol{B}\boldsymbol{C}^{-1}\boldsymbol{D}]I_0, \quad (3.11)$$

where the matrices $\boldsymbol{A}$, $\boldsymbol{B}$, $\boldsymbol{C}$ and $\boldsymbol{D}$ are

$$\begin{aligned}
\boldsymbol{A} &= j\omega \boldsymbol{L}_{\mathrm{rs}} - j\omega \tilde{\boldsymbol{Z}}_{\mathrm{rr}}[\boldsymbol{R}_{\mathrm{l}} + \tilde{\boldsymbol{Z}}_{\mathrm{rr}}]^{-1}\boldsymbol{L}_{\mathrm{rs}}, \\
\boldsymbol{B} &= j\omega \boldsymbol{L}_{\mathrm{rt}} - j\omega \tilde{\boldsymbol{Z}}_{\mathrm{rr}}[\boldsymbol{R}_{\mathrm{l}} + \tilde{\boldsymbol{Z}}_{\mathrm{rr}}]^{-1}\boldsymbol{L}_{\mathrm{rt}}, \\
\boldsymbol{C} &= \tilde{\boldsymbol{Z}}_{\mathrm{tt}} + \omega^2 \boldsymbol{L}_{\mathrm{tr}}[\boldsymbol{R}_l + \tilde{\boldsymbol{Z}}_{\mathrm{rr}}]^{-1}\boldsymbol{L}_{\mathrm{rt}}, \\
\boldsymbol{D} &= j\omega \boldsymbol{L}_{\mathrm{ts}} + \omega^2 \boldsymbol{L}_{\mathrm{tr}}[\boldsymbol{R}_l + \tilde{\boldsymbol{Z}}_{\mathrm{rr}}]^{-1}\boldsymbol{L}_{\mathrm{rs}}.
\end{aligned} \quad (3.12)$$

From (3.2), (3.9) and (3.10), the relation between the source voltage and the input current is expressed

$$V_0 = [E - \boldsymbol{F}\boldsymbol{C}^{-1}\boldsymbol{D}]I_0, \quad (3.13)$$

where the scalar E and matrix $\boldsymbol{F}$ are

$$\begin{aligned}
E &= r_0 + \omega^2 \boldsymbol{L}_{\mathrm{sr}}[\boldsymbol{R}_l + \tilde{\boldsymbol{Z}}_{\mathrm{rr}}]^{-1}\boldsymbol{L}_{\mathrm{rs}}, \\
\boldsymbol{F} &= j\omega \boldsymbol{L}_{\mathrm{st}} + \omega^2 \boldsymbol{L}_{\mathrm{sr}}[\boldsymbol{R}_l + \tilde{\boldsymbol{Z}}_{\mathrm{rr}}]^{-1}\boldsymbol{L}_{\mathrm{rt}}.
\end{aligned} \quad (3.14)$$

From (3.10) and (3.13), the currents induced in the transmitting resonators are derived

$$\boldsymbol{I}_{\mathrm{t}} = \frac{-\boldsymbol{C}^{-1}\boldsymbol{D}}{E - \boldsymbol{F}\boldsymbol{C}^{-1}\boldsymbol{D}}V_0. \quad (3.15)$$

Consequently, the output voltages can be adequately expressed as function of the source voltage as follows

$$\boldsymbol{V}_{\mathrm{r}} = \frac{\boldsymbol{A} - \boldsymbol{B}\boldsymbol{C}^{-1}\boldsymbol{D}}{E - \boldsymbol{F}\boldsymbol{C}^{-1}\boldsymbol{D}}V_0. \quad (3.16)$$

According to (3.12) and (3.14), the terms $\boldsymbol{A}$, $\boldsymbol{B}$, $\boldsymbol{C}$, $\boldsymbol{D}$, E and $\boldsymbol{F}$ are relevant to the loads $\boldsymbol{R}_l$. Thus, the load voltages $\boldsymbol{V}_{\mathrm{r}}$ depend on the load resistances.

Basically, the load voltages vary when one or more loads among R_{M+1}, R_{M+2}, $\ldots$, R_{M+N} change. However, when the loads are sufficiently large, the terms $\boldsymbol{A}$, $\boldsymbol{B}$, $\boldsymbol{C}$, $\boldsymbol{D}$, E and $\boldsymbol{F}$ in (3.16) can be approximated as follows

$$\begin{aligned}
\boldsymbol{A} &= j\omega\boldsymbol{L}_{\mathrm{rs}} - j\omega\tilde{\boldsymbol{Z}}_{\mathrm{rr}}[\boldsymbol{R}_l + \tilde{\boldsymbol{Z}}_{\mathrm{rr}}]^{-1}\boldsymbol{L}_{\mathrm{rs}} \approx j\omega\boldsymbol{L}_{\mathrm{rs}},\\
\boldsymbol{B} &= j\omega\boldsymbol{L}_{\mathrm{rt}} - j\omega\tilde{\boldsymbol{Z}}_{\mathrm{rr}}[\boldsymbol{R}_l + \tilde{\boldsymbol{Z}}_{\mathrm{rr}}]^{-1}\boldsymbol{L}_{\mathrm{rt}} \approx j\omega\boldsymbol{L}_{\mathrm{rt}},\\
\boldsymbol{C} &= \tilde{\boldsymbol{Z}}_{\mathrm{tt}} + \omega^2\boldsymbol{L}_{\mathrm{tr}}[\boldsymbol{R}_l + \tilde{\boldsymbol{Z}}_{\mathrm{rr}}]^{-1}\boldsymbol{L}_{\mathrm{rt}} \approx \tilde{\boldsymbol{Z}}_{\mathrm{tt}},\\
\boldsymbol{D} &= j\omega\boldsymbol{L}_{\mathrm{ts}} + \omega^2\boldsymbol{L}_{\mathrm{tr}}[\boldsymbol{R}_l + \tilde{\boldsymbol{Z}}_{\mathrm{rr}}]^{-1}\boldsymbol{L}_{\mathrm{rs}} \approx j\omega\boldsymbol{L}_{\mathrm{ts}},\\
E &= r_0 + \omega^2\boldsymbol{L}_{\mathrm{sr}}[\boldsymbol{R}_l + \tilde{\boldsymbol{Z}}_{\mathrm{rr}}]^{-1}\boldsymbol{L}_{\mathrm{rs}} \approx r_0,\\
\boldsymbol{F} &= j\omega\boldsymbol{L}_{\mathrm{st}} + \omega^2\boldsymbol{L}_{\mathrm{sr}}[\boldsymbol{R}_l + \tilde{\boldsymbol{Z}}_{\mathrm{rr}}]^{-1}\boldsymbol{L}_{\mathrm{rt}} \approx j\omega\boldsymbol{L}_{\mathrm{st}}.
\end{aligned} \tag{3.17}$$

Accordingly, the currents induced in the transmitting resonators calculated in (3.15) are approximated

$$\boldsymbol{I}_{\mathrm{t}} \approx \frac{-j\omega\tilde{\boldsymbol{Z}}_{\mathrm{tt}}^{-1}\boldsymbol{L}_{\mathrm{ts}}}{r_0 + \omega^2\boldsymbol{L}_{\mathrm{st}}\tilde{\boldsymbol{Z}}_{\mathrm{tt}}^{-1}\boldsymbol{L}_{\mathrm{ts}}}V_0. \tag{3.18}$$

It means that the currents in in the transmitting resonators are fixed, which is relevant to multiple K-inverters because constant voltage is transformed to constant currents against load variations. Consequently, the load voltages can be decided by the mutual inductances among the resonators and the source voltage as the formula below

$$\boldsymbol{V}_{\mathrm{r}} \approx \frac{j\omega\boldsymbol{L}_{\mathrm{rs}} + \omega^2\boldsymbol{L}_{\mathrm{rt}}\tilde{\boldsymbol{Z}}_{\mathrm{tt}}^{-1}\boldsymbol{L}_{\mathrm{ts}}}{r_0 + \omega^2\boldsymbol{L}_{\mathrm{st}}\tilde{\boldsymbol{Z}}_{\mathrm{tt}}^{-1}\boldsymbol{L}_{\mathrm{ts}}}V_0. \tag{3.19}$$

Equation (3.19) indicates that when the load resistances are sufficiently large, the proposed system has acted below:

1) The load voltages $\boldsymbol{V}_{\mathrm{r}}$ are stable against the load resistances because (3.19) is irrelevant to $\boldsymbol{R}_l$. For that reason, the ratios among the load voltages are independent of the load resistances. Additionally, the voltages induced in the receivers are mostly dominated by the transmitting currents $\boldsymbol{I}_{\mathrm{t}}$ because the use of low operation frequency will outstandingly suppress the cross-couplings among the receiving coils. According to (3.18), the transmitting currents $\boldsymbol{I}_{\mathrm{t}}$ are stable against the variations of the load resistances. Therefore, the induced voltages in the receivers are stable regardless of the load

variations. This is also considered as the additional explanation for being able to deliver constant voltages to the load resistances.

2) The load voltages as well as the ratios among them mainly depend on the mutual inductances $\boldsymbol{L}_{\mathrm{st}}$ between the source and the transmitting resonators, and the mutual inductances $\boldsymbol{L}_{\mathrm{rt}}$ between the transmitting and receiving resonators. Given certain positions of the receivers, we can regulate the load voltage ratios by changing the relative position of the transmitting resonators inside the charging platform because this will change in the mutual inductances $\boldsymbol{L}_{\mathrm{st}}$ and $\boldsymbol{L}_{\mathrm{rt}}$.

3) The load voltage ratio is irrelevant to the source voltage V_0.

3.2.3 Voltage control and effectiveness

The aforementioned three behaviors suggest that controlling the load voltages to reach their rated values is a simple two-step process as follows. First, given values of the rated voltages $V_{M+1}^{\star}$, $V_{M+2}^{\star}$, $\ldots$, $V_{M+N}^{\star}$ for N receivers, the arrangement of the transmitting resonators will be adjusted inside the charging platform until the ratio of the load voltages $V_{M+1} : V_{M+2} : \cdots : V_{M+N}$ reaches the ratio of the rated values $V_{M+1}^{\star} : V_{M+2}^{\star} : \cdots : V_{M+N}^{\star}$. Second, the source voltage V_0 will be increased or decreased until all the load voltages reach the correspondingly rated values.

The voltage control method takes effect when the load voltages are independent of the load resistances. For that to happen, according to (3.17), the following conditions must be remarkably satisfied

$$\begin{cases} \boldsymbol{U}_N \gg |\tilde{\boldsymbol{Z}}_{\mathrm{rr}} \boldsymbol{R}_l^{-1}|, & (3.20) \\ |\tilde{\boldsymbol{Z}}_{\mathrm{tt}}| \gg |\omega^2 \boldsymbol{L}_{\mathrm{tr}} \boldsymbol{R}_l^{-1} \boldsymbol{L}_{\mathrm{rt}}|, & (3.21) \\ |\boldsymbol{L}_{\mathrm{ts}}| \gg |\omega \boldsymbol{L}_{\mathrm{tr}} \boldsymbol{R}_l^{-1} \boldsymbol{L}_{\mathrm{rs}}|, & (3.22) \\ r_0 \gg |\omega^2 \boldsymbol{L}_{\mathrm{sr}} \boldsymbol{R}_l^{-1} \boldsymbol{L}_{\mathrm{rs}}|. & (3.23) \end{cases}$$

Therefore, several characteristics of the proposed method can be drawn as follows.

1) The cross coupling among the coils would be significantly suppressed and low operation frequency should be used if we need to achieve constant voltage functionality at low values of the load resistances. This feature is similar to the discovery in [133].

2) When the system has larger number of transmitting and receiving resonators, the load voltages would be more difficult to attain the stable values against the load variations. This means when the system is scaled up, the load voltages will be stabilized at larger load resistances.

3) The system can stabilize the load voltages at lower load resistances if the cross couplings $\boldsymbol{L}_{\rm tt}$ among the transmitting resonators and/or the mutual inductances $\boldsymbol{L}_{\rm ts}$ between the transmitting and receiving resonators are stronger.

3.2.4 RF-RF efficiency

The output power is derived by:

$$\begin{aligned} P_{\rm out} &= \frac{1}{2}{\rm Re}\{\boldsymbol{V}_{\rm r}^{\rm H}\boldsymbol{R}_l^{-1}\boldsymbol{V}_{\rm r}\} \\ &= \frac{1}{2}{\rm Re}\{[\boldsymbol{A}-\boldsymbol{B}\boldsymbol{C}^{-1}\boldsymbol{D}]^{\rm H}\boldsymbol{R}_l^{-1}[\boldsymbol{A}-\boldsymbol{B}\boldsymbol{C}^{-1}\boldsymbol{D}]\}|I_0|^2, \end{aligned} \tag{3.24}$$

The input power is calculated by:

$$P_{\rm in} = \frac{1}{2}{\rm Re}\{V_0^* I_0\} = \frac{1}{2}{\rm Re}\{E-\boldsymbol{F}\boldsymbol{C}^{-1}\boldsymbol{D}\}|I_0|^2. \tag{3.25}$$

Accordingly, the RF-to-RF efficiency is determined as following formula:

$$\eta = \frac{P_{\rm out}}{P_{\rm in}} = \frac{{\rm Re}\{[\boldsymbol{A}-\boldsymbol{B}\boldsymbol{C}^{-1}\boldsymbol{D}]^{\rm H}\boldsymbol{R}_l^{-1}[\boldsymbol{A}-\boldsymbol{B}\boldsymbol{C}^{-1}\boldsymbol{D}]\}}{{\rm Re}\{E-\boldsymbol{F}\boldsymbol{C}^{-1}\boldsymbol{D}\}}. \tag{3.26}$$

3.3. Simulation results

In order to confirm the effectiveness of the proposed voltage control method we carried out full-wave electromagnetic (EM) simulations using WIPL-D© Pro software. We conducted an investigation into the systems with two receivers and

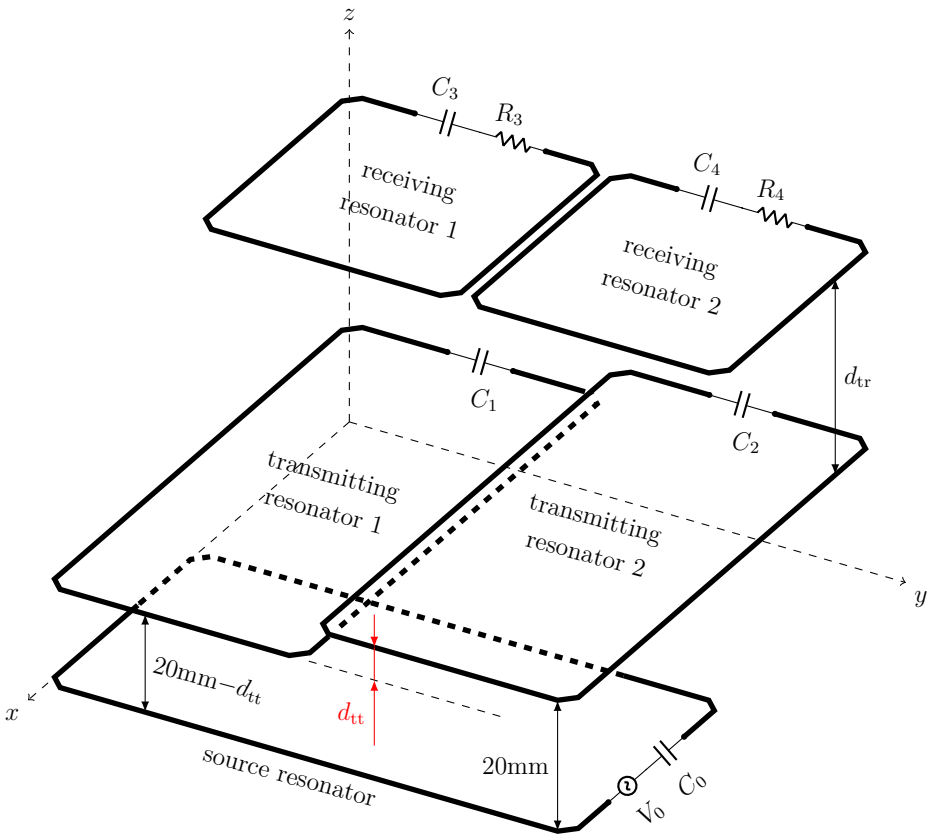

Figure 3.2. Simulation configuration of the two-receiver charging system

three receivers. In both systems all coils were the planar spiral coils. All coils were made of copper wire with conductivity of $5.8 \times 10^7 \mathrm{S} \cdot \mathrm{m}^{-1}$. The radius of wire was 1mm and the turn spacing was 1mm. It was assumed that the source resonator was driven by a power source. The power source supplied a sinusoidal constant voltage of 10V. The operating frequency of the power source was 200kHz with zero phase offset. It was also assumed that the power source had no internal resistance.

3.3.1 Two-receiver system

The simulation setting of the two-receiver system was described in Fig. 3.2. The sizes of the source, the transmitting coils were identical with 100mm × 200mm

while that of the receiving coils was 100mm × 100mm. The numbers of turn of the source, the transmitting and the receiving coils are 3, 8 and 3 respectively. Initially, TXs was 30mm distant from RXs (d_{tr} = 30mm) while the distance between TXs and the source resonator d_{st} is 20mm. Then, one transmitting coil was vertically lowered down from the initial position by steps to simulate the change of the arrangement of the transmitting resonators.

Fig. 3.3 showed the load voltages over the variations of the load resistances in two different arrangements of the two transmitting resonators. In these simulations, the load resistances varied from 5Ω to 500Ω. The results indicated that in two arrangements of the transmitting resonators the load voltages almost kept unchanged against the wide range of the load resistances. When the vertical distance between two transmitting resonators d_{tt} was 10mm, the ratio of two load voltages was about two ($V_4 : V_3 = 4.2\text{V} : 2.1\text{V}$) as shown in Fig. 3.3a. The ratio of the load voltages went to approximately 3.5 when d_{tt} was 16mm, while the load voltages were still kept constant against the variations of the load resistances. However, when the load resistance R_3 changed from 5Ω to 20Ω, the load voltage V_4 slightly increased from 4V to about 4.2V before stabilizing at 4.2V regardless of continuous increase of the load resistances. This was because when the load resistances were small, the impact of the cross couplings among the receiving coils become stronger due to the increases of the load currents. Therefore, the stability of the load voltages would be deteriorated.

The relation between the currents flowing in the transmitting resonators and the load resistances was shown in Fig. 3.4 . The simulation results highlighted that the transmitting currents were stable against the load variations. It agreed with the prediction in section 3.2.2. When the transmitting resonator 1 was at the position of 10mm lower than the initial position, the currents flowing in the transmitting resonators I_1 and I_2 were kept stable at about 3.4A and 2.6A

Fig. 3.5 illustrated the ratio between the two output voltages as a function of the vertical distance between the two transmitting coils. The estimated values, based on (3.19), and the simulation results have plotted in the same graph to verify the validity of the results. It was clear that when the vertical distance between two transmitting resonators increased, the ratio between two load voltages get bigger. For the system in this simulation, the ratio between two load volt-

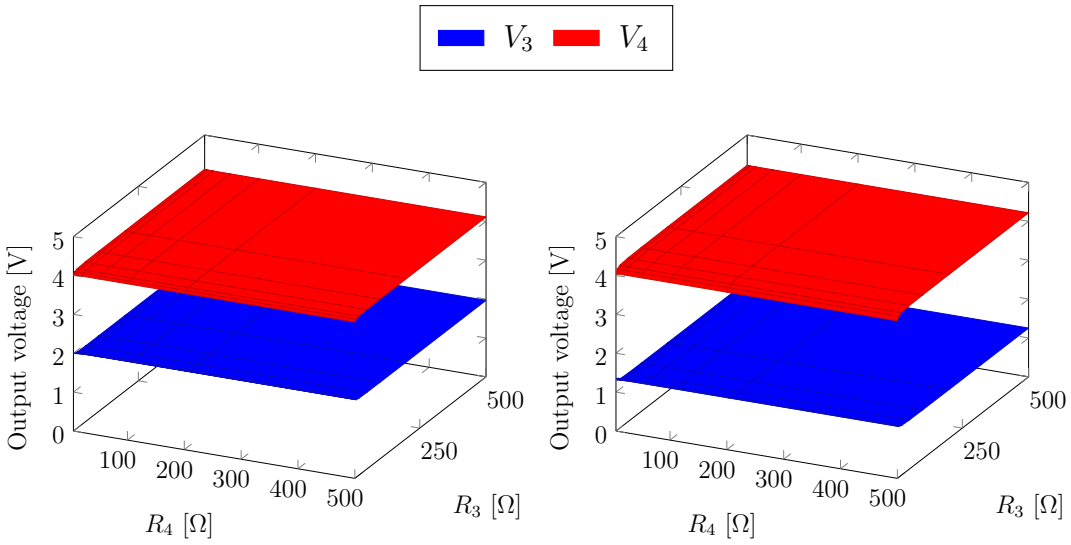

(a) $d_{\mathrm{tt}} = 10\mathrm{mm}$ (b) $d_{\mathrm{tt}} = 16\mathrm{mm}$

Figure 3.3. The load voltages as a function of the load resistances R_3 and R_4, with the vertical distance between two transmitting coils: (a) $d_{\mathrm{tt}} = 10\mathrm{mm}$ and (b) $d_{\mathrm{tt}} = 16\mathrm{mm}$.

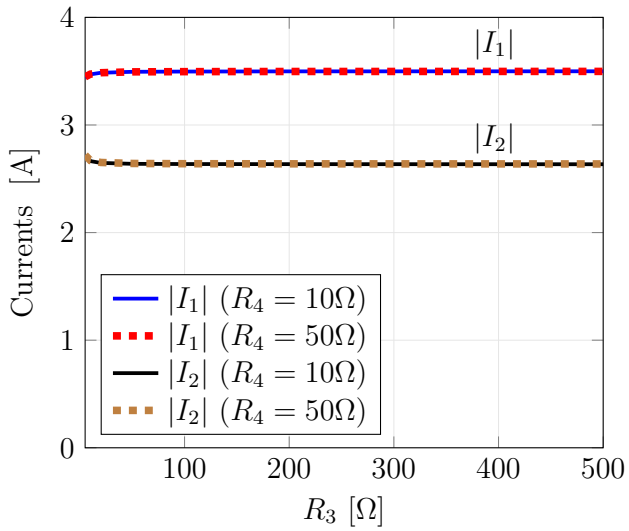

Figure 3.4. The amplitudes of the currents in the transmitting resonators

ages could reach the value of up to 3.5. The figure indicated that the simulation

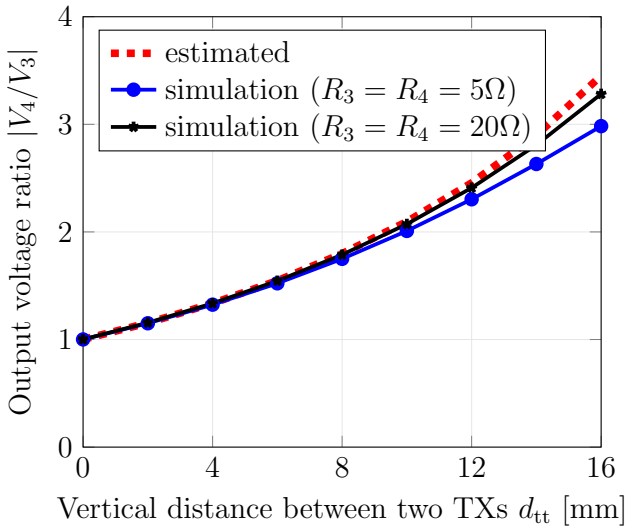

Figure 3.5. The load voltages as a function of the adjusting distance

results would approach the estimates as the load resistances became greater. For the case of the large load resistances, the simulation results would come nearer the estimated values calculated in (3.19) because the conditions (3.20) - (3.23) completely held. In contrast, the estimates was slightly different from the simulations as the load resistances were small, . Again, this was because the coupling effect from the receiving resonators was so strong that it could be not neglected in the calculation.

The variations of the output voltages over the change of the source voltage were illustrated in Fig. 3.6. The simulation results and the estimated values were plotted on the graph to validate the estimation of the output voltages in (3.19). The results indicated that the load voltages were proportional to the source voltage. The load voltages V_3 and V_4 were 2V and 4V respectively when the source voltage was 10V. The load voltages of 6V and 12V were obtained when the source voltage was adjusted to 30V. However, the ratio between the two load voltages did not change as the source voltage alters. The results confirmed that once the ratio between the two load voltages was fixed at the certain value, we could adjust the load voltages to make the load voltages meeting individually rated values.

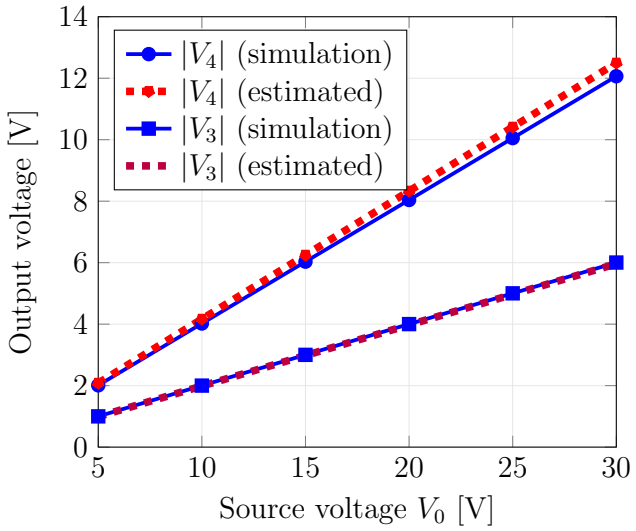

Figure 3.6. The load voltages when the vertical distance between two transmitting coils is equal to 10mm

Fig. 3.7 is the investigation of the RF-RF efficiency against the vertical distance between two transmitting coils d_{tt}. In these simulations the load resistances were selected to be 5Ω. It was indicated that the simulation results well matched the theoretical analysis in (3.26). The system could achieve higher efficiency as distance between the receiving resonators and the transmitting resonators d_{tr} was smaller. The transmission efficiency depended on not only the arrangement of the transmitting resonators but also the distance between the transmitting resonators and the receivers d_{tr}. When the distance between the transmitting resonators and the receivers was 30mm, the transmission efficiency could be 56% if the vertical distance between the transmitting resonators was 16mm. This number of transmission efficiency increased to 66% if we shortened the distance between the transmitting resonators and the receivers to 20mm for the same arrangement of the transmitting resonators. The transmission efficiency would reduce as The coupling between two transmitting coils became stronger and vice versa. Although the transmission efficiencies were not so high, they were still adequate for some low power applications, e.g., charging of up to several watts. Also, the achieved efficiencies were acceptable as all constant voltage designs

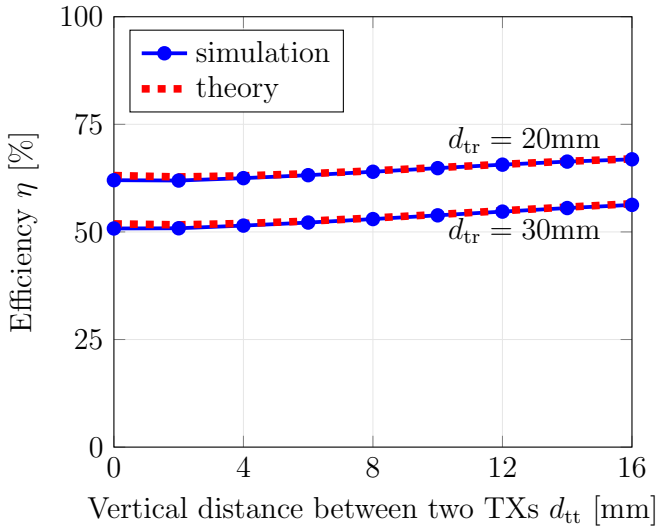

Figure 3.7. RF-RF efficiency as a function of vertical distance between two transmitting coils with load resistances of 5Ω

instinctively suffers from efficiency degradation.

Fig. 3.8 showed the RF-RF efficiency over the alternation of the two load resistances. The results highlighted that the system efficiency was inversely proportional to the load resistances. The system could achieve the transmission efficiency of about 80% when the load resistances were just 1Ω. This number of the transmission efficiency reduced to under 35% as two load resistances increased to 10Ω. It was observed that high efficiency could be achieved in the range of small load resistances. However, the output voltages were stable against load variations when load resistances altered in a larger range as proved in the previous parts. Therefore, it should be noticed of the tradeoff between the RF-RF efficiency and the stabilization of the output voltages when designing charging systems with the characteristic of stabilizing load voltages.

3.3.2 Three-receiver system

In order to confirm the scalability of the theory in Section 3.2.2, the simulation configuration of three receivers was carried out to investigate the output voltages

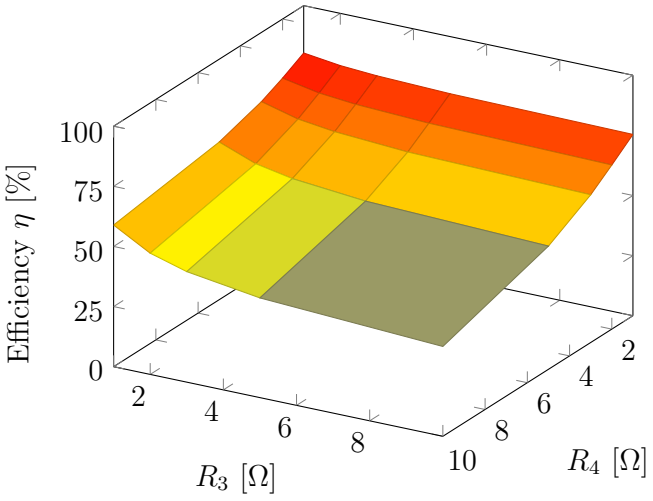

Figure 3.8. RF-RF efficiency as a function of two loads when vertical distance between two transmitting coils is equal to 10mm

against the load resistances. The three-receiver system was set up as shown in Fig. 3.9. The sizes of the source, the transmitting and the receiving coils were respectively 100mm×300mm, 100mm×200mm and 100mm×100mm. The source and the receiving coils were 3-turn spiral coils while the transmitting coils were 4-turn spiral coils. The number of the turns of the transmitting coils decreased from 8 in the two-receiver system to 4 in three-receiver system because of the limitation of the software. Initially, the distance between the source coil and three transmitting coils was 20mm and that between transmitting coils and receiving coils was 30mm. The load resistances changed from 5Ω to 100Ω to conduct an investigation into the output voltages.

Table 3.1 illustrated the load voltages over the variations of the load resistances when the middle transmitting resonator was lowered down 10mm in compared with the others. It was clear that when the load resistances were large, the load voltages could be stabilized against the load resistances. However, the load voltages lost the stability when the load resistances reduce to small values. Again, this was because the cross-couplings among the transmitting resonators decrease when the system was scaled up. It led the condition (3.21) could not be hold when the load resistances became small. Therefore, it was an explanation

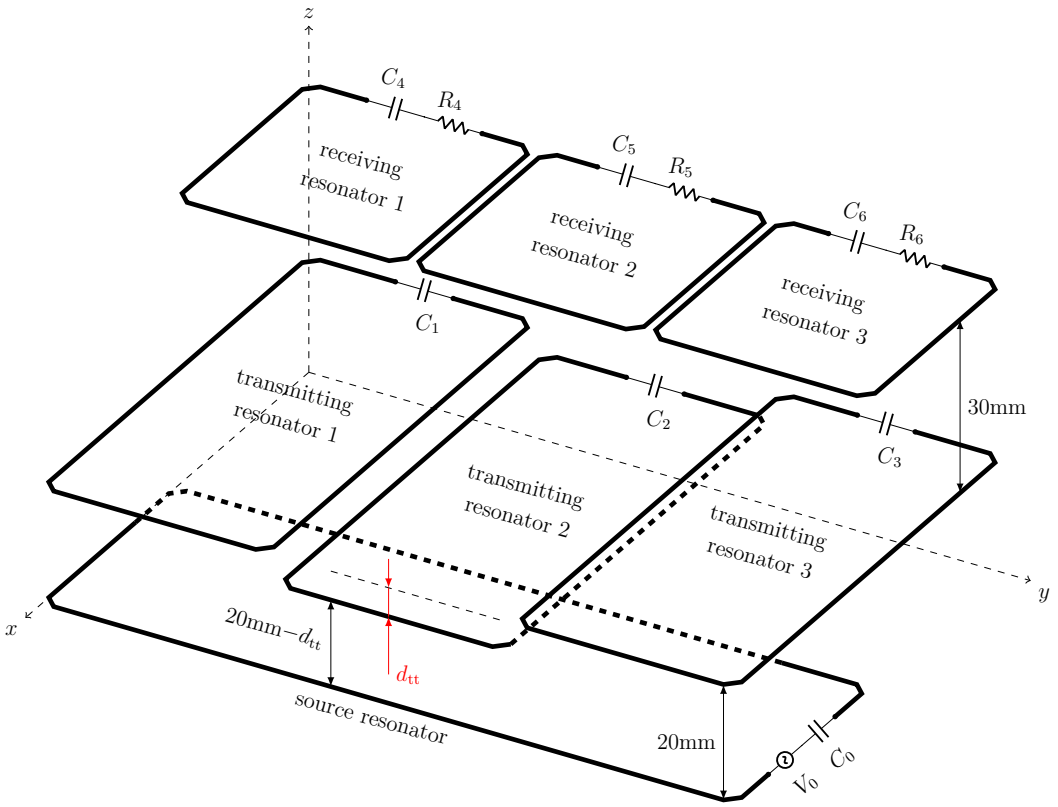

Figure 3.9. Simulation configuration of the three-receiver charging system

for the instability of the load voltages when the load resistances varied in small range.

3.3.3 Effect of Q-factor of the coils

Q-factors of the coils were the important factor because they would affect the performance of constant voltage designs for IPT systems. Table 3.2 in the next page showed the Q-factors of the coils utilized in the simulations in Section 3.3.1 and Section 3.3.2. As indicated in the table, the Q-factors of the coils in the previous investigations have an average values from around 70 to 120. This meant that the proposed scheme could achieve the expected stability and controllability for the coils with high Q-factors.

Next, the voltage stability and controllability of the proposed scheme were

Table 3.1. Simulation results: Output voltages against the load resistances for the configuration in Fig. 3.9

R_4 [Ω]	R_5 [Ω]	R_6 [Ω]	$\|V_4\|$ [V]	$\|V_5\|$ [V]	$\|V_6\|$ [V]
5	5	5	1.713	2.128	1.712
10	5	5	1.956	2.126	1.485
50	30	20	1.818	2.144	1.640
100	30	20	1.849	2.144	1.613
100	30	50	1.762	2.144	1.698
output voltages estimated in (3.19)			1.732	2.141	1.725

investigated when the Q-factors reduced from the values used in the previous subsections. In this investigation, the two loads of the system in Fig. 3.2 were set to be identically equal to 10Ω and the three loads of the system in Fig. 3.9 were identically equal to 10Ω also. The self-inductances of the coils were kept constant and their Q-factors were reduced by increasing the internal resistances. Using MATLAB, the simulation values in (3.16) and the estimated values were calculated in (3.19).

Fig. 3.10 in the previous page plotted the graph of the load voltages over the variations of the Q-factors of the source coil, the transmitting coils, and the receiving coils from 1 to 120. In Fig. 3.10, the subfigures (a), (b), (c) illustrated the results for the two-receiver system when the TX_2 lowered down 10mm while the subfigures (d), (e), (f) were those for the three-receiver system when we adjusted the TX_2 and the TX_3 down 10mm and 4mm respectively. As can be seen in the subfigures (a) and (d), when the quality factor of the source coil reduced, in each system, the simulation values still agreed with the approximated values of the load voltages, meaning that the load voltages in both systems were stabilized against the load resistances. Although the load voltages reduced, they were still stable against the load variations even when the Q-factor of the source coil reduced to under 20. This was because the condition (3.23) still held when r_0

Table 3.2. List of quality factor of the coils in the simulations

Symbol	**Parameter**	**Simulation value**
Two-receiver system		
Q_0	Quality factor of the source coil	77
Q_t	Quality factor of the transmitting coils	118
Q_r	Quality factor of the receiving coils	74
Three-receiver system		
Q_0	Quality factor of the source coil	83
Q_t	Quality factor of the transmitting coils	96
Q_r	Quality factor of the receiving coils	74

increased due to the decrease of Q_0. Next, the subfigures (b) and (e) showed that the simulation values of the load voltages approximated the estimated ones when the Q-factors of the transmitting coils decreased. It meant that the load voltages were still stable against the load variations when the Q-factors of the transmitting coils reduced. This was because the condition (3.21) still held. Finally, the effect of the receiving coil Q-factors was desribed in the subfigures (c) and (f). The load voltages were kept stable only when the Q-factors of the receiving coils were greater than 20. When the Q-factor reduced to under 20, the internal resistances of the receiving coils became greater. The condition (3.20) would not be satisfied. As a result, the simulation voltages were far from the estimated values. It was equivalent that the load voltages were not stable against the loads for this region of the receiving coils' Q-factors.

As an example to show that the load voltages kept stable when the approximated output voltages approximated the simulation values, Fig. 3.11 plotted the graph of the load voltages over the variations of the load resistances when the Q-factor of the receiving coils was 50 and the TX_2 lowered down 10mm in the two-receiver system. The load resistances changed from 10Ω to 100Ω but the load voltages were still stabilized. This result could be attributed to the fact that for the Q-factor of 50 the actual load voltages were near to the approximated ones as shown in Fig. 3.10c.

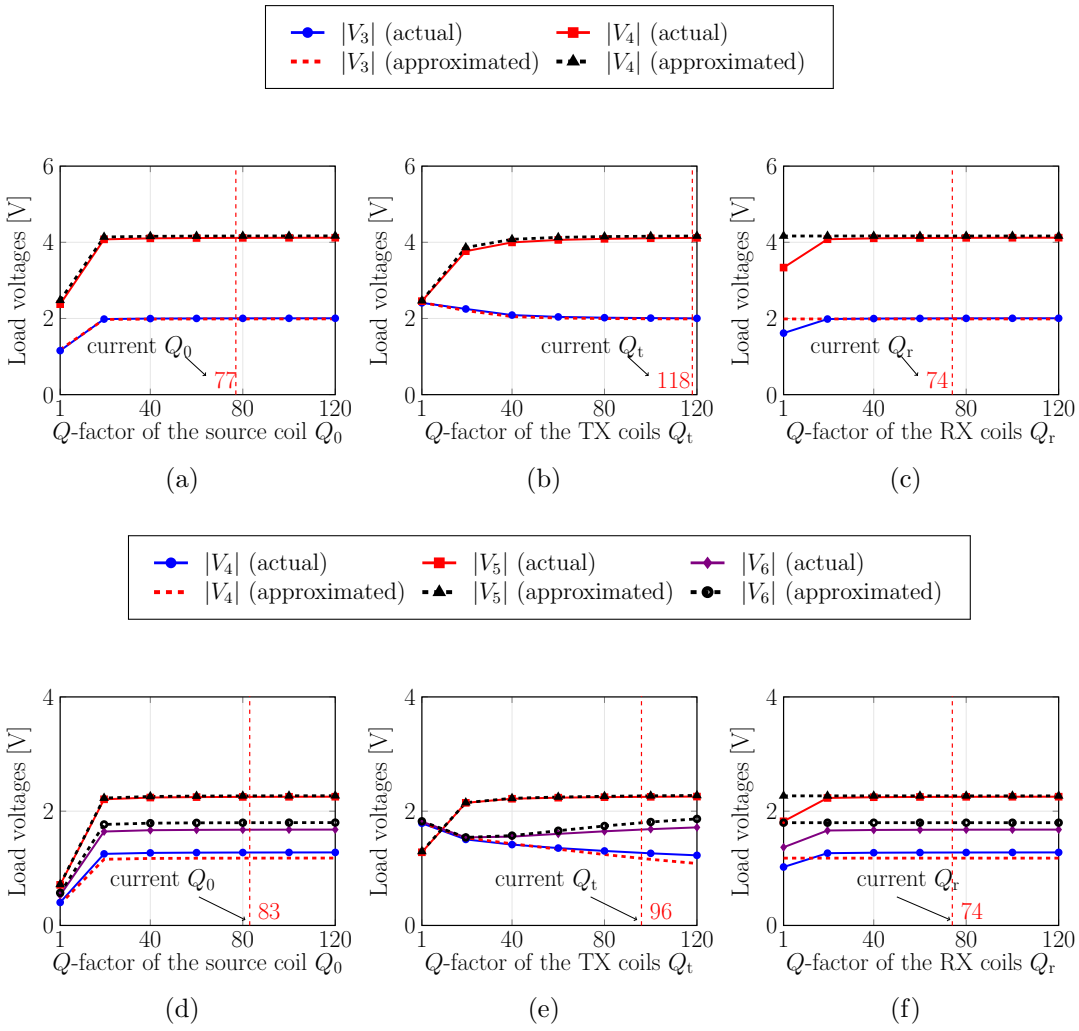

Figure 3.10. The effect of Q-factor of the coils on the load voltages: (a), (b), (c) the system with two receivers and (d), (e), (f) for the system with three receivers.

3.4. Experimental results

In order to confirm the feasibility of the proposed system, a demonstration system was constructed. The coupling network consisting of one source, two transmitting and two receiving resonators was illustrated in Fig. 3.12. The setup of the coupling network was identical to that of the simulation configuration in Fig. 3.2. The coils were made from 1mm-diameter copper wire. The turn number of the source, the transmitting and the receiving coils were 4, 10, and 5 respectively. The

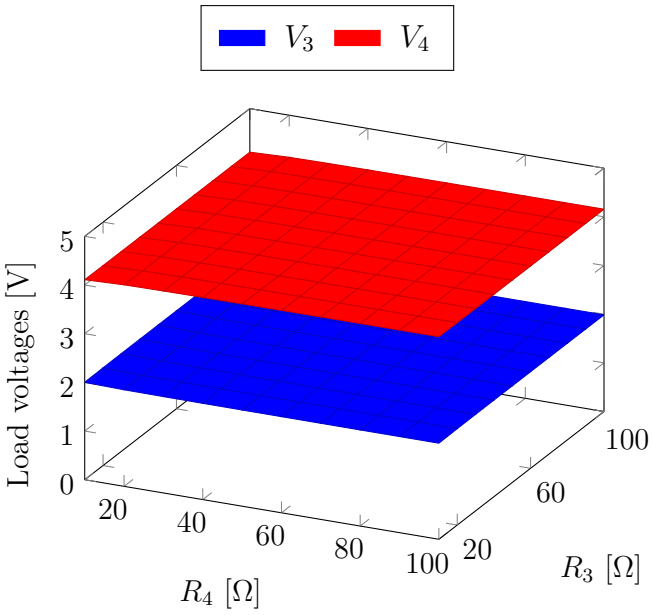

Figure 3.11. Load voltages as function of loads when $Q_r = 50$.

dimensions of the source and the transmitting coils were 100mm × 200mm, while those of the receiving coils were 100mm × 100mm. The self-inductance of each coil was cancelled out by a series resonant capacitor. Each resonant capacitor was implemented by combining several discrete capacitors. The measurements of the impedances of the resonators were taken by Vector Network Analyzer ZNBT 8. The list of the self-inductances of the coils and the corresponding resonant capacitances were showed in Table 4.1. Fig. 3.14 showed the setup of the demonstration system which could control two load voltages independently of the load resistances. A DC power supplied power for the RF inverter PATO23-1 to generate frequent square-wave signal with the frequency $f = 145$kHz. This signal was then used to be the input voltage of the coupling network. The square-wave signal was chosen as input voltage because of two reasons. For high operating frequencies, it was easier to generate square-wave signal than pure-sine-wave one [134]. For IPT systems, square-wave input voltage could give load voltage and current which were insignificantly different from using pure-sine wave [135]. Oscilloscope RTO 1004 was utilized to measure the output voltages as well as to

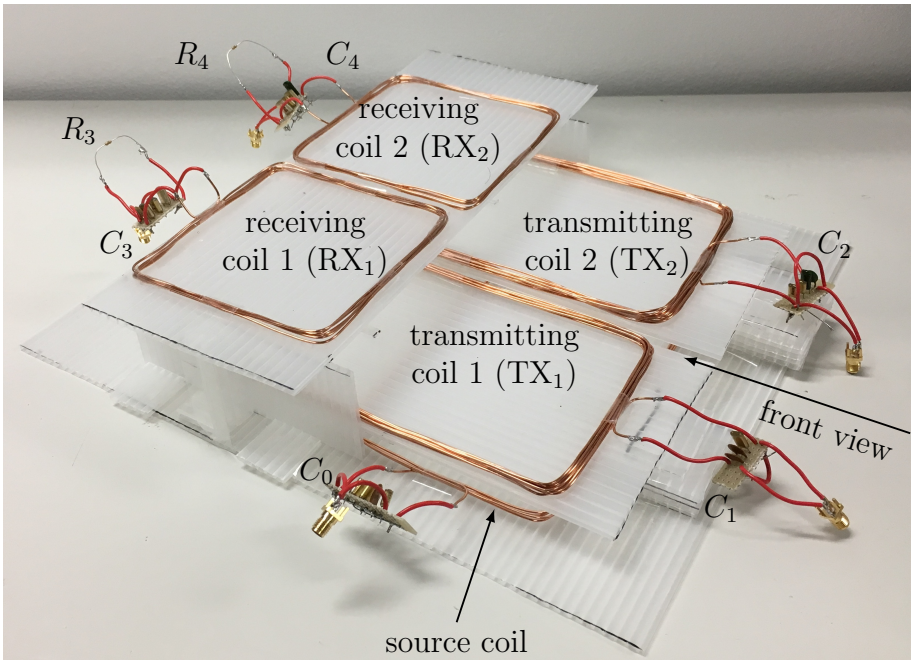

Figure 3.12. The experimental network with one source, two transmitting and two receiving resonators.

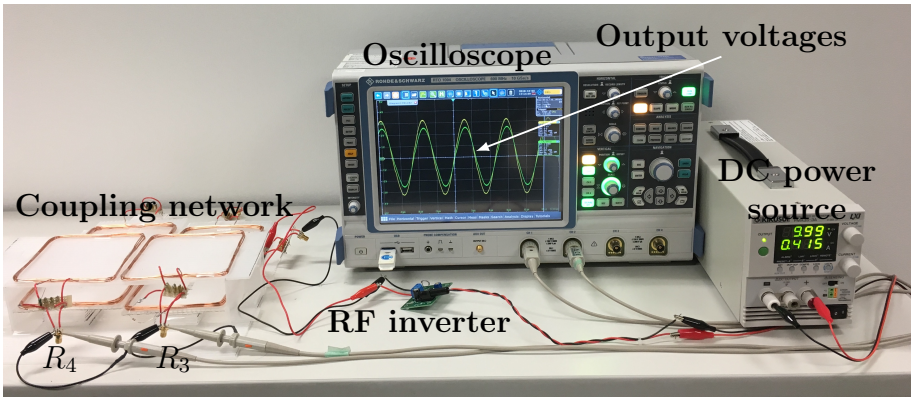

Figure 3.13. The experimental system for verification of controlling two load voltages in two-receiver IPT system.

capture their waveform.

In this work, we just focused on demonstrating the method of controlling

Table 3.3. List of parameter values in the prototype

Symbol	**Parameter**	**Practical value**
L_0	self-inductance of source coil	8.26µH
C_0	resonant capacitor for L_0	144nF
L_1	self-inductance of TX_1	42.92µH
C_1	resonant capacitor for L_1	28.15nF
L_2	self-inductance of TX_2	43.54µH
C_2	resonant capacitor for L_2	27.66nF
L_3	self-inductance of RX_1	7.8µH
C_3	resonant capacitor for L_3	154.7nF
L_4	self-inductance of RX_2	7.76µH
C_4	resonant capacitor for L_4	155nF

the load-independent output voltages, therefore the rectifier and the regulator were not included in the experiment for simplicity. Pure resistors were directly connected to the receivers of the system and considered as the loads. The loads altered among 10Ω, 20Ω, 30Ω, 56Ω, 91Ω to examine two load voltages. Initially, two transmitting resonators was 30mm distant from two receiving resonators and 20mm distant from the source resonator. The measurements were then evaluated by statistical parameters of mean and corrected sample standard deviation [136].

Table 3.4 shows the measures of the load voltages over the variations of the load resistances when two transmitting coils are on the initial arrangement as in Fig. 3.14a. The load voltages were measured in 25 times due to the changes of the load resistances. The results illustrated that the load voltages were kept stable against the variations the load resistances. In these results, the means of the measures of the load voltages V_3 and V_4 were 2.77V and 2.59V. The corrected sample standard deviation for the measures of V_3 was 0.2V, about 7.29% of the mean of V_3, while this number for those of V_4 was 0.14V, nearly 5.35% of the mean of V_4.

In the experimental arrangement as in Fig. 3.14b, the transmitting resonator

Table 3.4. Experimental results: Several measures of the output voltages against the load resistances for the arrangement in Fig. 3.14a

R_3 [Ω]	R_4 [Ω]	$\|V_3\|$ [V]	$\|V_4\|$ [V]
10	10	2.5692	2.332
10	20	2.5692	2.411
20	30	2.8458	2.6877
30	20	2.8854	2.6087
30	56	2.8854	2.6482
91	56	2.8458	2.6877
56	91	2.6877	2.5296

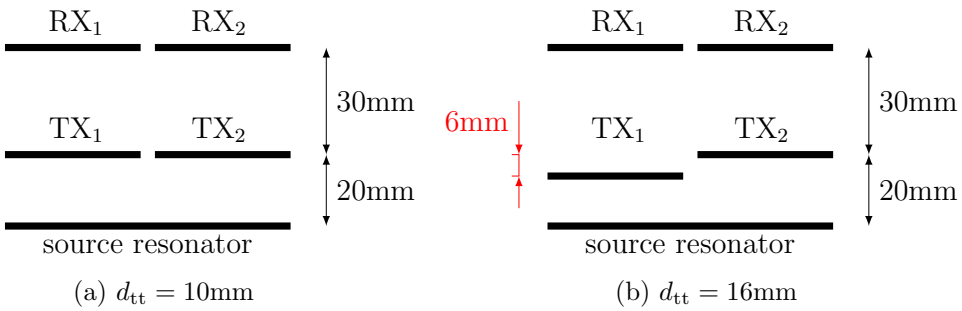

(a) $d_{\mathrm{tt}} = 10\mathrm{mm}$ (b) $d_{\mathrm{tt}} = 16\mathrm{mm}$

Figure 3.14. The load voltages as a function of the load resistances R_3 and R_4, with the vertical distance between two transmitting coils: (a) $d_{\mathrm{tt}} = 0\mathrm{mm}$ and (b) $d_{\mathrm{tt}} = 6\mathrm{mm}$.

1 was 6mm distant beneath the transmitting resonator 2. Fig. 3.15 in the previous page showed a snapshot of the voltage waveforms at the input and the output of the prototype with $R_3 = 56\Omega$ and $R_4 = 91\Omega$. The peak values of the load voltages over the variations of the load resistances were presented in Fig. 3.16. The results indicated that the load voltages were slightly far from the stable values when the load resistances varied in small range of from 10Ω to 30Ω. However, two load voltages kept stable when the load resistances were greater than 30Ω. Statistically, the means of the load voltages V_3 and V_4 were 2.08V and

2.70V respectively. The corresponding corrected sample standard deviations of the measures of the load voltages were 0.08V and 0.08V. The deviations were just equal to about 3.79% and 2.88% of the means of the measures of the two output voltages. In all the experiments, the corrected sample standard deviations of the measures of the load voltages were under 10% of the mean values. It meant that the load voltages were considered as to be stabilized against the load resistances. The results also indicated that lowering down one transmitting resonator could lead to a difference between two load voltages. It verified that the load voltage ratio could possibly be controlled by changing the arrangement of the transmitting resonators.

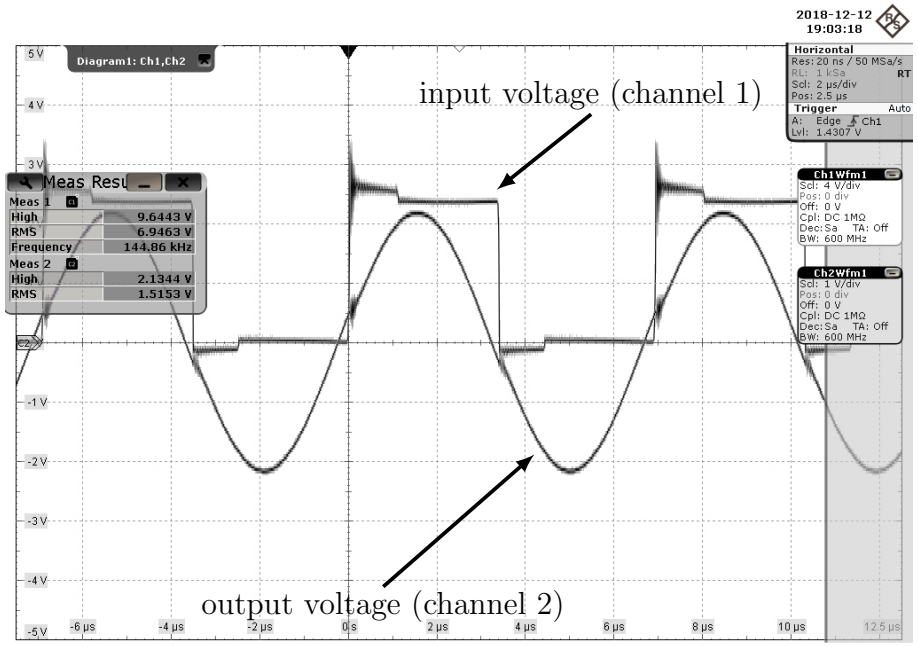

Figure 3.15. Snapshot of input voltage and output voltage in demonstration for $R_3 = 56\Omega$ and $R_4 = 91\Omega$.

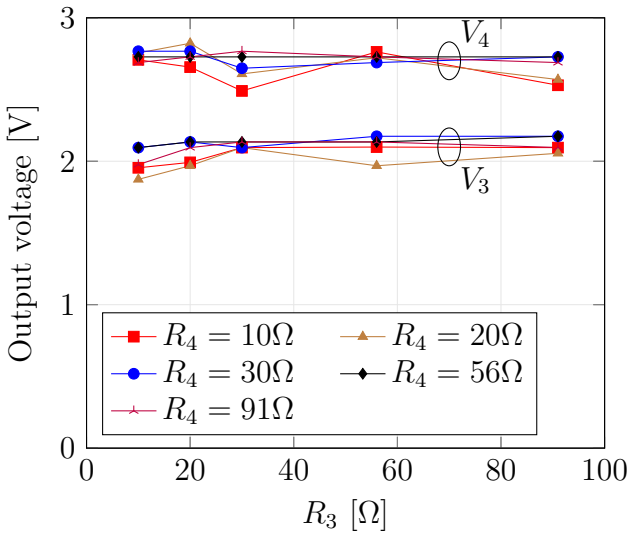

Figure 3.16. Load voltages as a function of the loads with the arrangement of the coil as in Fig. 3.14b.

3.5. Conclusion

This chapter has proposed an IPT platform to address the challenge of charging multiple receivers where each receiver required a rated voltage for its load. The proposed IPT charging platform consisted of one source resonator and multiple transmitting resonators. The theoretical analyses in this chapter indicated that when the load resistances were sufficiently large, the load voltages and their ratio were stable against load variations and depended only on the mutual inductances among the coils. Once the load voltages were stable against the load variations, they could be adjusted to rated voltages by effortlessly changing the relative position of the transmitting coils inside the charging platform. This adjustment could be done by a mechanical part. It was also highlighted that high transmission efficiency could be not achieved in the proposed system when the load voltages were stabilized against the wide range of the load resistances. The effectiveness of the load voltage control method has been confirmed via EM simulations of the two-receiver and the three-receiver IPT systems. For the two-receiver system, the ratio of up to 3.5 could be obtained between the two load voltages. For the three-

receive system, even under the load variations, stable load voltages have been observed at a more balanced ratio of about 1.7:2.1:1.7. The calculation using MATLAB indicated that the load voltages were still stable against the variations of the load resistances even with low Q-factors of the coils in the proposed IPT system. Finally, the feasibility of the proposed system was confirmed by the experiments with a two-receiver prototype. The system operated with a practical square-wave signal. In the experiment, it has been demonstrated that the system also had the ability to transfer stable voltages to the two loads with the deviations of under 7.29%. The effectiveness of the proposed IPT platform was verified by both the simulation results using ideal sinusoidal source and the experimental results using practical square-wave source.

Chapter 4

Load voltage stabilization in cooperative IPT system with K-inverter

4.1. Introduction

Last chapter proposed IPT charging platform to address the challenge that each receiver required a rated voltage for its load. However, in other scenario, there might be some receivers located far from charging platform, leading to the deterioration of the system performance because transmission distance is limited because of the coupling between transmitting coil and receiving coil [100]. In order to recover the performance, resonators were employed to support transmitter [17]. They are also known as relays. Relay has played an important role in IPT systems. Relays could be used for boosting charging voltage [130] or reducing impact of source internal resistance [113]. In another application, relay was designed to switch between constant current mode and constant voltage mode to meet the requirements of battery charging [105]. However, in mentioned systems above, relay coils played one role of supporting transmitter to transmit power to a distant receiver. In this chapter, in order to address the challenge of delivering power to distant receiver, instead of using additional relay, another receiver which could simultaneously help transmitter to transfer power to distant receiver and draw power itself was utilized. This kind of the system can be called cooperative

IPT system. LC tank or K-inverter was added to relay to realize cooperative characteristic while still stabilizing load voltages against load variations [P.C1], [P.C2], [P.C3].

4.2. Cooperative transmission with LC tank

4.2.1 System description

In this section, LC tank was added to relay to realize cooperative characteristic while keeping the load voltages stable against the load variation [P.C1].

Fig. 4.1 illustrated the schematic circuit of the cooperative IPT system using LC tank. A power source was used to drive the primary coil (L_0) to deliver power to the relay coil (L_1). Here, the power that the relay coil received was splitted into two parts. One part of the power was consumed by the load (R_1) which the relay carried. The rest of power was continuously deliver to the secondary coil (L_2) and consumed by the load (R_2) that the secondary coil carried. In this system, the self-inductance of each coil was cancelled out by a series resonant capacitance. Then, an additional LC tank was equipped for the relay to realize the stability of two output voltages against the variations of the load resistances.

In the model, there were several assumptions as follows. The power source had no internal resistance. The coupling between the primary coil and the secondary coil was very weak ($M_{02} = M_{20} \approx 0$). Internal resistances of the coils as well as

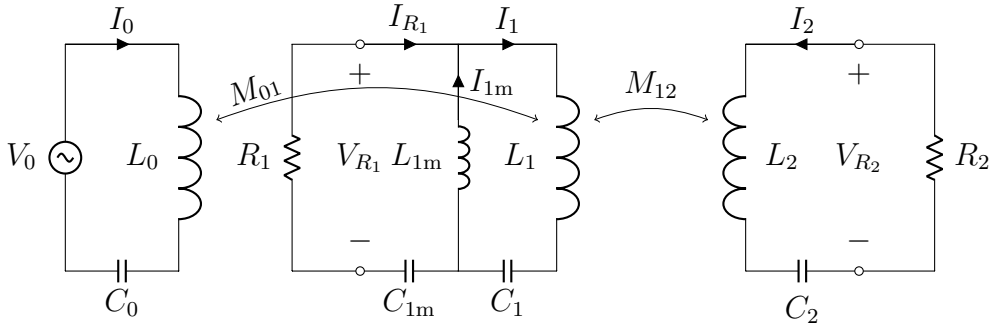

Figure 4.1. System model in cooperative IPT system using LC tank at relay

the compensatory inductors and capacitors were negligibly small. Therefore, we disregarded the internal resistances for simplicity in theoretical analysis.

According to Kirchhoff's laws, relations between voltages and currents were given

$$V_0 = (j\omega L_0 + \frac{1}{j\omega C_0})I_0 + j\omega M_{01} I_1, \tag{4.1}$$

$$V_{R_1} = -j\omega L_{1\mathrm{m}}(I_1 - I_{R_1}) + \frac{1}{j\omega C_{1\mathrm{m}}} I_{R_1}, \tag{4.2}$$

$$V_{R_2} = j\omega M_{21} I_1 + (j\omega L_2 + \frac{1}{j\omega C_2})I_2. \tag{4.3}$$

In above equations, the operating angular frequency of the power source was denoted by ω while $j = \sqrt{-1}$ was the imaginary unit. The mutual inductance between any two coils was M_{mn} where $m, n \in \{0, 1, 2\}$ and $m \neq n$. Because of the reciprocity of the network, we had $M_{mn} = M_{nm}$. V_0 was the complex voltage of the power source. V_{R_1} and V_{R_2} were two complex load voltages at the relay coil and the secondary one. I_0, I_1 and I_2 denoted for the complex currents in the primary, relay and secondary coils while the complex current in the load resistance carried by the relay coil was denoted by I_{R_1}. L_0, L_1 and L_2 were the self-inductances of the primary, relay and secondary coil respectively. R_1 and R_2 were the load resistances carried by the relay and secondary coils. C_0 and C_2 were the compensatory capacitances for the primary and the secondary coils while the combination of C_{1m}, L_{1m} and C_1 formed the compensation network between the relay coil L_1 and its load resistance R_1. The independence of two output voltages against the variations of the load resistances would be illustrated in the next section.

4.2.2 Load-independent output voltages

The compensatory components in compensation networks were designed to satisfy resonant relationship

$$\omega = \frac{1}{\sqrt{L_0 C_0}} = \frac{1}{\sqrt{L_1 C_1}} = \frac{1}{\sqrt{L_2 C_2}} = \frac{1}{\sqrt{L_{1\mathrm{m}} C_{1\mathrm{m}}}} \tag{4.4}$$

Combining (4.1), (4.2), (4.3) and (4.4), we obtained

$$V_0 = j\omega M_{01} I_1, \tag{4.5}$$

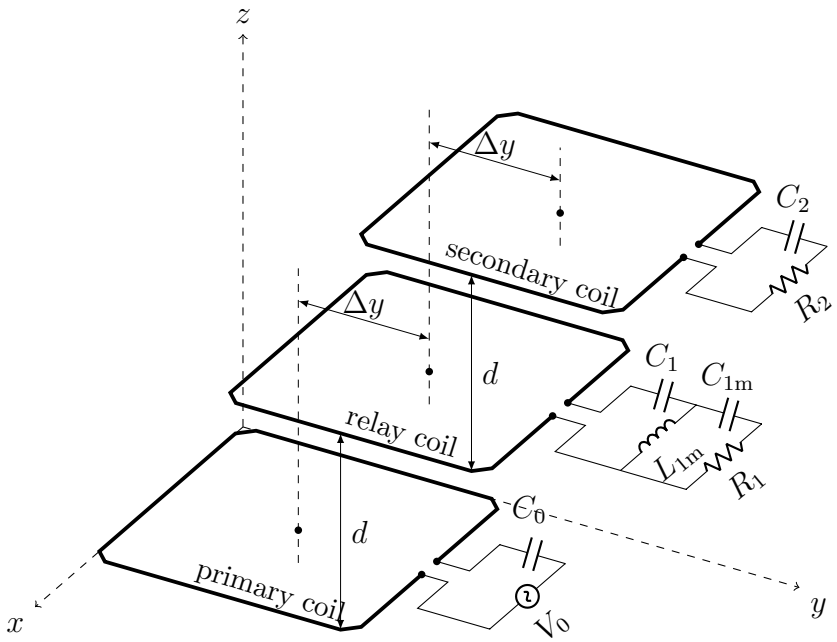

Figure 4.2. Simulation arrangement

$$V_{R_1} = -j\omega L_{1\mathrm{m}} I_1, \tag{4.6}$$

$$V_{R_2} = j\omega M_{21} I_1. \tag{4.7}$$

Therefore, the output voltages V_{R_1} and V_{R_2} could be expressed as

$$V_{R_1} = -\frac{L_{1\mathrm{m}}}{M_{01}} V_0, \tag{4.8}$$

$$V_{R_2} = \frac{M_{21}}{M_{01}} V_0. \tag{4.9}$$

Equations (4.8) and (4.9) highlighted that the output voltages were stable against the variations of the load resistances. It was clear that the output voltages were only decided by the source voltage, the compensatory inductor and the mutual inductance among the coils.

4.2.3 Simulation results

To verify the theoretical analysis in Section 4.2.2, WIPL software based simulations were carried out. Fig. 4.2 showed the simulation configuration. In the

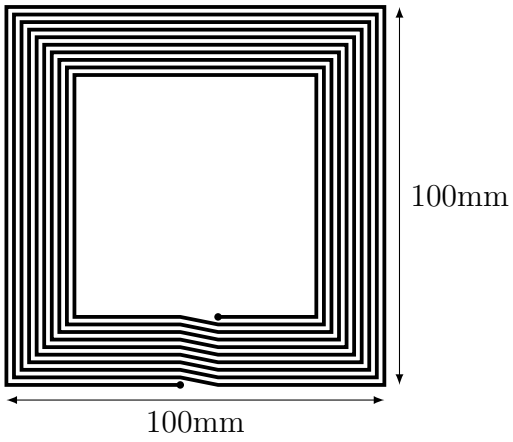

Figure 4.3. Coi layout used in the simulations.

simulations, the system included the primary, the relay and the secondary coils. The coils had an identical size of 100mm-by-100mm. Each coil was spiral coil with 10 turns as described in Fig. 4.3.

The material utilized to simulate the coils was 1mm-diameter copper wire with the conductivity of $58\mathrm{MS\,m^{-1}}$. The horizontal distance between two perpendicular axes of two adjacent coils was denoted by Δy. The power source used in the simulations was 5V sine-wave voltage and supposed to had no internal resistance. The operating frequency of the power source was set to be 200kHz. The loads varied from 10Ω to 100Ω to investigate the voltages of two loads carried by the relay and the secondary coils. In order to simulate the negligibly weak coupling between the primary coil and the secondary one, Δy was adjusted to be 55mm as illustrated in Fig. 4.4.

In the simulations, the compensatory components were set to make the output voltages V_{R_1} and V_{R_2} provided by the relay coil and the secondary coil to be equal to the source voltage. More specifically, for the output voltage V_{R_1}, the impedance of the compensatory inductor $L_{1\mathrm{m}}$ was set to equal to the mutual coupling between the primary coil and the relay one according to (4.8). For the output voltage V_{R_2}, the relay was distant from the primary and the secondary coil with the same distance d of 30mm. This would ensure M_{01} equals to M_{12} according to (4.9).

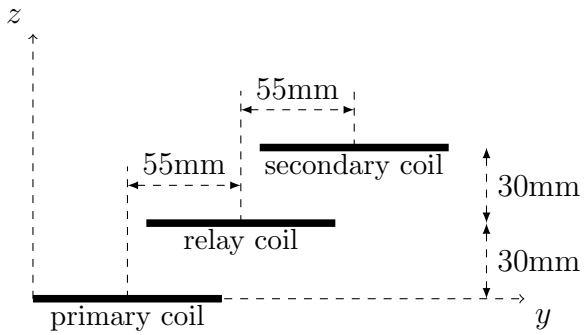

Figure 4.4. Side projection of the coils in the simulation.

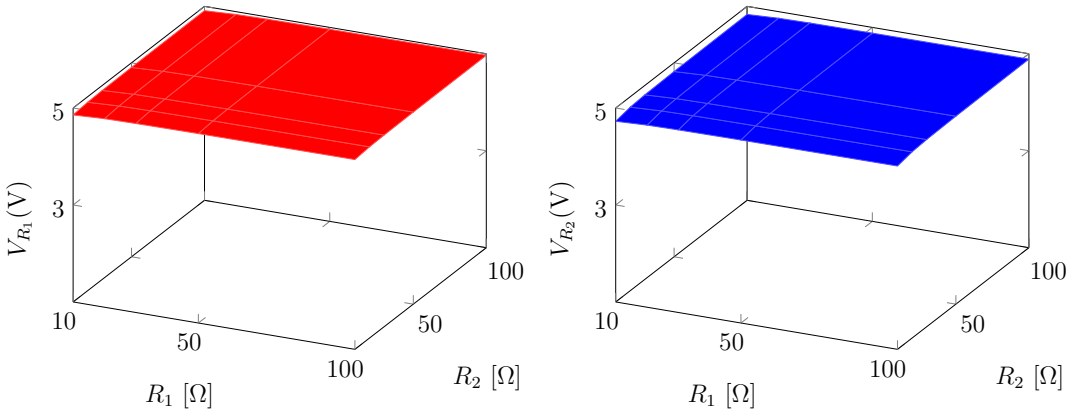

(a) V_{R_1} (b) V_{R_2}

Figure 4.5. Load voltages as a function of the loads with the configuration in Fig. 4.4.

Fig. 4.5 plotted the graph of the output voltages over the variations of the load resistances. The results highlighted that the output voltages were stabilized against the variations of two load resistances. Two output voltages V_1 and V_2 were kept constant at 4.9V and 4.8V. The output voltages were slightly different from the source voltage. This could be caused by the internal resistances of the coils and the mutual coupling between the primary coil and the secondary one. Although internal resistances and the mutual coupling were small but they still had impact on the stability of two output voltages.

The simulation results confirmed that by using LC tank the relay could si-

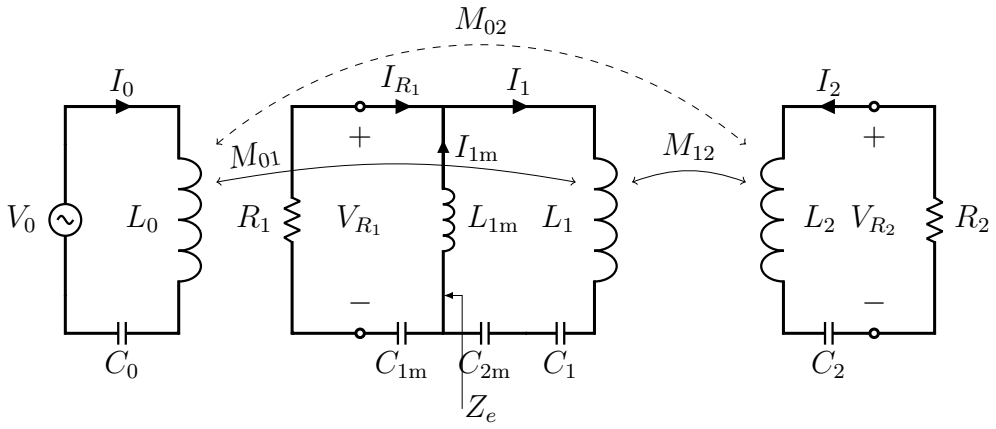

Figure 4.6. System model for cooperative IPT system using K-inverter at the relay.

multaneously draw power itself and support transmitter to deliver power to a distant receiver. Furthermore, LC tank structure also helped not only to deliver a constant voltage to the distant receiver but also to stabilize its load voltage against the load variations. However, this structure suffered the deterioration of transmission efficiency because the imaginary part of the relay circuit was not eliminated completely. An improvement by using K-inverter will be explained in next section.

4.3. Cooperative transmission with K-inverter

In the cooperative IPT system using LC tank, even though the load voltages were stable against the load variations, the cooperative IPT system could not achieve high transmission efficiency because the imaginary part of the total impedance of the relay circuit was not completely eliminated. In order to improve the efficiency, a K-inverter was used instead of LC tank to realize the cooperative characteristic of the relay as well as stabilize load voltages against load variations.

4.3.1 System description

Similar to the cooperative IPT system using LC tank, the cooperative IPT system using K-inverter also included the transmitter, the relay and the distant receiver as described in Fig. 4.6. In this model, the constant voltage source V_0 operating at frequency f (angular frequency $\omega = 2\pi f$) drove the transmitter with primary coil L_0. The relay coil L_1 would receive power transmitted from the primary coil through the mutual inductance M_{01} between them. One part of the power that the relay received was consumed by its load R_1. Another part of the received power was transmitted to the secondary coil L_2 through the mutual inductance M_{12} between the relay coil and the secondary coil. Then, this amount of the power was consumed by the load R_2 carried by the secondary coil.

As analogous to the cooperative IPT system in [P.C1], the self-inductance of each was compensated by a series resonant capacitor first. Then a K-inverter, under the form of CLC topology ($C_{1\mathrm{m}}$−$L_{1\mathrm{m}}$-$C_{2\mathrm{m}}$) in this case, was added to the relay to realize the characteristics of cooperative transmission and load voltage stability. The power source was assumed to have no internal resistances. The internal resistances of the coils were ignored in theoretical analysis for simplicity because they were negligibly small in comparison to the mutual couplings and the load resistances.

According to Kirchhoff's laws, relations between voltages and currents are given

$$V_0 = (j\omega L_0 + \frac{1}{j\omega C_0})I_0 + j\omega M_{01}I_1 + j\omega M_{02}I_2, \tag{4.10}$$

$$\begin{aligned} -j\omega L_{1\mathrm{m}}(I_1 - I_{R_1}) &= j\omega M_{10}I_0 \\ &+ (j\omega L_1 + \frac{1}{j\omega C_1} + \frac{1}{j\omega C_{1\mathrm{m}}})I_1 + j\omega M_{12}I_2, \end{aligned} \tag{4.11}$$

$$0 = -j\omega L_{1\mathrm{m}}(I_1 - I_{R_1}) + (R_1 + \frac{1}{j\omega C_{1\mathrm{m}}})I_{R_1}, \tag{4.12}$$

$$0 = j\omega M_{20}I_0 + j\omega M_{21}I_1 + (R_2 + j\omega L_2 + \frac{1}{j\omega C_2})I_2. \tag{4.13}$$

In the equations above, M_{kl} is the mutual inductance between any two coil where $k, l \in \{0, 1, 2\}$ and $k \neq l$. I_0, I_1 and I_2 were the complex currents in the corresponding coils. I_{R_1} and $I_{1\mathrm{m}}$ were the complex currents flowing in the load resistance R_1 and in compensatory inductor $L_{1\mathrm{m}}$. C_0, C_1 and C_2 were the series

compensatory capacitors used to cancel out the self-inductances of the primary, the relay and the secondary coils. C_1 and CLC topology formed by $C_{1\mathrm{m}}, L_{1\mathrm{m}}$ and $C_{2\mathrm{m}}$ were combined to form the compensation network between load resistance R_1 and relay coil.

The input power was

$$P_{\mathrm{in}} = \frac{1}{2}\mathrm{Re}\{V_0^* I_0\} \tag{4.14}$$

where x^* denoted for the conjugate of the complex number x.

The out power consumed by the loads was

$$P_{\mathrm{out}} = \frac{1}{2}\left(\frac{|V_{R_1}|^2}{R_1} + \frac{|V_{R_2}|^2}{R_2}\right) \tag{4.15}$$

where $|x|$ was the amplitude of the complex number x; V_{R_1} and V_{R_2} were respectively complex voltages of the loads R_1 and R_2. The load voltages were expressed in (4.24) and (4.25) of the next page.

The RF-RF efficiency was derived

$$\eta = \frac{P_{\mathrm{out}}}{P_{\mathrm{in}}} \tag{4.16}$$

4.3.2 Efficiency improvement

The compensatory components were designed to satisfy resonant relationship:

$$\begin{aligned}\omega &= \frac{1}{\sqrt{L_0 C_0}} = \frac{1}{\sqrt{L_1 C_1}} = \frac{1}{\sqrt{L_2 C_2}} \\ &= \frac{1}{\sqrt{L_{1\mathrm{m}} C_{1\mathrm{m}}}} = \frac{1}{\sqrt{L_{1\mathrm{m}} C_{2\mathrm{m}}}}\end{aligned} \tag{4.17}$$

In Fig. 4.6, the equivalent impedance Z_e when looking from the relay coil L_1 to the load resistance R_1 was

$$Z_e = \frac{\omega^2 L_{1\mathrm{m}}^2}{R_1} + j\omega L_{1\mathrm{m}} \tag{4.18}$$

For the compensation scheme of C_1-$L_{1\mathrm{m}}$-$C_{1\mathrm{m}}$ introduced in [P.C1], the relay circuit could not achieve resonance because the imaginary part of the equivalent impedance Z_e was not eliminated completely. Therefore, the efficiency was deteriorated. When using K-inverter instead of LC tanke, the total impedance

corresponding to the current I_1 in the relay coil was

$$Z_{\text{total}} = Z_e + \frac{1}{j\omega C_{2\text{m}}} + j\omega L_1 + \frac{1}{j\omega C_1} = \frac{\omega^2 L_{1\text{m}}^2}{R_1} \tag{4.19}$$

Equation (4.19) shows that when using K-inverter instead of LC tank, not only the load resistance R_1 was transformed but also the imaginary part of the total impedance was completely removed. It meant that the relay circuit was considered as a resonator with small internal resistance. Consequently, the power could be relayed to the secondary coil with higher efficiency than the system introduced in [P.C1].

4.3.3 Output voltage stability against load variations

According to Kirchhoff's law, the relations between voltages and currents were expressed as follows:

$$V_0 = j\omega M_{01} I_1 + j\omega M_{02} I_2, \tag{4.20}$$

$$j\omega L_{1\text{m}} I_{R_1} = j\omega M_{10} I_0 + j\omega M_{12} I_2, \tag{4.21}$$

$$0 = -j\omega L_{1\text{m}} I_1 + R_1 I_{R_1}, \tag{4.22}$$

$$0 = j\omega M_{20} I_0 + j\omega M_{21} I_1 + R_2 I_2. \tag{4.23}$$

Combining (4.20)-(4.23), the output voltages could be derived as in (4.24) and (4.25).

$$V_{R_1} = \frac{-j\omega L_{1\text{m}}}{j\omega M_{01} + \dfrac{\omega^2 M_{02} M_{21}}{R_2} + \dfrac{\omega^2 M_{02} M_{20}}{R_2} \dfrac{-\dfrac{\omega^2 L_{1\text{m}}^2}{R_1} - \dfrac{\omega^2 M_{12} M_{21}}{R_2}}{j\omega M_{10} - \dfrac{\omega^2 M_{12} M_{20}}{R_2}}} V_0, \tag{4.24}$$

$$V_{R_2} = \frac{j\omega M_{20} \dfrac{-\dfrac{\omega^2 L_{1\text{m}}^2}{R_1} - \dfrac{\omega^2 M_{12} M_{21}}{R_2}}{j\omega M_{10} - \dfrac{\omega^2 M_{12} M_{20}}{R_2}} + j\omega M_{21}}{j\omega M_{01} + \dfrac{\omega^2 M_{02} M_{21}}{R_2} + \dfrac{\omega^2 M_{02} M_{20}}{R_2} \dfrac{-\dfrac{\omega^2 L_{1\text{m}}^2}{R_1} - \dfrac{\omega^2 M_{12} M_{21}}{R_2}}{j\omega M_{10} - \dfrac{\omega^2 M_{12} M_{20}}{R_2}}} V_0. \tag{4.25}$$

When the load resistances R_1 and R_2 were sufficiently large, the output voltages V_{R_1} and V_{R_2} were approximated:

$$V_{R_1} \approx -\frac{L_{1\mathrm{m}}}{M_{01}} V_0, \tag{4.26}$$

$$V_{R_2} \approx \frac{M_{21}}{M_{01}} V_0. \tag{4.27}$$

Equations (4.26) and (4.27) indicated that when the load resistances were sufficiently large, two output voltages were stabilized against the variations of the load resistances. They only depended on source voltage, compensatory inductor and the mutual inductances between two adjacent coils. Therefore, adding K-inverter to the relay, we could realize the cooperative characteristic while still stabilizing the load voltages against the load variations.

4.3.4 Simulation results

In order to confirm the effectiveness of the proposed system, some simulations using WIPL-D were carried out. Fig. 4.7 described the simulation arrangement. In these simulations, the size of all the coils is 10cm-by-10cm. Copper wire with the conductivity of $58\mathrm{MS\,m^{-1}}$ was used to construct the coils. The constant voltage source of 5V was utilized to supply power for the primary coil. Two load resistances R_1 and R_2 changed from 10Ω to 100Ω to examine two output voltages and the efficiency. For simplicity, the compensatory inductor $L_{1\mathrm{m}}$ is selected to be equal to the mutual inductance between the primary coil and the secondary coil. The relay coil was placed to be equidistant between the primary coil and the secondary coil with distance d. In the simulations, d was equal to 60mm. Therefore, for the simulation setting, two output voltages would be equal to the source voltage according to (4.26) and (4.27). The transmission efficiency of the proposed system analyzed in Section 4.3.1 would be compared with those of the system in [P.C1] and the system using resonators.

For the simulations of the system using resonators and the system in [P.C1], the arrangement and all parameters are the same as those of the system described above, except for compensation networks which were designed as in [P.C1]. In systems using resonators, the compensation scheme of series, series and series

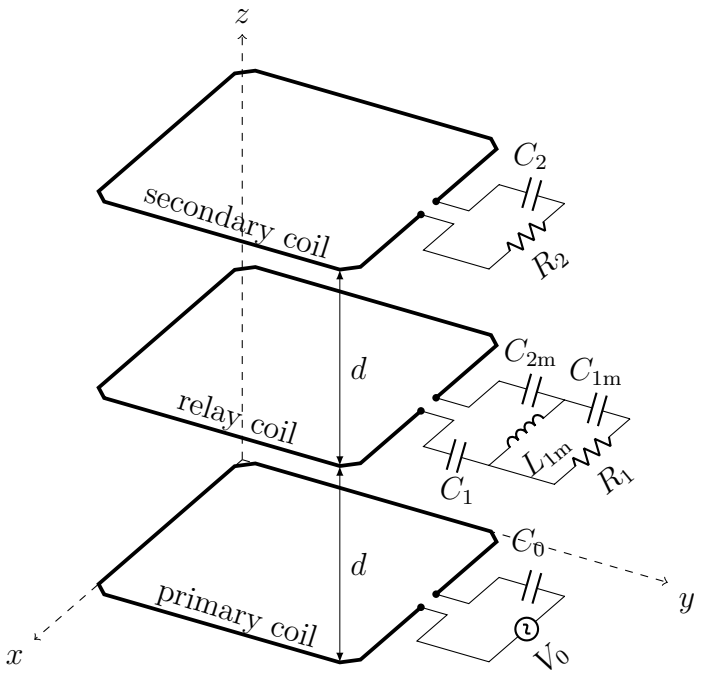

Figure 4.7. Simulation arrangement for cooperative IPT system using K-inverter.

(S-S-S) was applied where the capacitance of each compensatory capacitor would cancel out the self-inductance of the corresponding coil. There was only one load carried by the secondary coil.

Fig. 4.8 plotted the graph of the output voltages over the variations of the load resistances. It was clear that two output voltages were stabilized at 5V regardless of the variations of the load resistances. The simulation results were consistent with those estimated in (4.26) and (4.27). When the load resistances varied in small range, two output voltages were slightly different from the estimated values. This was caused by the impact of the internal resistances and the coupling among the coils.

The simulation results indicated that the proposed system could achieve higher transmission efficiency than the system in [P.C1] and the conventional one did. When the load resistance R_1 was equal to 10Ω, the transmission efficiency of the proposed system was 15% greater than that of the cooperative system in [P.C1]. This gap of transmission efficiency increased to about 20% when the load

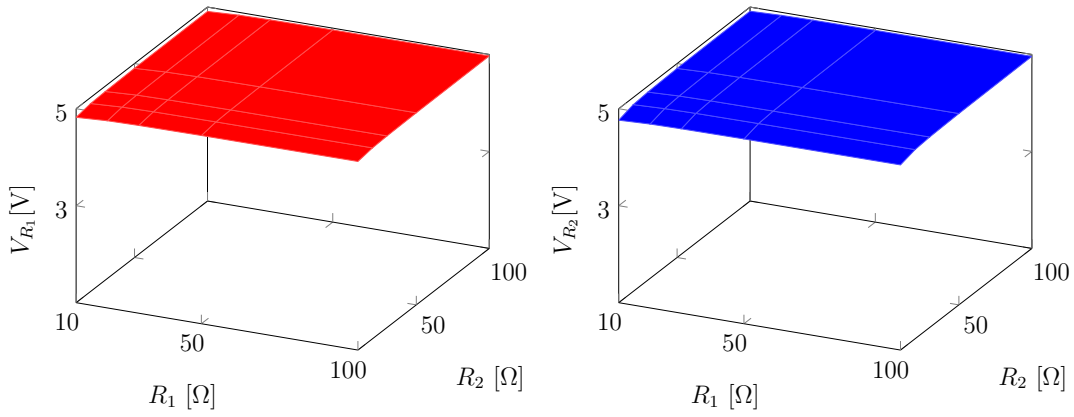

(a) V_{R_1} (b) V_{R_2}

Figure 4.8. Load voltages as a function of the loads.

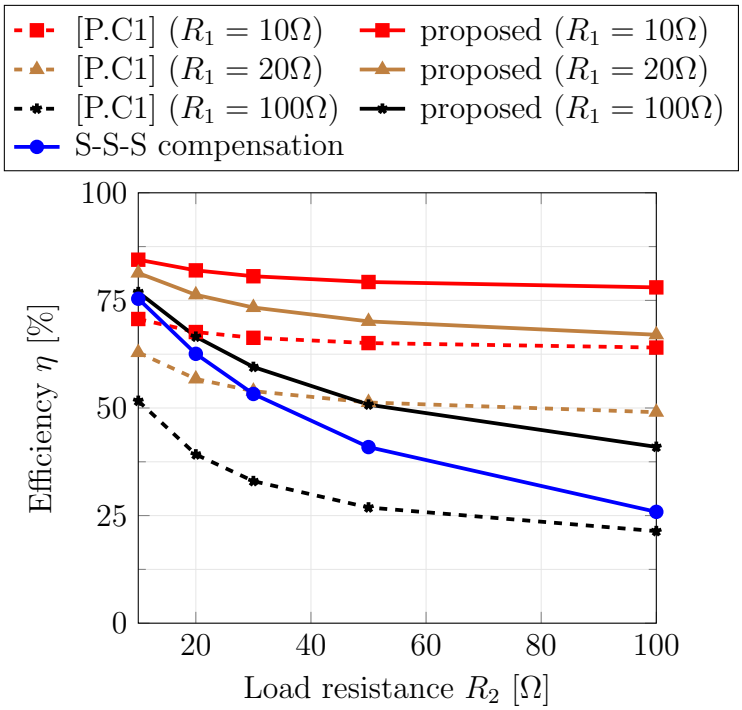

Figure 4.9. Efficiency over the loads.

resistance R_1 was 100Ω. The efficiency in [P.C1] did not always outperform the conventional one. However, for the proposed system, the transmission efficiency

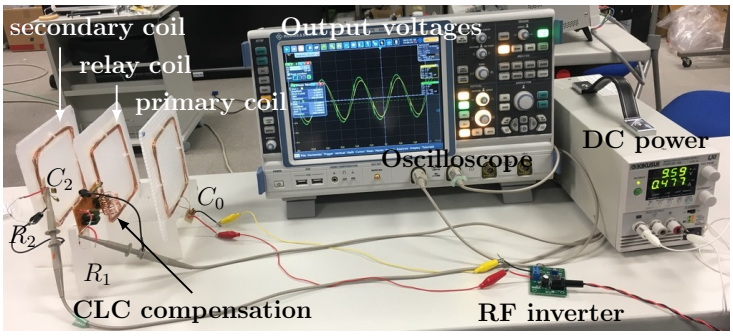

Figure 4.10. Experimental system to demonstrate cooperative IPT system using K-inverter.

was completely improved with the wide range of the load resistances. For the same load resistance R_2, the transmission efficiency increased when the load resistance R_1 decreased. When R_1 was very large, the performance of the proposed system approached that of the system using resonators.

4.3.5 Experimental results

The feasibility of the cooperative ITP system using K-inverter was verified by a demonstration system as shown in Fig. 4.10. In the experiments, the primary coil had 5 turns while the relay and the secondary coils had 10 turns. The size of all the coils was 10cm-by-10cm. The distance between any two adjacent coils was 75mm. The list of the components used the demonstration system were illustrated in Table 4.1. The RF inverter generated square-wave voltage with operation frequency of 200kHz. This signal was considered as the input voltage of the system. Each load resistance changed among 10Ω, 20Ω, 56Ω and 91Ω to examine the output voltages.

Fig. 4.11 illustrated the output voltages over the variations of the load resistances. The experimental results indicated that the output voltage V_{R_1} was stabilized at 1.6V while the output voltage V_{R_2} was stable around 1.3V. Even though there are the variations of two load resistances, two output voltages keep stable. Similar to the simulation results, the output voltages were slightly different from the stable values as the load resistances were in small range. This

Table 4.1. List of parameter values in the demonstration

Symbol	Parameter	Practical value
L_0	self-inductance of primary coil	7.75µH
C_0	resonant capacitor of L_0	81.79nF
L_1	self-inductance of relay coil	27.17µH
C_1	resonant capacitor of L_1	23.5nF
$C_{1\mathrm{m}}, C_{2\mathrm{m}}$	compensatory capacitors	467.3nF
$L_{1\mathrm{m}}$	compensatory inductor	0.22µH
L_2	self-inductance of secondary coil	26.94µH
C_2	resonant capacitor of L_2	23.5nF

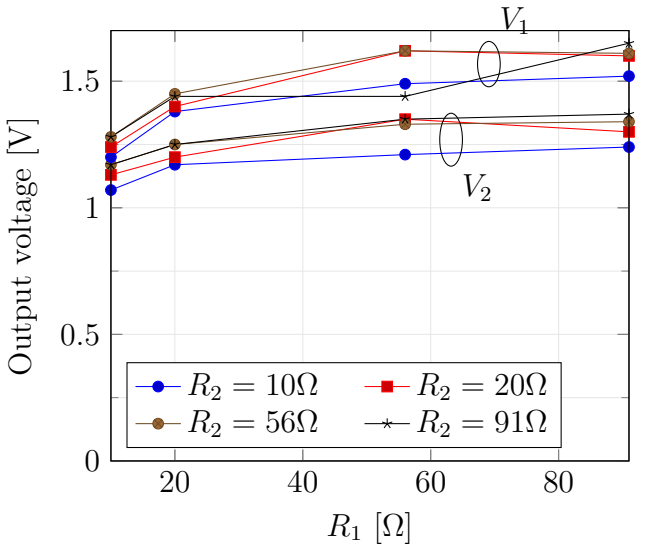

Figure 4.11. Load voltages as a function of the loads in demonstration system.

was because of the impact of the internal resistances of the coils. Another reason was the real components of the compensation networks could not obtain perfect resonant relationship.

The theoretical analysis and numerical results confirmed cooperative IPT system using K-inverter at relay could help to improve efficiency in comparison with the one using LC tank at relay while still stabilizing two load voltages against

the variations of the load resistances. Recently, cooperative transmission could be done by using two-coil repeater in IPT systems [111, 137, 138]. However, two-coil repeater structure could suffer the deterioration of transmission efficiency in comparison with the cooperative IPT system using K-inverter for voltage-gain-free design. The comparison between will be illustrated in next section.

4.4. Efficiency comparison of cooperative IPT systems

Two cooperative three-terminal inductive power transfer systems were considered. Each system included a transmitter (TX), a relay (RX_1) and a distant receiver (RX_2). In both systems, the relay terminal could simultaneously support transmitter to transfer a part of power to the distant receiver and draw power itself and. The power sources in both systems were assumed to be identical with constant voltage V_s and operating frequency f (angular frequency $\omega = 2\pi f$). To easily distinguish two systems, the system using K-inverter [P.C2] was named the cooperative IPT system using common-coil relay or common-coil cooperative IPT system. Meanwhile, the system utilizing two-coil relay in [111, 137, 138] was named the cooperative IPT system using separated-coil relay or separated-coil cooperative IPT system.

4.4.1 System description

More specifically, the schematic circuit of the cooperative IPT system using common-coil relay was illustrated in Fig. 4.12a. the transmitting coil L_0 would deliver power to the relay L_1 via the mutual inductance M_{01} between the transmitting coil and the relay coil. The relay would draw a part of power and transmit the rest of power to the distant receiving coil L_2 via the mutual inductance M_{12} between it and the distant receiving coil. The compensation networks in this system was totally similar to those in [P.C2]. Specifically, the compensatory components were designed

$$\omega = \frac{1}{\sqrt{L_0 C_0}} = \frac{1}{\sqrt{L_2 C_2}} = \frac{1}{\sqrt{LC}} = \frac{1}{\sqrt{(L_1 + L)C_1}}. \tag{4.28}$$

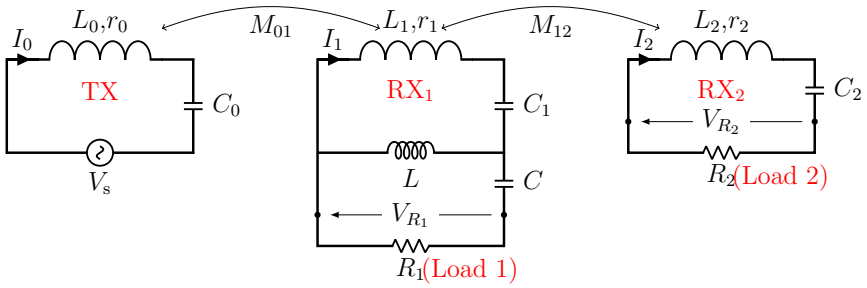

(a) Using common-coil relay

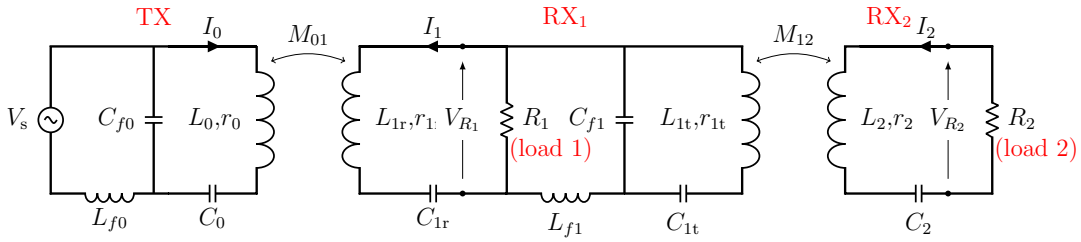

(b) Using separated-coil relay

Figure 4.12. Cooperative IPT systems.

The two load voltages are given by [P.C2]

$$|V_{R_1}| \approx \frac{L}{M_{01}}|V_s|, \tag{4.29}$$

$$|V_{R_2}| \approx \frac{M_{21}}{M_{01}}|V_s|, \tag{4.30}$$

where $|x|$ was denoted for the amplitude of the complex number x.

Meanwhile, the IPT system using separated-coil relay in [137] was described as in Fig. 4.12b. Different from the system using common-coil relay, the relay of this system included two coils L_{1r} and L_{1t}. It was assumed that the mutual inductance between these two coils of the relay was completely eliminated. The coil L_{1r} of the relay would take charge of receive power from the transmitting coil via the mutual M_{01}. Here, a part of of the power was consumed by the load R_1. Then, the rest of the power would transfer to the coil L_{1t} and reach to the distant receiving coil L_2 via the mutual inductance M_{12} between the them. The power that the distant receiver received was consumed by the load R_2. In the cooperative IPT system using separated-coil relay, CLC topology was employed

for the coils L_0 and $L_{1\mathrm{t}}$ while series compensatory capacitor was utilized for the coils. $L_{1\mathrm{r}}$ and L_2. The compensatory components were given by the resonant relationship as follows

$$\begin{aligned}\omega &= \frac{1}{\sqrt{L_0 C_0}} = \frac{1}{\sqrt{L_2 C_2}} = \frac{1}{\sqrt{L_{1\mathrm{r}} C_{1\mathrm{r}}}} \\ &= \frac{1}{\sqrt{L_{f0} C_{f0}}} = \frac{1}{\sqrt{L_{f1} C_{f1}}} = \frac{1}{\sqrt{(L_{1\mathrm{t}} + L_{f1}) C_{1\mathrm{t}}}}\end{aligned} \tag{4.31}$$

The two load voltages in this system are given by [137]

$$|V_{R_1}| \approx \frac{M_{01}}{L_{f0}} |V_{\mathrm{s}}|, \tag{4.32}$$

$$|V_{R_2}| \approx \frac{M_{21}}{L_{f1}} \frac{M_{01}}{L_{f0}} |V_{\mathrm{s}}| \tag{4.33}$$

In both systems, the internal resistance of the coil $\#i$ was denoted by r_i where $i \in \{0, 1, 2, 1\mathrm{r}, 1\mathrm{t}\}$.

The input power in both systems was given

$$P_{\mathrm{in}} = \frac{1}{2} \mathrm{Re}\{V_{\mathrm{s}}^* I_{\mathrm{s}}\} \tag{4.34}$$

where x^* denotes for the conjugate of the complex number x, I_{s} is the source current.

The power consumed by the loads in both systems was expressed

$$P_{\mathrm{out}} = \frac{1}{2} \left(\frac{|V_{R_1}|^2}{R_1} + \frac{|V_{R_2}|^2}{R_2} \right) \tag{4.35}$$

The RF-RF efficiency in both systems was

$$\eta = \frac{P_{\mathrm{out}}}{P_{\mathrm{in}}} \tag{4.36}$$

4.4.2 RF-RF efficiency comparison

This this investigation, equivalent circuit technique has been used to derive the load voltage stability and to analyze the RF-RF efficiency. The equivalent circuits of the two systems were described as in Fig. 4.13.

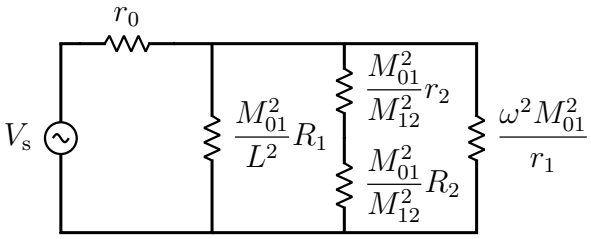

(a) For the system in Fig. 4.12a

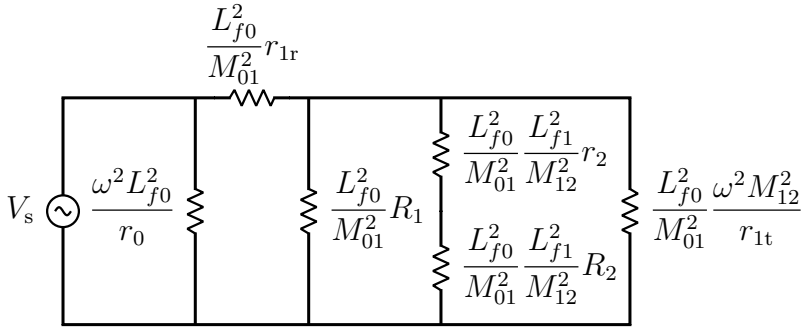

(b) For the system in Fig. 4.12b

Figure 4.13. Equivalent circuits.

According to the equivalent circuits, if the internal resistances of the coils were negligibly small to the loads, the equivalent loads in the both systems were considered to connect in parallel to the source. Consequently, the load voltages only depended on the mutual inductances, the compensatory inductors and the source voltage. It matched the theoretical analysis in (4.29), (4.30), (4.32) and (4.33).

To fairly compare RF-RF efficiency between two systems, the parameters of the two systems would be identical. Specifically, all coils in two systems were identical in terms of self-inductance and internal resistance $L_1 = L_{1r} = L_{1t}$, $r_1 = r_{1r} = r_{1t}$. The compensatory components in the compensation networks had no internal resistance and identical $L = L_{f0} = L_{f1}, C = C_{f0} = C_{f1}, C_1 = C_{1t}$. The mutual inductances through which the power was transferred were similar in both systems.

In this investigation, both systems were designed so that the source voltage was delivered to load voltages without gain. Therefore, for the system in Fig.

4.12a, the mutual inductances and the compensatory inductor were set as follows

$$M_{01} = M_{12} = L. \tag{4.37}$$

Similarly, for the system in Fig. 4.12b, the mutual inductances and the compensatory inductors were set as follows

$$M_{01} = L_{f0}; M_{12} = L_{f1}. \tag{4.38}$$

As a result, the equivalent circuits of two systems were nearly similar, except that the system in Fig. 4.12b had an additional term of $\omega^2 L_{f0}^2/r_0$ in comparison with the system in Fig. 4.12a. This term would be the cause of energy loss in the system in Fig. 4.12b. However, this loss did not happen in the system in Fig. 4.12a according to Fig. 4.13a. It meant that energy loss could be reduced in the cooperative IPT system using common-coil relay in compared with the cooperative IPT system using separated-coil relay.

4.4.3 Simulation results

WIPL-D-based simulations were used to verify the theoretical analysis. In both systems, all coils had an identical size of 10cm-by-10cm. Wire whose conductivity was $58\mathrm{MS\,m^{-1}}$ was used to make the coils. The power source of 5V was used to drive the transmitting coil. The power source had no internal resistance and operated at the frequency of 200kHz. Two loads R_1 and R_2 changed from 5Ω to 100Ω to evaluate two output voltages and the RF-RF efficiency.

For the simulations of the cooperative IPT system using common-coil relay, the transmitter (TX), the relay ($\mathrm{RX_1}$) and the distant receiver ($\mathrm{RX_2}$) were arranged coaxially as shown in Fig. 4.14a. The compensatory inductor was set as in (4.37). The relay $\mathrm{RX_1}$ was distant d_1 from the transmitter TX and d_2 from the distant receiver $\mathrm{RX_2}$.

For the simulations of the cooperative IPT system using separated-coil relay, the system was arranged as in Fig. 4.14b. Here, two coils of the relay were placed far away each other to eliminate the coupling between two coils. Similar to the cooperative system using common-coil relay, the distances from the relay to the transmitter and from the relay to the final receiver were d_1 and d_2 respectively. The compensatory inductors were set as in (4.38).

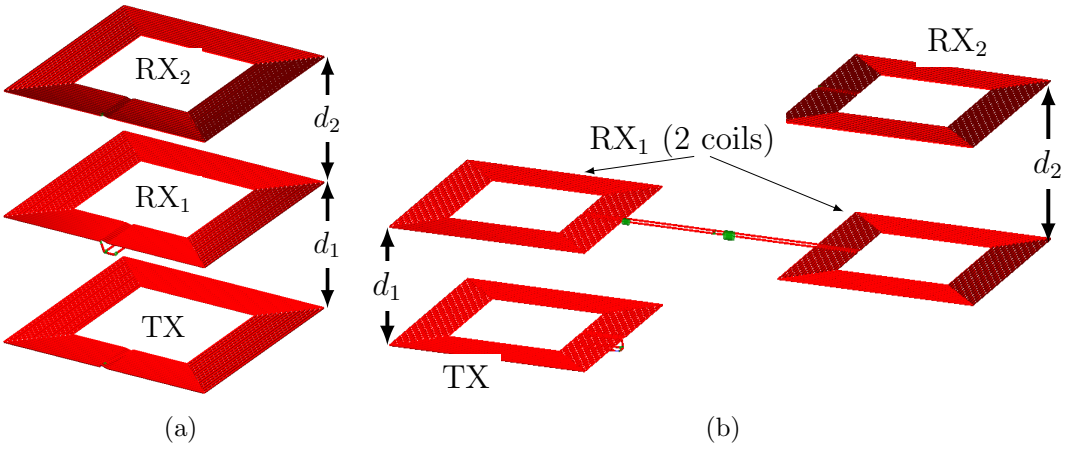

Figure 4.14. Simulation configurations for the cooperative IPT system: (a) using common-coil relay, (b) using separated-coil relay.

Fig. 4.15 illustrated the simulation results of the load voltages over the variations of the loads. In these simulations, d_1 and d_2 were initially set to be 60mm. The results confirmed that in both systems, either using common-coil relay or separated-coil relay, the load voltages were stabilized at approximately 5V when the loads changed from 5Ω to 100Ω. The results verified the theoretical analysis of the load voltages in (4.29), (4.30), (4.32) and (4.33). When the both distances d_1 and d_2 increased from 60mm to 100mm and the compensatory inductors changed according to the changes of the mutual inductances, two load voltages were still kept stable at 5V against the load variations .

The comparison of RF-RF efficiency between two systems in Fig. 4.12a and Fig. 4.12b was illustrated in Fig. 4.16. It could be seen that the system using common-coil relay could achieve higher efficiency than the one using separated-coil relay. The efficiency of the system using common-coil relay was 10% greater than the one using separated-coil relay when the loads were 25Ω. This gap rose to 15% as the loads were equal to 75Ω. The trend of the results was still held as the distances increase to 100mm. It meant in this case, the system using common-coil relay could still outperform the one using separated-coil relay.

In order to evaluate the load voltage stability as well as efficiency of two systems in other arrangements of the coils, the distance, either d_1 or d_2, was

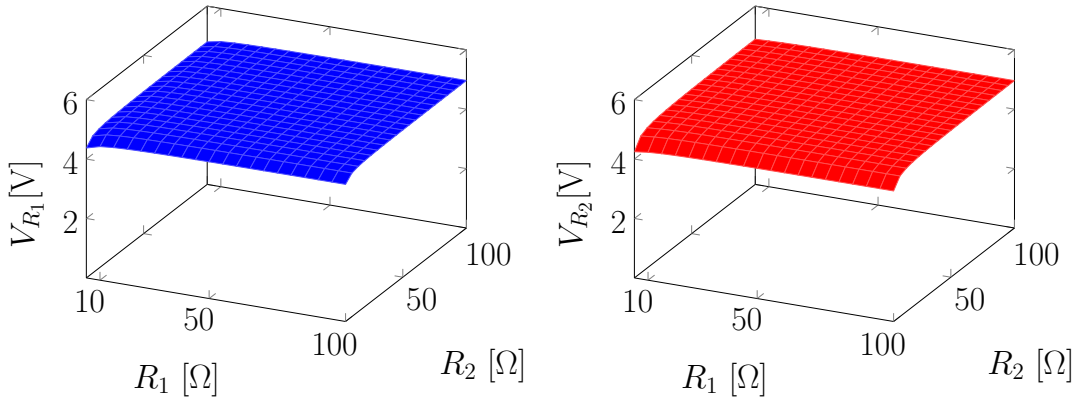

(a) using common-coil relay

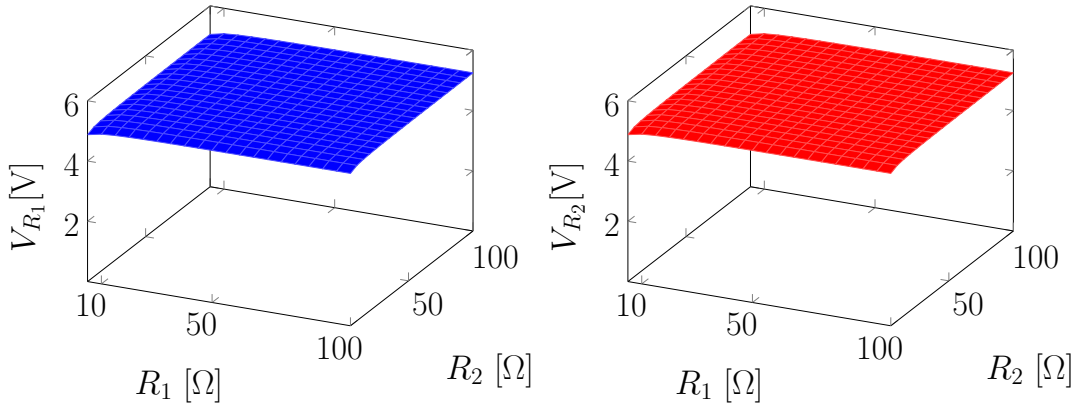

(b) using separated-coil relay

Figure 4.15. The load voltages as a function of the loads for $d_1 = d_2 = 60$mm in cooperative IPT systems.

changed while other parameters of the system were fixed. Accordingly, the pair of (d_1, d_2) was set to be (50mm, 60mm), (70mm, 60mm), (60mm, 50mm) or (60mm, 70mm) to investigate two systems. The graph of the load voltages as a function of the load variations when the pair of (d_1, d_2) was equal to (50mm, 60mm) was illustrated in Fig. 4.17. It was clear that the both systems could keep the load voltages unchanged against the variations of the loads. The simulation results matched the theoretical analysis in (4.29), (4.30), (4.32) and (4.33). In other arrangements of the coils, both systems still stabilized the load voltages against the load variations.

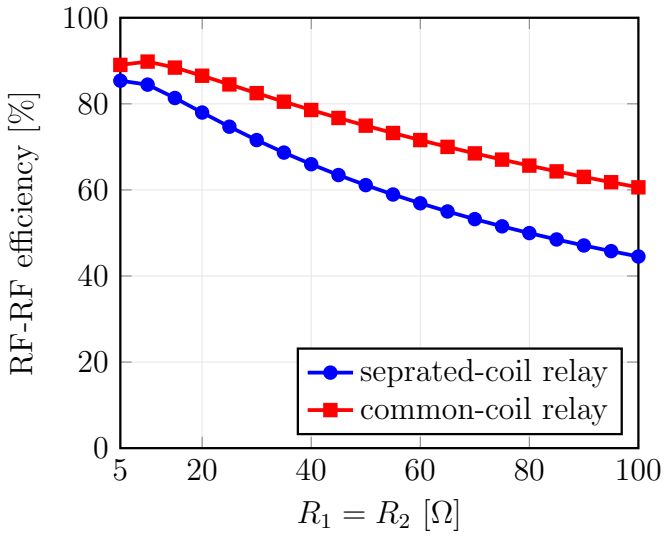

(a) $d_1 = d_2 = 60$mm

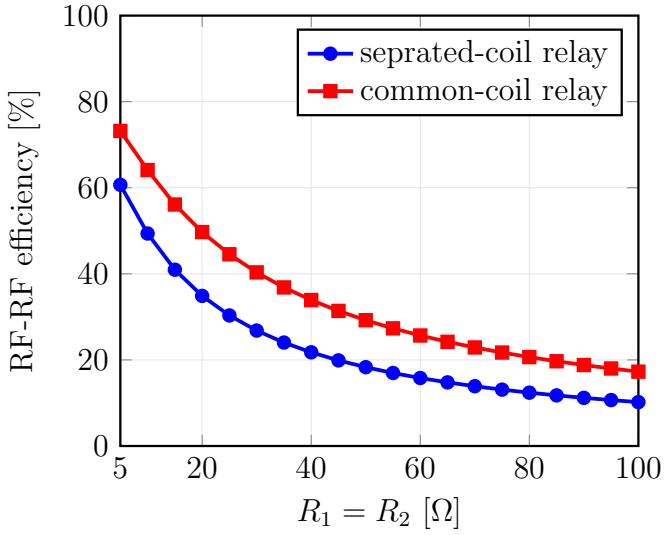

(b) $d_1 = d_2 = 100$mm

Figure 4.16. RF-RF efficiency over the loads in cooperative IPT systems.

For four arrangements of the coils, the system using common-coil relay could achieve higher RF-RF efficiency than the one using separated-coil relay as the loads varied from 5Ω to 100Ω. The graph of RF-RF efficiency over the load variations for various coil arrangements was plotted in Fig. 4.18. It was seen

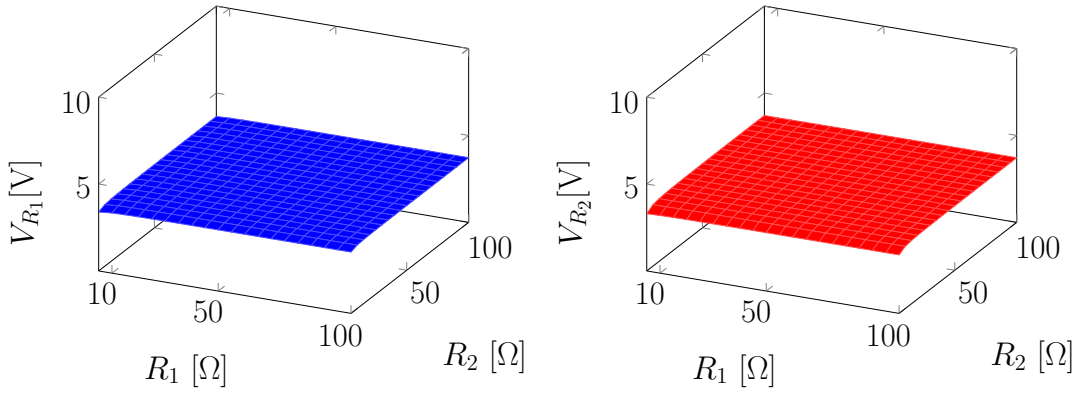

(a) using common-coil relay

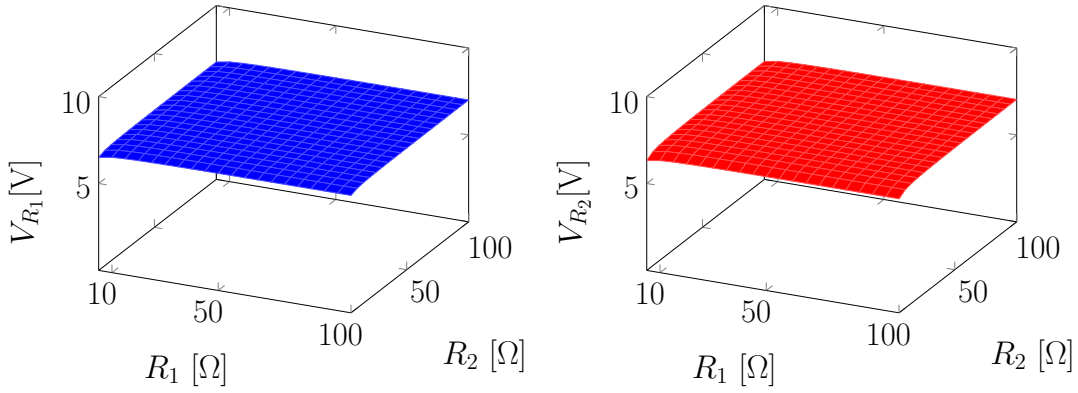

(b) using seprated-coil relay

Figure 4.17. The load voltages as a function of the loads for $d_1 = 50$mm and $d_1 = 60$mm in cooperative IPT systems .

that this advantage of the system using common-coil relay over the one using separated-coil relay was still hold for the other coil arrangements.

4.5. Conclusion

This chapter presented the cooperative IPT system where the relay could simultaneously draw power itself and transmit the rest of received power to the distant receiver while still keeping the load voltages stable against the load variations. Two types of compensation networks, consisting of LC tank and K-inverter, were

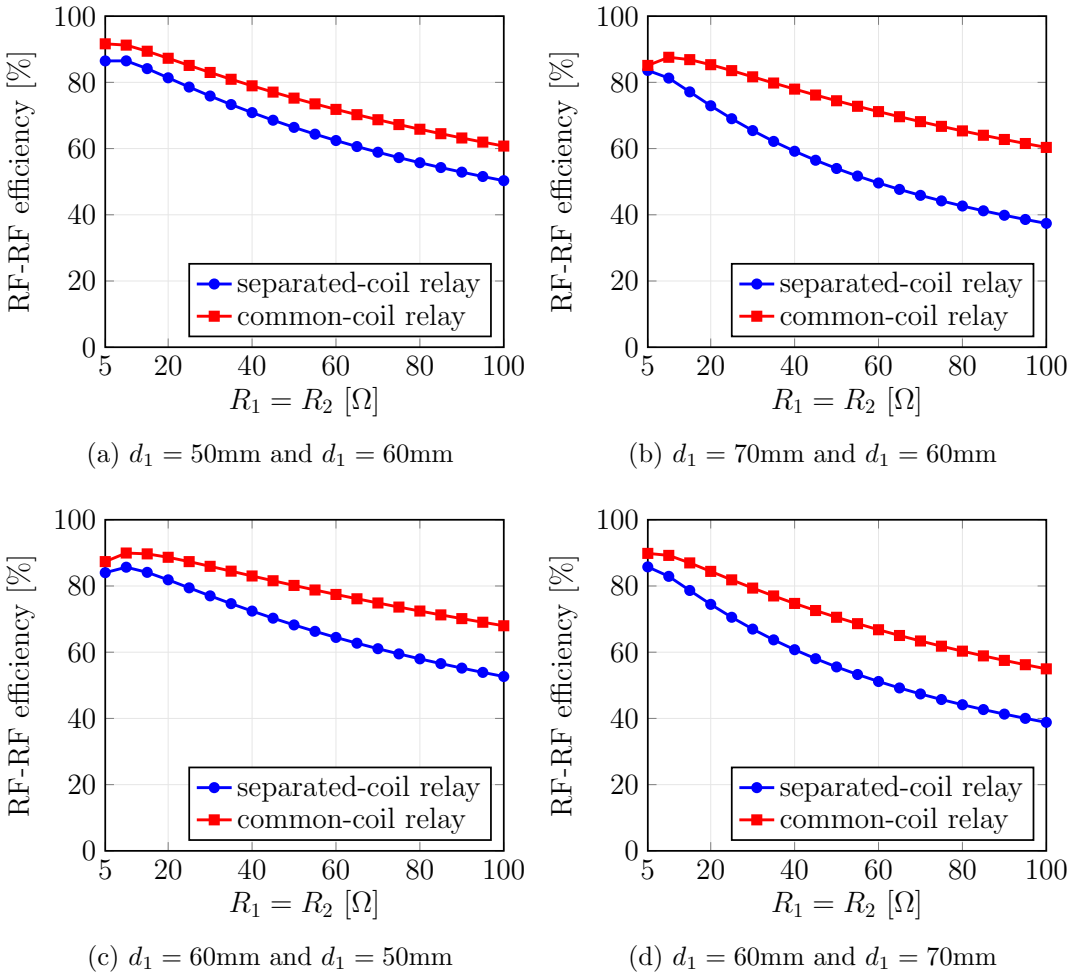

(a) $d_1 = 50$mm and $d_1 = 60$mm

(b) $d_1 = 70$mm and $d_1 = 60$mm

(c) $d_1 = 60$mm and $d_1 = 50$mm

(d) $d_1 = 60$mm and $d_1 = 70$mm

Figure 4.18. RF-RF efficiency over the loads in cooperative IPT systems.

applied for the relay to transform it to cooperative receiver. This chapter also highlighted that the cooperative IPT system using K-inverter could achieve better performance of efficiency in comparison with the one using LC tank. Moreover, the cooperative IPT system using K-inverter also attained higher efficiency than the one using two-coil repeater to relay the power transmission for voltage-gain-free design.

Chapter 5

Power separation and load voltage stabilization in multiple-frequency IPT system with K-inverter

5.1. Introduction

The previous systems have been proposed to deliver rated voltages to multiple loads or realize cooperative characteristic while stabilizing load voltages against load variations under single operating frequency. Recently, IPT technology's development has witnessed that operating frequencies have been diverged in different types of applications [139]. This divergence motivates the development of multiple-frequency IPT charging systems. There are two main solutions for this problem. The first solution is to propose one-to-multiple charging systems where single transmitter is able to deliver power of multiple frequencies to multiple receiver. In contrast, the second solution is to design multiple-to-multiple charging systems where each transmitter operates at an individual frequency to deliver power to corresponding receiver. However, one-to-multiple charging systems are more preferable than multiple-to-multiple systems because of its compact and simple transmitter. Furthermore, multiple-frequency one-to-multiple IPT sys-

tems is a potential candidate for being used in public parking charging lots [51] or universal wireless charging pads [88].

In order to charge multiple receivers operating at multiple frequencies, the authors in [140] proposed an inverter generating a nearly half-cycle sinusoidal current which was considered as being synthesized from three harmonics. In this proposal, the amplitudes of the harmonics significantly decreased to the order of the harmonic. This would limit operation frequencies at harmonics only as well as the number of receivers. In other design, multiple sources were connected in series to a transmitter to deliver power to multiple receivers [141]. However, because the transmitter had only one resonant frequency, the power of the frequencies far from the resonant frequency would be hardly transferred via the transmitter. To address this problem, the authors in [142] employed the compensation of LC tanks at transmitter side to deliver power of multiple frequencies out of transmitting coil. Nevertheless, the design of the compensation network in this proposal depended on the loads.

In this chapter, two-frequency one-to-two inductive power transfer systems in which each pair of source and receiver works on an individual frequency was proposed [P.W2], [P.C4]. Two sources shared either a common transmitting coil or a common resonator to deliver power to two receiver. A novel K-inverter was introduced to separate power of two frequencies and stabilize the load voltages against the load variations. Therefore, the proposed system could achieve full voltage control for the loads that could not be done in the previous studies.

5.2. Multiple-frequency IPT system with common transmitting coil

5.2.1 System description

The schematic circuit of the two-frequency IPT system using a common transmitting coil was shown in Fig. 5.1 in the next page. Two voltage-constant sources V_{s1} and V_{s2} operated at two different frequencies, f_1 and f_2 (angular frequencies $\omega_1 = 2\pi f_1$, $\omega_2 = 2\pi f_2$), respectively. Two sources simultaneously utilized the common transmitting coil L_0 to transfer power to two receivers RX_1 (coil L_1)

and RX_2 (coil L_2). Each source would deliver power to the receiver operating at similar frequency. In the system model, M_{mn} denoted the mutual inductance between the m-th coil and the n-th coil where $m, n \in \{0, 1, 2\}$ and $m \neq n$.

In transmitter side, C_{f1}, L_{f1}, $C_{\mathrm{s1\_}f2}$, $L_{\mathrm{s1\_}f2}$ and jX_{s1} were combined to be equivalent to CLC compensation network operating at the frequency f_1 between the source V_{s1} and the transmitting coil.

$$\frac{1}{j\omega_1 C_{f1}} + j\omega_1 L_{f1} = 0 \tag{5.1}$$

$$\frac{j\omega_1 L_{\mathrm{s1\_}f2}}{1 - \omega_1^2 C_{\mathrm{s1\_}f2} L_{\mathrm{s1\_}f2}} + jX_{\mathrm{s1}} + j\omega_1(L_{f1} + L_0) = 0 \tag{5.2}$$

Inside this compensation network, the capacitor $C_{\mathrm{s1\_}f2}$ and the inductor $L_{\mathrm{s1\_}f2}$ were resonant at the frequency f_2

$$\frac{1}{j\omega_2 C_{\mathrm{s1\_}f2}} + j\omega_2 L_{\mathrm{s1\_}f2} = 0 \tag{5.3}$$

Accordingly, this pair of LC would prevent the interference from power of the frequency f_2. Similarly, the combination of C_{f2}, L_{f2}, $C_{\mathrm{s2\_}f1}$, $L_{\mathrm{s2\_}f1}$ and C_{s2} was considered as CLC compensation network operating at the frequency f_2 between

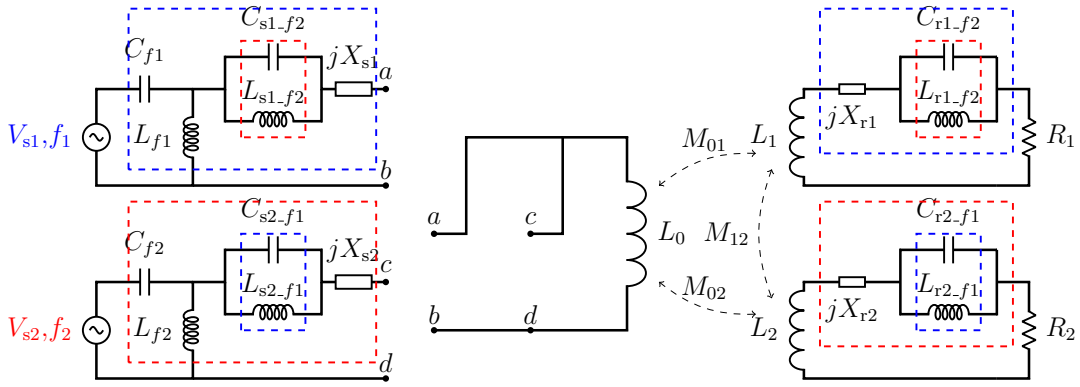

Figure 5.1. System model of multiple-frequency one-to-two IPT system using transmitting coil.

the source V_{s2} and the transmitting coil

$$\frac{1}{j\omega_2 C_{f2}} + j\omega_2 L_{f2} = 0, \tag{5.4}$$

$$\frac{j\omega_2 L_{s2\_f1}}{1 - \omega_2^2 C_{s2\_f1} L_{s2\_f1}} + jX_{s2} + j\omega_2(L_{f2} + L_0) = 0 \tag{5.5}$$

The pair of the capacitor C_{s1_f1} and the inductor L_{s2_f1} resonant at the frequency f_1 would mitigate the power of the frequency f_1

$$\frac{1}{j\omega_1 C_{s2\_f1}} + j\omega_1 L_{s2\_f1} = 0 \tag{5.6}$$

In receiver side, for the receiver RX_1, the combination of the reactance X_{r1}, C_{r1_f2} and L_{r1_f2} formed equivalent series compensation network between the coil L_1 and the load R_1

$$\frac{j\omega_1 L_{r1\_f2}}{1 - \omega_1^2 C_{r1\_f2} L_{r1\_f2}} + jX_{r1} + j\omega_1 L_1 = 0 \tag{5.7}$$

The pair of C_{r1_f2} and L_{r1_f2} resonant at f_2 would prevent the power of the frequency f_2 in the RX_1 circuit.

$$\frac{1}{j\omega_2 C_{r1\_f2}} + j\omega_2 L_{r1\_f2} = 0 \tag{5.8}$$

Correspondingly, for the receiver RX_2 operating at the frequency f_2, the combination of the reactance X_{r2}, C_{r2_f1} and L_{r2_f1} formed equivalent series compensation network between the coil L_2 and the load R_2.

$$\frac{j\omega_2 L_{r2\_f1}}{1 - \omega_2^2 C_{r2\_f1} L_{r2\_f1}} + jX_{r2} + j\omega_2 L_2 = 0 \tag{5.9}$$

The pair of C_{r2_f1} and L_{r2_f1} would prevent the power of the frequency f_1 in the RX_2 circuit.

$$\frac{1}{j\omega_1 C_{r2\_f1}} + j\omega_1 L_{r2\_f1} = 0 \tag{5.10}$$

5.2.2 Power separation and load voltage stability

Without the loss of generality, the operation of the source V_{s1} was considered first. According to the superposition theory, the source V_{s2} was equivalent to

short circuit to the operation of the source V_{s1}. Therefore, the impedance looked from two points c and d to the source V_{s2} was

$$Z_{cd}(f_1) = \frac{j\omega_1 L_{s2\_f1}}{1-\omega_1^2 C_{s2\_f1} L_{s2\_f1}} + \frac{1}{j\omega_1 C_{s2}} + \frac{j\omega_1 L_{f2}}{1-\omega_1^2 C_{f2} L_{f2}} \tag{5.11}$$

where C_{s2} was calculated from jX_{s2}. $Z_{cd}(f_1)$ would approach infinity because of (5.6). As a result, two points c and d were considered as open to the operation of the source V_{s1}. Similarly, at the frequency f_1, the equivalent impedance of RX_2 is

$$Z_2(f_1) = \frac{j\omega_1 L_{r2\_f1}}{1-\omega_1^2 C_{r2\_f1} L_{r2\_f1}} + \frac{1}{j\omega_1 C_2} + j\omega_1 L_2 + R_2 \tag{5.12}$$

where the capacitor C_2 (jX_{r2}) was calculated by (5.9). We have $Z_2(f_1)$ would approach infinity because of (5.10). Hence, RX_2 could not receive the power of the frequency f_1. Finally, the power supplied by the source V_{s1} was transferred to RX_1 only. For similar analysis of the operation of the source V_{s2}, RX_2 could receive power transmitted by the source V_{s2} only. Even though two sources shared the common transmitting coil to deliver power to the two receivers, the power link of each pair of source-receiver was completely separated.

Accordingly, the operation of each pair of source-receiver was independent of each other. The compensation network at transmitter side was CLC circuit and that at receiver side was series. Consequently, the load voltages were stabilized against the variations of the loads

$$V_{R_1} = -\frac{M_{01}}{L_{f1}} V_{s1} \tag{5.13}$$

$$V_{R_2} = -\frac{M_{02}}{L_{f2}} V_{s2} \tag{5.14}$$

5.2.3 Simulation results

The power separation as well as the stability of the output voltages in the proposed system would be confirmed by LTSpice software based simulations. Fig. 5.2 illustrated the simulation setup of the proposed system. 80kHz and 110kHz were selected as two operating frequencies. Two source voltages supplied the constant voltages of 10V. The compensatory inductors L_{f1} and L_{f2}

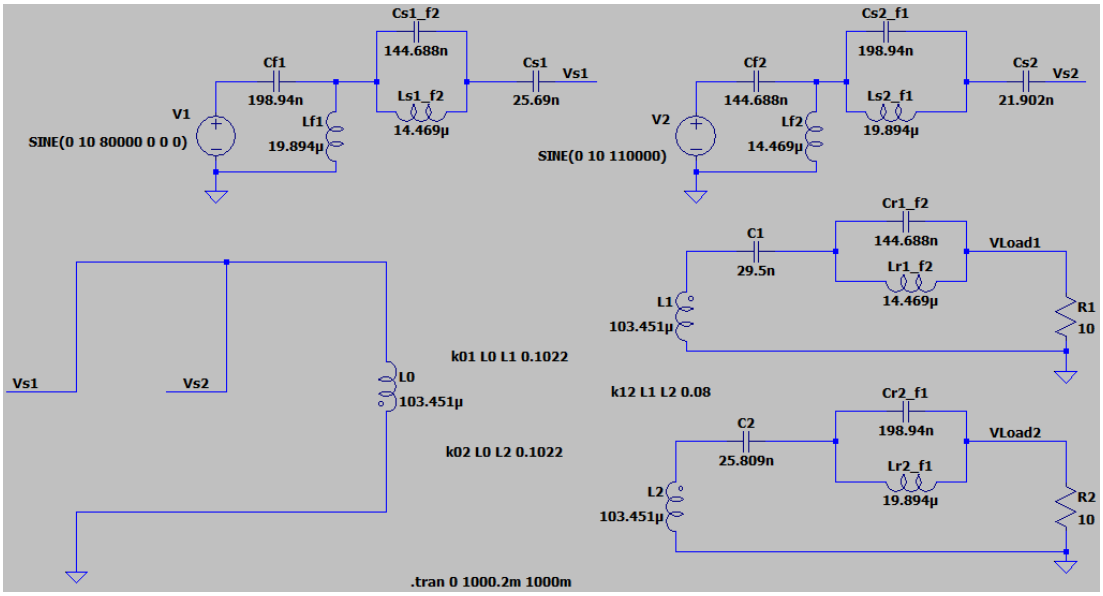

Figure 5.2. Simulation setting for two-frequency one-to-two IPT system using transmitting coil.

were set so that their impedances at corresponding frequency were equal to 10Ω ($\omega_1 L_{f1} = \omega_2 L_{f2} = 10\Omega$). The other compensatory components were designed as in the equations in Section 5.2.1. The coupling coefficients among the coils were set to be $k_{01} = k_{02} = 0.1022$ and $k_{12} = 0.08$. Therefore, the corresponding mutual inductances were $M_{01} = M_{02} = 10.573\mu$H and $M_{12} = 8.276\mu$H.

The waveforms and Fast Fourier Transform (FFT) of the currents flowing in C_{s1} and C_{s2} for the loads of 10Ω were plotted in Fig. 5.3. The results in Fig. 5.3b illustrated that the current $I_{C_{s1}}$ mainly comprised the power of the frequency 80kHz. Similarly, the current $I_{C_{s2}}$ mainly comprised the power of the frequency 110kHz according to the simulation results in Fig. 5.3c. The interference between the current flowing in C_{s1} and C_{s2} was negligibly small, or it could be considered as no interference. It matched the theoretical analysis in the previous section.

The waveforms and FFT of the load voltages were illustrated in Fig. 5.4. Similarly, it was clear that each receiver only received the power of the frequency at which it was operating only. The simulation results in Fig. 5.4a matched the formulas (5.13) and (5.14) where estimated load voltages $|V_{R_1}| = V_{s1} M_{01} / L_{f1} =$

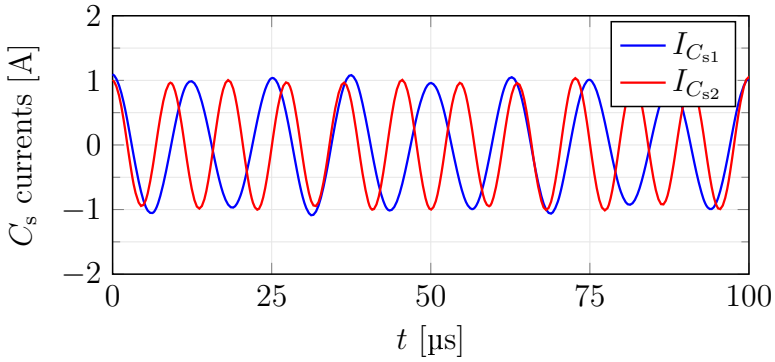

(a) Waveforms

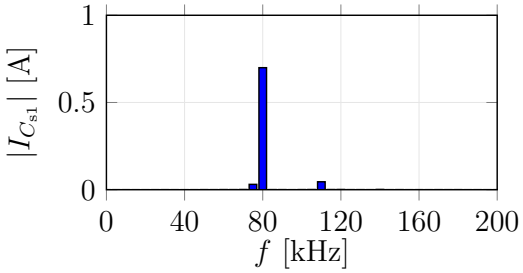

(b) FFT of the current in C_{s1}

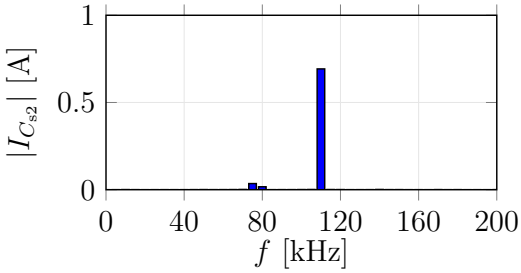

(c) FFT of the current in C_{s2}

Figure 5.3. The currents flowing in C_{s1} and C_{s2}.

5.314V and $|V_{R_2}| = V_{s2}M_{02}/L_{f2} = 7.307$V. Fig. 5.4b and Fig. 5.4c highlighted that RX_1 only received the power of the frequency f_1 and RX_2 only received the power of only frequency f_2. It implied that the power of each operating frequency was completely separated for each pair of source-receiver.

5.2.4 Experimental results

The feasibility of the proposed system was verified by the experiments. Fig. 5.5 showed the experiment setup. Two frequencies of 170kHz and 200kHz were selected as the operating frequencies of two sources. In order to evaluate the transmission ability, the transmission factors among the sources and the receivers were measured by Vector Network Analyzer.

The inductances of the coils: $L_0 = 147.67$µH, $L_1 = 56.26$µH, $L_2 = 60.67$µH. Compensatory components: $C_{f1} = C_{s2_f1} = 56$nF, $C_{f2} = C_{s1_f2} = 39$nF, $L_{f1} =$

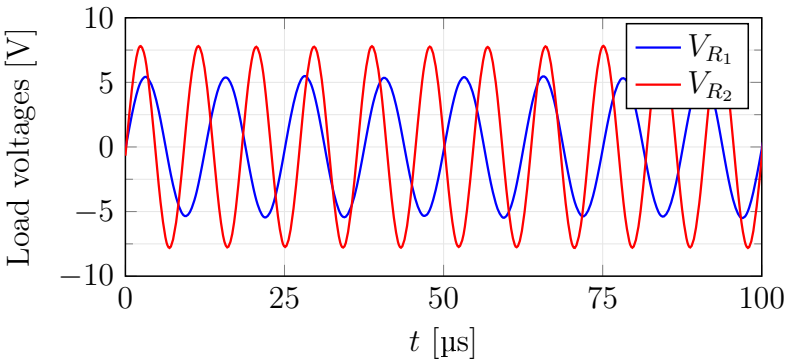

(a) Waveforms

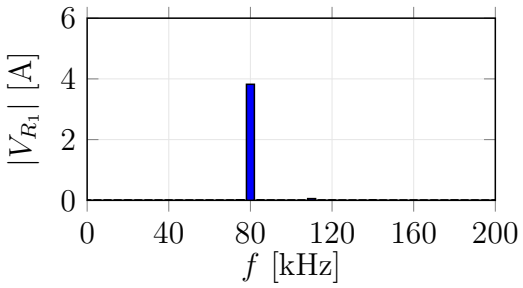

(b) FFT of the load voltage V_{R_1}

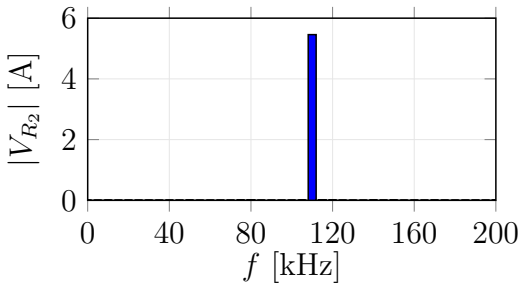

(c) FFT of the load voltage V_{R_2}

Figure 5.4. The load voltages.

$L_{\text{s2\_}f1} = 15.82\mu\text{H}$, $L_{f2} = L_{\text{s1\_}f2} = 16.31\mu\text{H}$, $C_{\text{s1}} = 3.9\text{nF}$ (jX_{s1}), $C_{\text{s2}} = 5\text{nF}$ (jX_{s2}), $C_{\text{r1\_}f2} = C_{\text{r2\_}f1} = 82\text{nF}$, $L_{\text{r1\_}f2} = 7.8\mu\text{H}$, $L_{\text{r2\_}f1} = 10.8\mu\text{H}$.

Fig. 5.6 in next page illustrated the measures of the transmission factors (S_{12}) between each source and each load. First, Fig. 5.6a indicated that there was no interference between two sources when the transmission factors were -26.29dB at 170kHz and -21.73dB at 200kHz. Similarly, Fig. 5.6b showed that there was no power exchange between two receivers because the transmission factors between them were -27.81dB and -29.29dB at 170kHz and 200kHz respectively. Correspondingly, the receivers could not receive the power transmitted by the frequency-mismatched sources because the transmission factors between one source and frequency-mismatched receiver were under -30dB as shown in Fig. 5.6c and Fig. 5.6d. In contrast, Fig. 5.6e illustrated that the source 1 could transfer power to RX_1 at the operating frequency of 170kHz when the transmis-

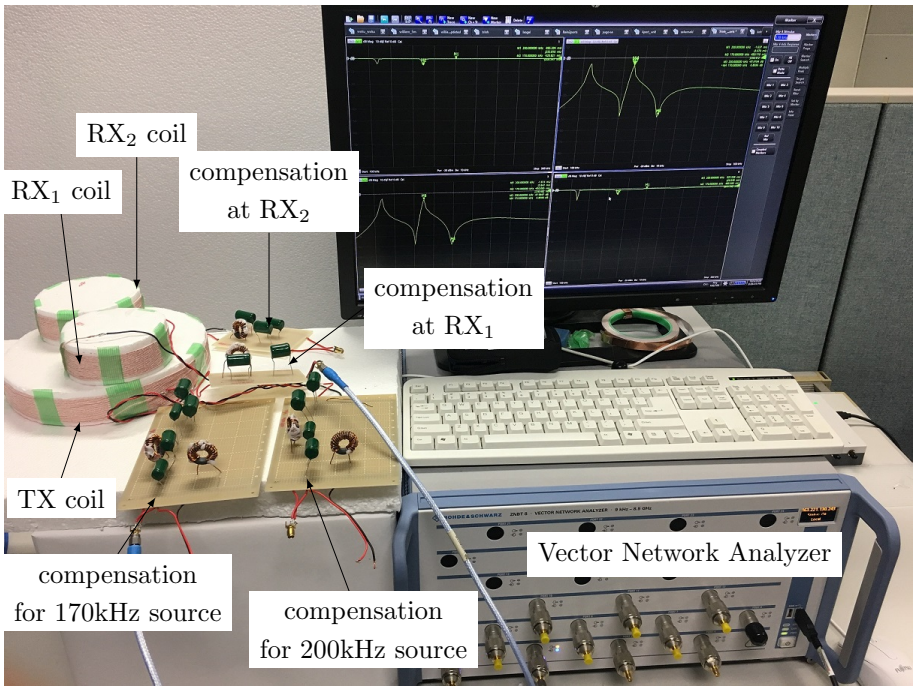

Figure 5.5. Demonstration of two-frequency one-to-two IPT system using common transmitting coil.

sion factor of this pair was −5.89dB. Similarly, the power of the frequency of 200kHz could be transmitted from the source 2 to RX_2 because the transmission factor of this pair was −5.16dB. The transmission factor between one source and its frequency-matched receiver was decided by the coupling between the transmitting coil and the corresponding receiving coil. Since $Z_{cd}(f_1)$ and $Z_{ab}(f_2)$ could not practically approach infinity, there would be power leakage from source 1 to source 2 and vice versa. It would deteriorate the transmission factors of the power links between sources and their corresponding receivers.

In summary, this work proposed one-to-two inductive power transfer system in which one transmitter was simultaneously driven by two sources operating at two different frequencies to deliver power two receivers. Although the theoretical analysis and simulation results indicated that the power of each power link of source-receiver was completely separated, the demonstration system showed the transmission factor between one source to the corresponding receiver was still

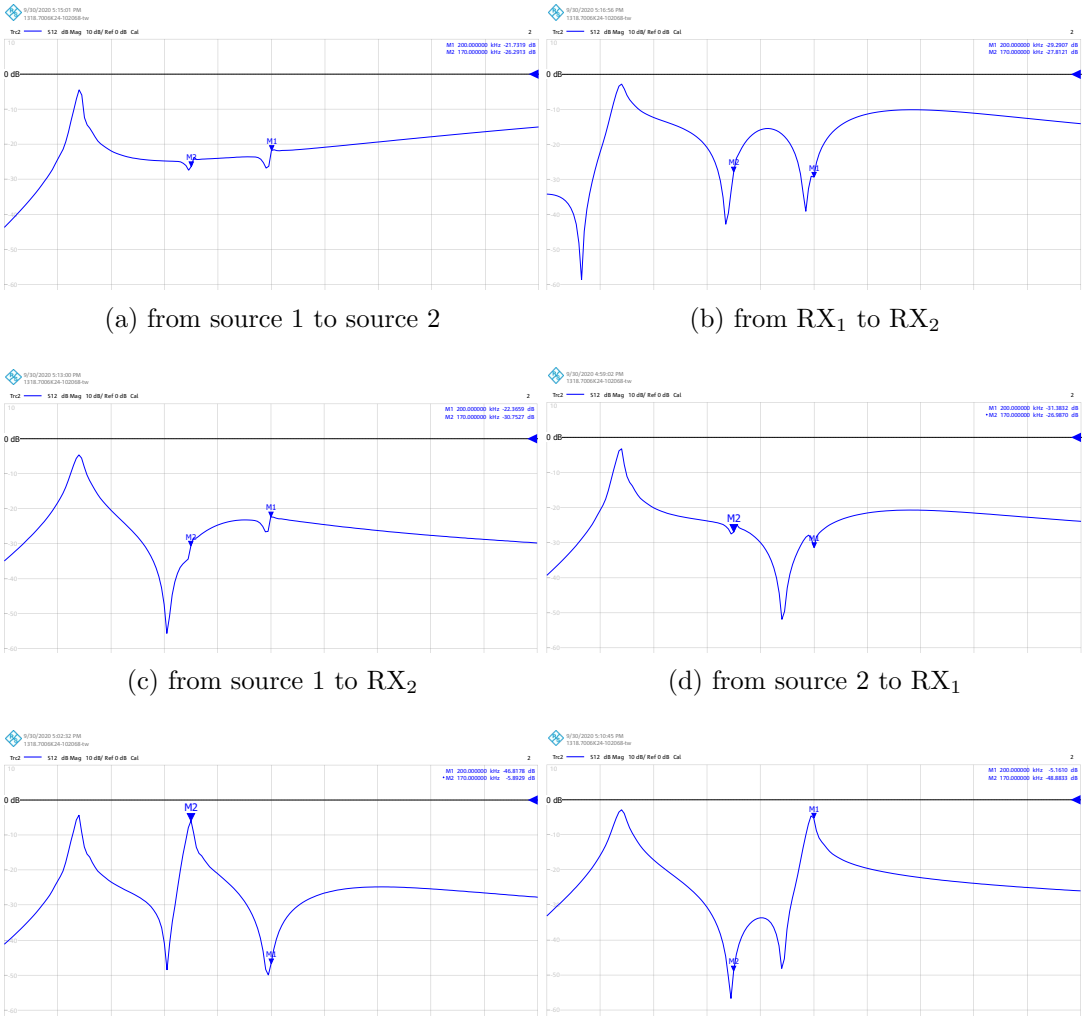

(a) from source 1 to source 2

(b) from RX_1 to RX_2

(c) from source 1 to RX_2

(d) from source 2 to RX_1

(e) from source 1 to RX_1

(f) from source2 to RX_2

Figure 5.6. Transmission factors in frequency domain (S_{12})

low. This was because the equivalent impedance of frequency-mismatched source circuit did not approach infinity as expected. Therefore they would affect the power link of other pair of source-receiver. This effect could be reduced by using common transmitting resonator instead of common transmitting coil. It was illustrated in next section.

5.3. Multiple-frequency IPT system with common transmitting resonator

5.3.1 System description

Fig. 5.7 showed the schematic circuit of the multiple-frequency IPT system using common transmitting resonator. In this system, the transmitting resonator, consisting of the coil L_0 and series compensatory capacitor C_0, was simultaneously driven by two sources V_{s1} and V_{s2}. Two operating frequencies were f_1 and f_2 with angular frequencies $\omega_1 = 2\pi f_1$, $\omega_2 = 2\pi f_2$. For simplicity, it was assumed that the internal resistances were negligibly small.

The reactance X_{s1} and the compensatory components, C_{f1}, L_{f1}, C_{s1_f2}, L_{s1_f2}, C_0 were combined to form compensation network between the source V_{s1} and the transmitting coil L_0. They were designed with the following relationship

$$\frac{1}{j\omega_1 C_{f1}} + j\omega_1 L_{f1} = 0 \tag{5.15}$$

$$\frac{j\omega_1 L_{s1\_f2}}{1-\omega_1^2 C_{s1\_f2} L_{s1\_f2}} + jX_{s1} + \frac{1}{j\omega_1 C_0} + j\omega_1(L_{f1}+L_0) = 0 \tag{5.16}$$

Inside the compensation network, the capacitor C_{s1_f2} and the inductor L_{s1_f2}

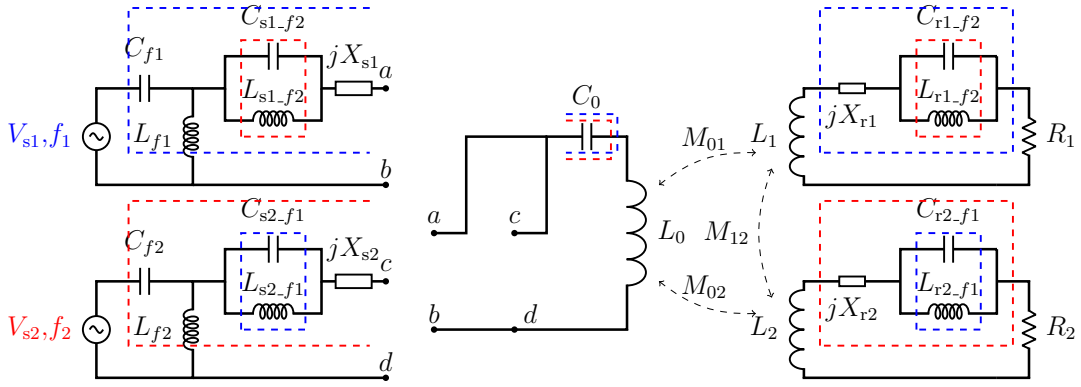

Figure 5.7. System model of multiple-frequency one-to-two IPT system using transmitting resonator.

were resonant at the frequency f_2

$$\frac{1}{j\omega_2 C_{\mathrm{s1\_}f2}} + j\omega_2 L_{\mathrm{s1\_}f2} = 0. \tag{5.17}$$

This pair of inductor-capacitor would be a band-stop filter eliminating the power of the frequency f_2 out of the circuit [143]. Similarly, the reactance X_{s2} was combined with the compensatory components, C_{f2}, L_{f2}, $C_{\mathrm{s2\_}f1}$, $L_{\mathrm{s2\_}f1}$ and C_0 to form the compensation network between the source V_{s2} and the transmitting coil L_0. They were designed based on the following relationship

$$\frac{1}{j\omega_2 C_{f2}} + j\omega_2 L_{f2} = 0, \tag{5.18}$$

$$\frac{j\omega_2 L_{\mathrm{s2\_}f1}}{1 - \omega_2^2 C_{\mathrm{s2\_}f1} L_{\mathrm{s2\_}f1}} + jX_{\mathrm{s2}} + \frac{1}{j\omega_2 C_0} + j\omega_2 (L_{f2} + L_0) = 0. \tag{5.19}$$

The capacitor $C_{\mathrm{s1\_}f1}$ and the inductor $L_{\mathrm{s2\_}f1}$ were resonant at the frequency f_1 to prevent the power of frequency f_1

$$\frac{1}{j\omega_1 C_{\mathrm{s2\_}f1}} + j\omega_1 L_{\mathrm{s2\_}f1} = 0. \tag{5.20}$$

As mentioned in the previous section, for the operation of one source, the equivalent impedance of the frequency-mismatched source could not be infinity in practice because the components of the band-stop filter were not ideal. In such case, the power link of the other source and the corresponding receiver would be significantly affected by the equivalent impedance of the frequency-mismatched source. This could happen because the impedance of the frequency-mismatched source was just several times greater than the equivalent impedance of the transmitter. Therefore, to reduce the equivalent impedance of the transmitter, the compensatory capacitor C_0 was added to the transmitting coil. It would help reducing the effect of the frequency-mismatched source on the transmitter. Consequently, the appearance of C_0 would enhance the isolation between two power streams.

For the receiver side, for RX_1, the reactance, denoted by jX_{r1}, was combined with $C_{\mathrm{r1\_}f2}$ and $L_{\mathrm{r1\_}f2}$ to form series compensation network between the coil L_1 and the load R_1

$$\frac{j\omega_1 L_{\mathrm{r1\_}f2}}{1 - \omega_1^2 C_{\mathrm{r1\_}f2} L_{\mathrm{r1\_}f2}} + jX_{\mathrm{r1}} + j\omega_1 L_1 = 0 \tag{5.21}$$

where $C_{\mathrm{r1\_}f2}$ and $L_{\mathrm{r1\_}f2}$ were resonant at f_2 to reject the power of the frequency f_2

$$\frac{1}{j\omega_2 C_{\mathrm{r1\_}f2}} + j\omega_2 L_{\mathrm{r1\_}f2} = 0. \tag{5.22}$$

Analogously, for RX_2, the reactance, denoted by jX_{r2}, was combined with $C_{\mathrm{r2\_}f1}$ and $L_{\mathrm{r2\_}f1}$ to form a series compensation network between the receiving coil L_2 and the load R_2

$$\frac{j\omega_2 L_{\mathrm{r2\_}f1}}{1-\omega_2^2 C_{\mathrm{r2\_}f1} L_{\mathrm{r2\_}f1}} + jX_{\mathrm{r2}} + j\omega_2 L_2 = 0, \tag{5.23}$$

$$\frac{1}{j\omega_1 C_{\mathrm{r2\_}f1}} + j\omega_1 L_{\mathrm{r2\_}f1} = 0 \tag{5.24}$$

where $C_{\mathrm{r2\_}f1}$ and $L_{\mathrm{r2\_}f1}$ were resonant at the frequency f_1 to reject the power of the frequency f_1.

In the system model, the mutual inductance between the m-th coil and the n-th coil is denoted by M_{mn} where $m, n \in \{0, 1, 2\}$ and $m \neq n$. By employing the band-stop filters inside the compensation networks, the power of each pair of source-receiver was completely separated. Moreover, the compensation networks also helped to keep the load voltages stable against the load variations. The superior characteristics of the multiple-frequency system would be theoretically proved in next section.

5.3.2 Power separation and load voltage stability

Because of the symmetry of the system structure, the operation of the system caused by the source V_{s1} was considered first. The operation of the system caused by the source V_{s2} could be analyzed analogously. For the operation of the source V_{s1}, the source V_{s2} was considered as short circuit due to superposition theory. The equivalent impedance between two points c and d was

$$Z_{cd}(f_1) = \frac{j\omega_1 L_{\mathrm{s2\_}f1}}{1-\omega_1^2 C_{\mathrm{s2\_}f1} L_{\mathrm{s2\_}f1}} + \frac{1}{j\omega_1 C_{\mathrm{s2}}} + \frac{j\omega_1 L_{f2}}{1-\omega_1^2 C_{f2} L_{f2}} \tag{5.25}$$

where the capacitor C_{s2} was the calculation result of the reactance X_{s2} decided by (5.19). Here, $Z_{cd}(f_1)$ would approach infinity because of (5.20). Therefore, this

circuit between two points c and d considered as open circuit for the operation of the source V_{s1}.

For receiver side, at the operation frequency f_1, the total impedance of RX_2 circuit was

$$Z_2(f_1) = \frac{j\omega_1 L_{\mathrm{r2\_}f1}}{1-\omega_1^2 C_{\mathrm{r2\_}f1} L_{\mathrm{r2\_}f1}} + \frac{1}{j\omega_1 C_{\mathrm{r2}}} + j\omega_1 L_2 + R_2 \tag{5.26}$$

where the capacitor C_{r2} was the calculation result of the reactance X_{r2} decided by (5.23). $Z_2(f_1)$ would approach infinity because of (5.24). Therefore, RX_2 could not receive power transmitted by the source V_{s1}. As a result, the power supplied by V_{s1} was delivered to RX_1 only. This pair of source-receiver was considered as compensated by CLC at transmitter side according to (5.16), (5.15) and by series at receiver side according to (5.21).

Analogously, the theoretical analysis for the power transmission between the source V_{s2} and RX_2 was analyzed in the same way. Consequently, two power links between two pairs of source-receiver were completely separated although two sources simultaneously shared the common transmitting resonator to deliver power to two receivers. Since each pair of source-receiver operated with the compensation scheme of CLC-series as analyzed, the load voltages were given by

$$V_{R_1} = -\frac{M_{01}}{L_{f1}} V_{\mathrm{s1}}, \tag{5.27}$$

$$V_{R_2} = -\frac{M_{02}}{L_{f2}} V_{\mathrm{s2}} \tag{5.28}$$

Two equations above indicated that each load voltage was independent of the parameters from the frequency-mismatched source and receiver. Therefore, any power control for each load would not affect the operation of the other pair of source-receiver.

5.3.3 Simulation results

To verify the power separation and constant load voltages in the multiple-frequency IPT system using common transmitting resonator, LTSpice-based simulations were carried out. Two power sources were set to be 10V. Two frequencies of 170kHz and 200kHz were selected to be operating frequencies. The specific

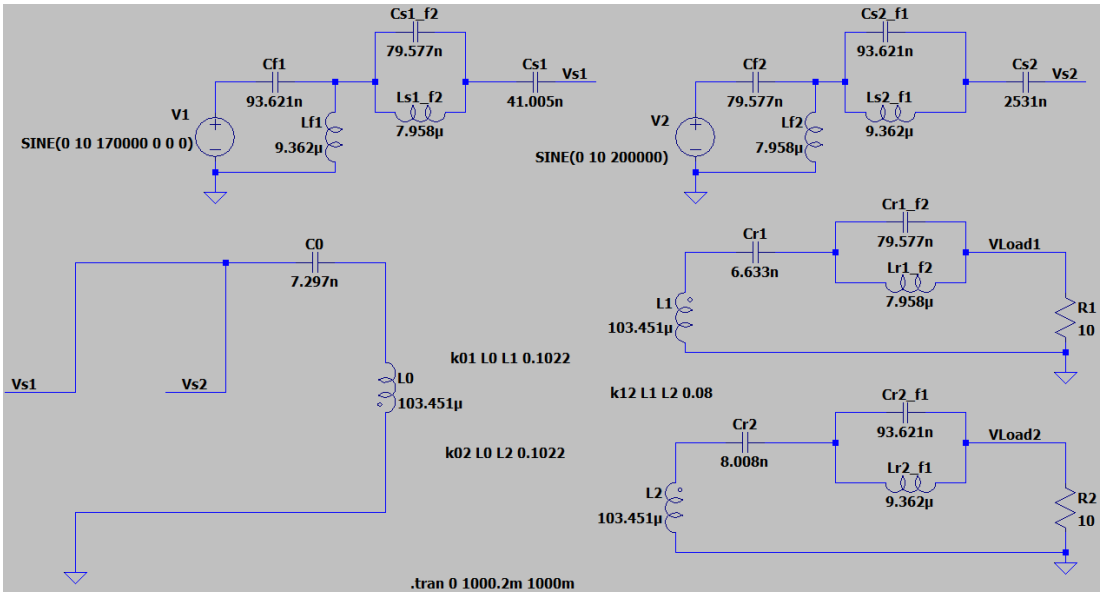

Figure 5.8. Simulation setting for two-frequency IPT system using common transmitting resonator.

parameters of the system was illustrated in Fig. 5.8. In the simulations, the impedances of the compensatory inductors L_{f1} and L_{f2} were set to be 10Ω at their corresponding frequencies ($\omega_1 L_{f1} = \omega_2 L_{f2} = 10\Omega$). The relationship among the compensatory components was given by the equations in Section 5.3.1. In order to simulate coupling among the coils, the coupling coefficients were set as $k_{01} = k_{02} = 0.1022$ and $k_{12} = 0.08$. Accordingly, the corresponding mutual inductances were $M_{01} = M_{02} = 10.573\mu$H and $M_{12} = 8.276\mu$H.

Fig. 5.9 showed the waveforms and Fast Fourier Transform (FFT) of the currents flowing in C_{s1} and C_{s2}. The results indicated that the current $I_{C_{s1}}$ mainly comprised the power of the frequency 170kHz while the current $I_{C_{s1}}$ mainly comprised the power of the frequency 200kHz only. It matched the theoretical analysis that there was no interference between two sources.

The waveforms and FFT of the load voltages were illustrated inFig. 5.10. Similarly, these results highlighted that the receiver RX_1 could receive the power of the frequency 170kHz while the receiver RX_2 could receive the power of the frequency 200kHz. Additionally, the load voltages in the simulation results matched

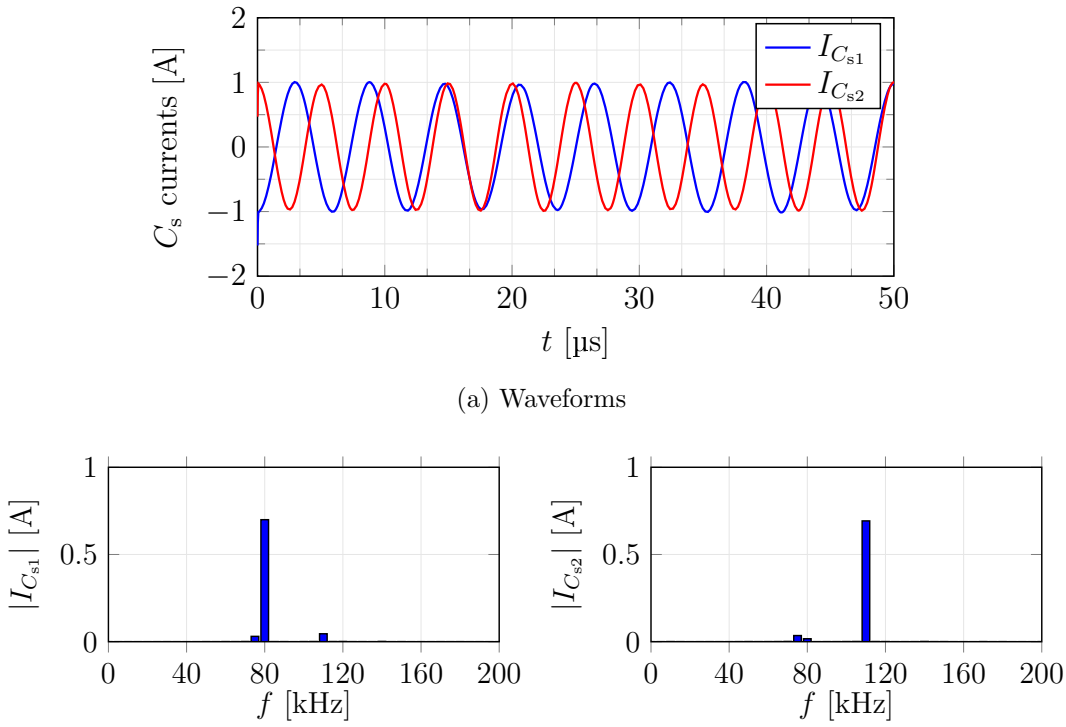

(a) Waveforms

(b) FFT of the current in C_{s1}

(c) FFT of the current in C_{s2}

Figure 5.9. The currents flowing in C_{s1} and C_{s2}.

the estimates in (5.27), (5.28) where the load voltages were estimated to be $|V_{R_1}| = |V_{s1}M_{01}/L_{f1}| = 11.3\text{V}$ and $|V_{R_2}| = |V_{s2}M_{02}/L_{f2}| = 13.3\text{V}$.

The stability of the load voltages against the load variations was evaluated by changing the loads among the values of 10Ω, 20Ω and 50Ω. The results shown in Table 5.1 highlighted that the two load voltages were stabilized at about 11.1V and 13.4V even though the loads altered among 10Ω, 20Ω and 50Ω.

5.3.4 Experimental results

The feasibility of the proposed system was confirmed by a demonstration system which was shown in Fig. 5.11. The schematic circuit of the demonstration system was similar to the system model in Fig. 5.7. Two operating frequencies were 170kHz and 200kHz. Table 5.2 showed the specific parameters of the demonstration system. The evaluation of the transmission factors among the sources and

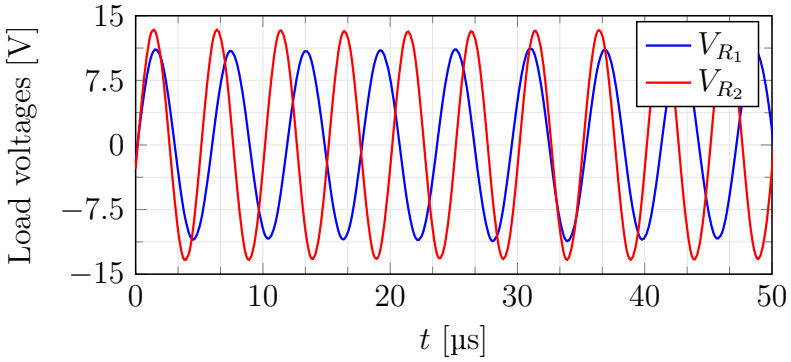

(a) Waveforms

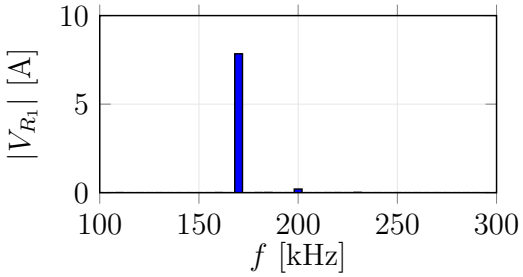

(b) FFT of the load voltage V_{R_1}

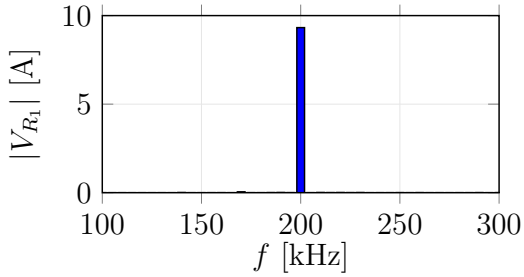

(c) FFT of the load voltage V_{R_2}

Figure 5.10. The load votlages.

the receivers was done using Vector Network Analyzer.

Fig. 5.12 in the next page illustrated the transmission factors among the sources and the receivers. According to the results in Fig. 5.12a, power could not be transferred between two sources because the transmission factors between them were −30.6dB and −31.5dB at 170kHz and 200kHz. Similarly, the transmission factors of −23.79dB and −22.62dB, in Fig. 5.12b, between two receivers verified that there was no power exchanged between two receivers at both operating frequencies. Additionally, the power links between one source and the frequency-mismatched receiver were negligibly weak because the transmission factors between them were under −20dB as shown in Fig. 5.12c and Fig. 5.12d. Finally, the transmission factor of −1.89dB could be achieved between V_{s1} and RX_1 as shown in Fig. 5.12e. It indicated that the source V_{s1} could deliver power to RX_1 at the operating frequency 170kHz. The transmission factor was −1.89dB

Table 5.1. The load voltages against the load variations

R_1 (Ω)	R_2 (Ω)	V_{R_1} (V)	V_{R_2} (V)
10	10	10.998	13.178
10	20	10.987	13.405
10	50	10.958	13.492
20	10	11.095	13.183
20	20	11.092	13.406
20	50	11.081	13.494
50	10	11.152	13.18
50	20	11.141	13.406
50	50	11.132	13.492

Table 5.2. The parameters of the experimental system

Symbol	Value	Symbol	Value
C_{f1}	56nF	L_0	147.67µH
L_{f1}	15.82µH	C_0	4.95nF
$C_{\mathrm{s1\_}f2}$	39nF	L_1	56.26µH
$L_{\mathrm{s1\_}f2}$	16.31µH	C_{r1}	10nF
C_{s1}	18.1nF	$L_{\mathrm{r1\_}f2}$	7.8µH
C_{f2}	39nF	$C_{\mathrm{r1\_}f2}$	82nF
L_{f2}	16.31µH	L_2	60.67µH
$C_{\mathrm{s2\_}f1}$	56nF	C_{r2}	4.5nF
$L_{\mathrm{s2\_}f1}$	15.82µH	$L_{\mathrm{r2\_}f1}$	10.8µH
C_{s2}	-	$C_{\mathrm{r2\_}f1}$	82nF

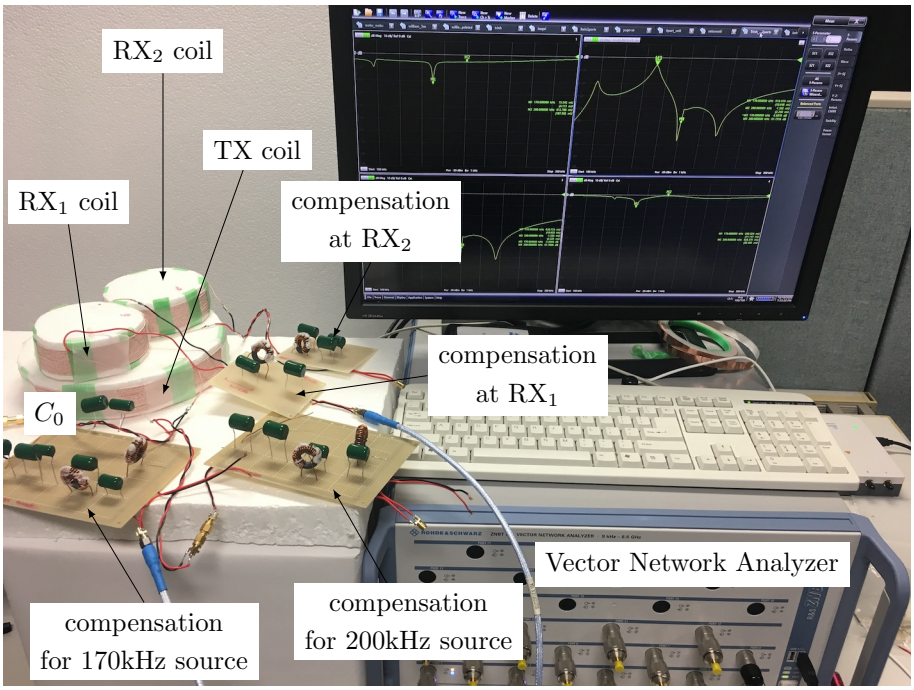

Figure 5.11. Experimental system two-frequency one-to-two IPT system using common transmitting resonator.

because it was decided by the ratio between the mutual inductance M_{01} and the compensatory inductance L_{f1} as in (5.27). Identically, the results in Fig. 5.12e highlighted that the source V_{s2} could deliver power to RX$_2$ at the operating frequency 200kHz because the transmission factor between them was -1.23dB.

5.4. Conclusion

This chapter presented the multiple-frequency one-to-multiple IPT systems where multiple pairs of source-receiver share a common transmitting channel to operate at individual frequency. Initially, multiple sources drove a common transmitting coil to deliver power to corresponding receivers. K-inverter and band-reject filter were combined to separate power link of each pair of source-receiver and stabilize load voltage of corresponding receiver. The theoretical analysis and the

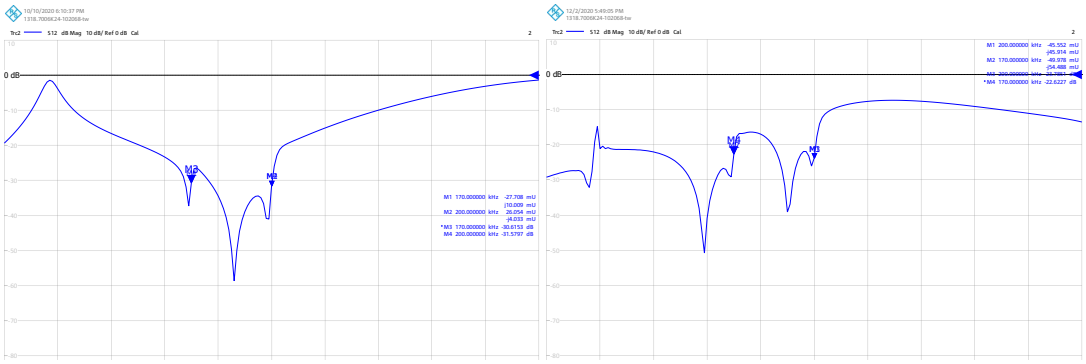

(a) from source 1 to source 2

(b) from RX_1 to RX_2

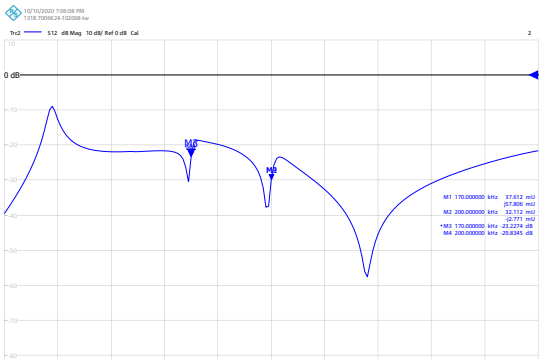

(c) from source 1 to RX_2

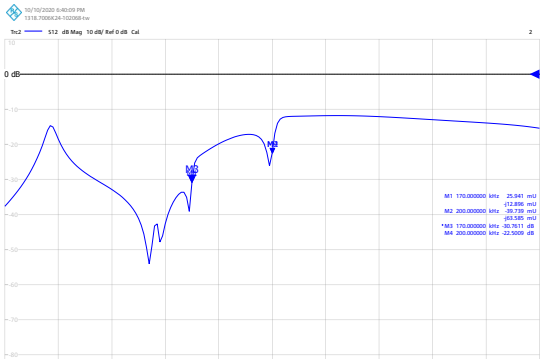

(d) from source 2 to RX_1

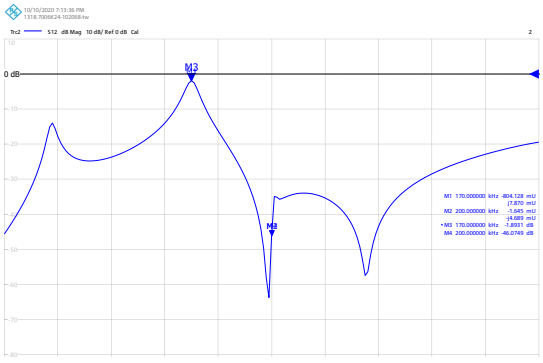

(e) from source 1 to RX_1

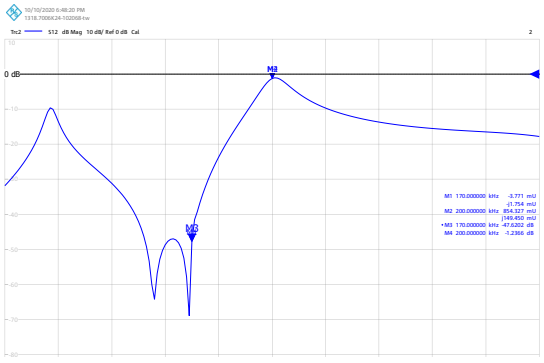

(f) from source2 to RX_2

Figure 5.12. Transmission factors in frequency domain (S_{12})

simulation results indicated that the power link of each pair of source-receiver was completely isolated from the operation of the other pairs of source-receiver. However, in practice, the transmission factor of each link was affected by the

equivalent impedances of the frequency-mismatched source circuits. Then, instead of using a common transmitting coil, multiple sources drove a resonator to deliver power to corresponding receiver. The theoretical analysis and the simulation results showed that the combination of K-inverter and band-reject filter still separated power link of each pair of source-receiver in this system. Furthermore, by using a common transmitting resonator, the transmission factors of the sources and the corresponding receiver were significantly improved in comparison with using a common transmitting coil. The experimental results verified the theoretical analysis.

Chapter 6

Conclusion

The objective of this dissertation was to propose single-transmitter multiple-receiver IPT system which could stabilize the load voltages against the load variations under different conditions. First, when charging multiple receivers, each receiver often required a rated voltage for its load. Second, some receivers were located far from charging platform, leading to the deterioration of the system performance. Third, each receiver required not only a rated voltage for its load but also an individual operating frequency.

This dissertation utilized K-inverter to design three multiple-receiver IPT systems to address the corresponding challenges, . Firstly, multiple transmitting resonators were inserted between source resonator and multiple receivers to control the load voltages. This structure formed multiple K-inverters at transmitter side. It enabled the load voltages to be decided by the mutual inductances among the resonators and the source voltage only. As a result, the load voltages could be controlled by adjusting the characteristic impedances of the K-inverters, equivalent to adjusting the arrangement of the multiple transmitting resonators. Secondly, the cooperative IPT systems were developed from a relay-based IPT system where the relay was equipped an additional LC tank or K-inverter to simultaneously draw power itself and transmit the rest of received power to the distant receiver. Moreover, using LC tank or K-inverter, the cooperative IPT systems also stabilized the two load voltages stable against the load variations. However, using K-inverter-based structure attained higher performance than LC tank structure. It also indicated that the cooperative IPT system with single-coil relay outper-

formed the one with two-coil repeater while still keeping two load voltages stable against the load variations. Finally, multiple-frequency one-to-multiple IPT system was proposed to satisfy the requirement of multiple operating frequencies in multiple receivers. K-inverters were combined with band-reject filters to separate the power link of each pair of source-corresponding receiver and to stabilize the load voltages. As a result, full voltage control for each load could be achieved without affecting the operation of other pairs of source and corresponding receiver.

This dissertation has addressed the challenges in charging multiple receiver. The feasibility of these solutions enabled to realize universal charging platforms in future.

Publications and Conferences

Journals

[P.J1] **Quoc-Trinh Vo**, Quang-Thang Duong, and Minoru Okada, "Load-independent voltage control for multiple-receiver inductive power transfer systems," IEEE Access, vol. 7, pp. 139 450–139 461, September 2019

Conferences

[P.C1] **Quoc-Trinh Vo**, Quang-Thang Duong, and Minoru Okada, "Cooperative transmission in three-coil inductive power transfer system with load-independent output voltages," in 2019 International Workshop on Antenna Technology (iWAT). IEEE, March 2019

[P.C2] **Quoc-Trinh Vo**, Quang-Thang Duong, and Minoru Okada, "Efficiency improvement for three-coil cooperative inductive power transfer systems," in 2019 IEEE Wireless Power Transfer Conference (WPTC). IEEE, June 2019

[P.C3] **Quoc-Trinh Vo**, Quang-Thang Duong, and Minoru Okada, "Efficiency comparison between cooperative inductive power transfer," in 2020 International Conference on Advanced Technologies for Communications (ATC), October 2020

[P.C4] **Quoc-Trinh Vo**, Quang-Thang Duong, and Minoru Okada, "Cross-talk mitigation using band-stop filters for multiple-frequency one-to-multiple

inductive power transfer," in 15th European Conference on Antennas and Propagation (EuCAP), March 2021

Workshops

[P.W1] **Quoc-Trinh Vo**, Quang-Thang Duong, and Minoru Okada, "Transmitter-side voltage control for two-receiver inductive power transfer systems," in 2018 Asian Wireless Power Transfer (AWPT), November 2018

[P.W2] **Quoc-Trinh Vo**, Quang-Thang Duong, and Minoru Okada, "Two-frequency One-to-Two Inductive Power Transfer System with Load-independent Output Voltages," in 2020 Asian Wireless Power Transfer (AWPT), December 2020

Acknowledgements

Firstly, I would like to express my gratitude to Professor Minoru Okada, Associate Professor Takeshi Higashino, Assistant Professor Duong Quang Thang and Assistant Professor Chen Na for their kind guidance and support. This dissertation would be not completed without their advice, comments as well as countless discussion.

I would like to thank Professor Yuichi Hayashi. His comments and questions during my research progress helped to improve my research.

I would like to thank my laboratory members, especially WPT group members, who supported me in my experiments as well as daily life. That made my life in NAIST more memorable.

I would like to thank Ms. Miki Kioi, my laboratory's secretariat, for supporting me during the last three years.

Finally, I would like to thank my family for all of their supports and encouragements.

References

[1] M. D. Godfrey, Mathematical Theory of Electrodynamic Phenomena by Andre-Marie Ampere. Unpublished, 2015.

[2] P. Day, The Philosopher's Tree: A Selection of Michael Faraday's Writings. Taylor & Francis, 1999.

[3] D. J. Griffiths, Introduction to Electrodynamics. Prentice-Hall, 1999.

[4] J. C. Maxwell, "A dynamical theory of the electromagnetic field," Philosophical Transactions of the Royal Society of London, vol. 155, pp. 459–512, December 1865.

[5] N. Tesla, "System of transmission of electrical energy," USA Patent US645 576, March 20, 1900.

[6] ——, "The transmission of electric energy without wires," Electrical World and Engineer, no. 1483, pp. 23 760–23 761, March 1904.

[7] ——, "Apparatus for transmitting electrical energy," USA Patent US1 119 732, December 1, 1914.

[8] A. Marincic, "Nikola tesla and the wireless transmission of energy," IEEE Transactions on Power Apparatus and Systems, vol. PAS-101, no. 10, pp. 4064–4068, October 1982.

[9] N. Tesla, "Experiments with alternate currents of very high frequency and their application to methods of artificial illumination," Transactions of the American Institute of Electrical Engineers, vol. VIII, no. 1, pp. 266–319, January 1891.

[10] M. A. Houran, X. Yang, and W. Chen, "Magnetically coupled resonance WPT: Review of compensation topologies, resonator structures with misalignment, and EMI diagnostics," Electronics, vol. 7, no. 11, p. 296, November 2018.

[11] Y. Zeng, B. Clerckx, and R. Zhang, "Communications and signals design for wireless power transmission," IEEE Transactions on Communications, vol. 65, no. 5, pp. 2264–2290, May 2017.

[12] G. A. Landis, "Applications for space power by laser transmission," in Laser Power Beaming, J. V. Walker and E. E. M. IV, Eds. SPIE, May 1994.

[13] L. Summerer and O. Purcell, "Concepts for wireless energy transmission via laser," in International Conference on Space Optical Systems and Applications (ICSOS), 2009.

[14] B. Clerckx, R. Zhang, R. Schober, D. W. K. Ng, D. I. Kim, and H. V. Poor, "Fundamentals of wireless information and power transfer: From RF energy harvester models to signal and system designs," IEEE Journal on Selected Areas in Communications, vol. 37, no. 1, pp. 4–33, January 2019.

[15] Y. Zeng, R. Zhang, and T. J. Lim, "Wireless communications with unmanned aerial vehicles: opportunities and challenges," IEEE Communications Magazine, vol. 54, no. 5, pp. 36–42, May 2016.

[16] N. Tesla, "High frequency oscillators for electro-therapeutic and other purposes," Proceedings of the IEEE, vol. 87, no. 7, p. 1282, July 1999.

[17] A. Kurs, A. Karalis, R. Moffatt, J. D. Joannopoulos, P. Fisher, and M. Soljacic, "Wireless power transfer via strongly coupled magnetic resonances," Science, vol. 317, no. 5834, pp. 83–86, July 2007.

[18] G. A. Covic and J. T. Boys, "Inductive power transfer," Proc. IEEE, vol. 101, no. 6, pp. 1276–1289, June 2013.

[19] S. D. Barman, A. W. Reza, N. Kumar, M. E. Karim, and A. B. Munir, "Wireless powering by magnetic resonant coupling: Recent trends in wire-

less power transfer system and its applications," Renewable Sustainable Energy Rev., vol. 51, pp. 1525–1552, November 2015.

[20] V. Cirimele, F. Freschi, and M. Mitolo, "Inductive power transfer for automotive applications: State-of-the-art and future trends," in 2016 IEEE Industry Applications Society Annual Meeting. IEEE, October 2016.

[21] V. Shevchenko, O. Husev, R. Strzelecki, B. Pakhaliuk, N. Poliakov, and N. Strzelecka, "Compensation topologies in IPT systems: Standards, requirements, classification, analysis, comparison and application," IEEE Access, vol. 7, pp. 120 559–120 580, 2019.

[22] Z. Zhang, H. Pang, A. Georgiadis, and C. Cecati, "Wireless power transfer-an overview," IEEE Trans. Ind. Electron., vol. 66, no. 2, pp. 1044–1058, February 2019.

[23] J. Schuder, H. Stephenson, and J. F. Townsend, "Energy transfer into a closed chest by means of stationary coupling coils and a portable high-power oscillator." Transactions - American Society for Artificial Internal Organs, vol. 7, pp. 327–31, 1961.

[24] J. C. Schuder and H. E. Stephenson, "Energy transport to a coil which circumscribes a ferrite core and is implanted within the body," IEEE Transactions on Biomedical Engineering, vol. BME-12, no. 3 and 4, pp. 154–163, July 1965.

[25] J. C. Schuder, J. H. Gold, and H. E. Stephenson, "An inductively coupled RF system for the transmission of 1 kW of power through the skin," IEEE Transactions on Biomedical Engineering, vol. BME-18, no. 4, pp. 265–273, July 1971.

[26] T. Sun, X. Xie, G. Li, Y. Gu, Y. Deng, and Z. Wang, "A two-hop wireless power transfer system with an efficiency-enhanced power receiver for motion-free capsule endoscopy inspection," IEEE Transactions on Biomedical Engineering, vol. 59, no. 11, pp. 3247–3254, November 2012.

[27] B. H. Waters, A. P. Sample, P. Bonde, and J. R. Smith, "Powering a ventricular assist device (VAD) with the free-range resonant electrical energy delivery (FREE-d) system," Proceedings of the IEEE, vol. 100, no. 1, pp. 138–149, January 2012.

[28] A. Banerjee, S. A. Saba, S. Rana, and S. Chakraborty, "Bionic eye - a review," in 2020 8th International Conference on Reliability, Infocom Technologies and Optimization (Trends and Future Directions) (ICRITO). IEEE, June 2020.

[29] A. Yakovlev, S. Kim, and A. Poon, "Implantable biomedical devices: Wireless powering and communication," IEEE Commun. Mag., vol. 50, no. 4, pp. 152–159, April 2012.

[30] D. Ahn and S. Hong, "Wireless power transmission with self-regulated output voltage for biomedical implant," IEEE Trans. Ind. Electron., vol. 61, no. 5, pp. 2225–2235, May 2014.

[31] X. Meng, D. Qiu, B. Zhang, and W. Xiao, "Output voltage stabilization control without secondary side measurement for implantable wireless power transfer system," in 2018 IEEE PELS Workshop on Emerging Technologies: Wireless Power Transfer (Wow). IEEE, June 2018.

[32] J. A. Taylor, Z. N. Low, J. Casanova, and J. Lin, "A wireless power station for laptop computers," in 2010 IEEE Radio and Wireless Symp. (RWS). IEEE, January 2010.

[33] J. Kim, H. chang Son, D. hyeon Kim, and Y. jin Park, "Optimal design of a wireless power transfer system with multiple self-resonators for an LED TV," IEEE Transactions on Consumer Electronics, vol. 58, no. 3, pp. 775–780, August 2012.

[34] M. Kesler, "Highly resonant wireless power transfer:safe, efficient, and over distance," 2013, (accessed 2020-12-05). [Online]. Available: http://large.stanford.edu/courses/2016/ph240/surakitbovorn1/docs/kesler.pdf

[35] X. Mou and H. Sun, "Wireless power transfer: Survey and roadmap," in 2015 IEEE 81st Vehicular Technology Conference (VTC Spring). IEEE, May 2015.

[36] R.-C. Kuo, P. Riehl, A. Satyamoorthy, W. Plumb, P. Tustin, and J. Lin, "A 3d resonant wireless charger for a wearable device and a mobile phone," in 2015 IEEE Wireless Power Transfer Conference (WPTC). IEEE, May 2015.

[37] D. van Wageningen and T. Staring, "The qi wireless power standard," in Proceedings of 14th International Power Electronics and Motion Control Conference EPE-PEMC 2010. IEEE, September 2010.

[38] S. Y. Hui, "Planar wireless charging technology for portable electronic products and qi," Proceedings of the IEEE, vol. 101, no. 6, pp. 1290–1301, June 2013.

[39] P. S. Riehl, A. Satyamoorthy, H. Akram, Y.-C. Yen, J.-C. Yang, B. Juan, C.-M. Lee, F.-C. Lin, V. Muratov, W. Plumb, and P. F. Tustin, "Wireless power systems for mobile devices supporting inductive and resonant operating modes," IEEE Trans. Microw. Theory Techn., vol. 63, no. 3, pp. 780–790, March 2015.

[40] G. A. Covic and J. T. Boys, "Modern trends in inductive power transfer for transportation applications," IEEE Journal of Emerging and Selected Topics in Power Electron., vol. 1, no. 1, pp. 28–41, March 2013.

[41] J. L. Villa, J. Sanz, and J. Sallan, "Inductive battery charging system for electric vehicles," in 2013 World Electric Vehicle Symposium and Exhibition (EVS27). IEEE, November 2013.

[42] R. Bosshard and J. W. Kolar, "Multi-objective optimization of 50 kW/85 kHz IPT system for public transport," IEEE Journal of Emerging and Selected Topics in Power Electronics, vol. 4, no. 4, pp. 1370–1382, December 2016.

[43] Y. J. Jang, "Survey of the operation and system study on wireless charging electric vehicle systems," Transportation Research Part C: Emerging Technologies, vol. 95, pp. 844–866, October 2018.

[44] H. A. Fadhil, S. G. Abdulqader, and S. A. Aljunid, "Implementation of wireless power transfer system for smart home applications," in 2015 IEEE 8th GCC Conference & Exhibition. IEEE, feb 2015.

[45] Y. J. Jang, Y. D. Ko, and S. Jeong, "Optimal design of the wireless charging electric vehicle," in 2012 IEEE International Electric Vehicle Conference. IEEE, mar 2012.

[46] ICNIRP, "ICNIRP statement on the guidelines for limiting exposure to time-varying electric, magnetic, and electromagnetic fields (up to 300ghz)," Health Physics, vol. 97, no. 3, pp. 257–258, September 2009.

[47] IEEE, "IEEE standard for safety levels with respect to human exposure to radio frequency electromagnetic fields, 3 kHz to 300 GHz," 1992.

[48] ——, "IEEE standard for safety levels with respect to human exposure to electromagnetic fields, 0-3 kHz," 2002.

[49] M. Clemens, M. Zang, M. Alsayegh, and B. Schmuelling, "High resolution modeling of magnetic field exposure scenarios in the vicinity of inductive wireless power transfer systems." in 2018 IEEE International Magnetics Conference (INTERMAG). IEEE, April 2018.

[50] S. Park, "Investigating human exposure to a practical wireless power transfer system using and the effect about key parameters of dosimetry," PLOS ONE, vol. 15, no. 8, p. e0236929, August 2020.

[51] Z. Zhang, K. T. Chau, C. Qiu, and C. Liu, "Energy encryption for wireless power transfer," IEEE Trans. Power Electron., vol. 30, no. 9, pp. 5237–5246, September 2015.

[52] M. N. Sadzali, A. Ali, M. M. Azizan, and M. A. M. Albreem, "The security energy encryption in wireless power transfer," in 3RD Electronic and

Green Materials Internatinal Conference 2017 (EGM 2017), vol. 1885. AIP Conference Proceedings, September 2017.

[53] M. Rahmanil, "Frequency hopping in cognitive radio networks: A survey," in 2015 IEEE International Conference on Wireless for Space and Extreme Environments (WiSEE). IEEE, December 2015.

[54] Q.-T. Duong and M. Okada, "A secure inductive power transfer using 2× 2 MIMO," in 2018 IEEE PELS Workshop on Emerging Technologies: Wireless Power Transfer (Wow). IEEE, June 2018.

[55] T. Ohira, "Maximum available efficiency formulation based on a black-box model of linear two-port power transfer systems," IEICE Electron. Express, vol. 11, no. 13, pp. 20 140 448–20 140 448, July 2014.

[56] ——, "Extended k-Q product formulas for capacitive- and inductive-coupling wireless power transfer schemes," IEICE Electron. Express, vol. advpub, 2014.

[57] Q.-T. Duong and M. Okada, "kQ-product formula for multiple-transmitter inductive power transfer system," IEICE Electron. Exp., vol. 14, no. 3, pp. 20 161 167–20 161 167, 2017.

[58] M. Fu, T. Zhang, X. Zhu, P. C.-K. Luk, and C. Ma, "Compensation of cross coupling in multiple-receiver wireless power transfer systems," IEEE Trans. Ind. Informat., vol. 12, no. 2, pp. 474–482, April 2016.

[59] Q.-T. Duong and M. Okada, "Analysis of reactance compensation for eliminating cross-coupling in multiple-receiver inductive power transfer," in 2017 11th European Conference on Antennas and Propagation (EUCAP), March 2017, pp. 492–495.

[60] ——, "Maximum efficiency formulation for multiple-input multiple-output inductive power transfer systems," IEEE Trans. Microw. Theory Techn., vol. 66, no. 7, pp. 3463–3477, July 2018.

[61] D. Schieber, "On the inductance of printed spiral coils," Archiv für Elektrotechnik, vol. 68, no. 3, pp. 155–159, May 1985.

[62] C. Zierhofer and E. Hochmair, "Geometric approach for coupling enhancement of magnetically coupled coils," IEEE Trans. Biomed. Eng., vol. 43, no. 7, pp. 708–714, July 1996.

[63] W. Hurley and M. Duffy, "Calculation of self- and mutual impedances in planar sandwich inductors," IEEE Trans. Magn., vol. 33, no. 3, pp. 2282–2290, May 1997.

[64] Y. Cheng and Y. Shu, "A new analytical calculation of the mutual inductance of the coaxial spiral rectangular coils," IEEE Trans. Magn., vol. 50, no. 4, pp. 1–6, April 2014.

[65] S. Aldhaher, D. C. Yates, and P. D. Mitcheson, "Design and development of a class EF_2 inverter and rectifier for multimegahertz wireless power transfer systems," IEEE Transactions on Power Electronics, vol. 31, no. 12, pp. 8138–8150, December 2016.

[66] X. Liu, C. Xia, and X. Yuan, "Study of the circular flat spiral coil structure effect on wireless power transfer system performance," Energies, vol. 11, no. 11, p. 2875, October 2018.

[67] H. Cai, L. Shi, and Y. Li, "Harmonic-based phase-shifted control of inductively coupled power transfer," IEEE Trans. Power Electron., vol. 29, no. 2, pp. 594–602, February 2014.

[68] S. Aldhaher, D. C. Yates, and P. D. Mitcheson, "Load-independent class e/EF inverters and rectifiers for MHz-switching applications," IEEE Trans. Power Electron., vol. 33, no. 10, pp. 8270–8287, October 2018.

[69] J. Liu, Q. Deng, W. Wang, and Z. Li, "Modeling and control of inverter zero-voltage-switching for inductive power transfer system," IEEE Access, vol. 7, pp. 139 885–139 894, 2019.

[70] P. C. K. Luk and S. Aldhaher, "Analysis and design of a class d rectifier for a class e driven wireless power transfer system," in 2014 IEEE Energy Conversion Congress and Exposition (ECCE). IEEE, September 2014.

[71] M. Liu, M. Fu, and C. Ma, "Parameter design for a 6.78-MHz wireless power transfer system based on analytical derivation of class e current-driven rectifier," IEEE Transactions on Power Electronics, vol. 31, no. 6, pp. 4280–4291, June 2016.

[72] M. Zargham and P. G. Gulak, "Maximum achievable efficiency in near-field coupled power-transfer systems," IEEE Trans. Biomed. Circuits Syst., vol. 6, no. 3, pp. 228–245, June 2012.

[73] I.-J. Yoon and H. Ling, "Investigation of near-field wireless power transfer under multiple transmitters," IEEE Antennas Wireless Propag. Lett., vol. 10, pp. 662–665, 2011.

[74] J. Kim, H.-C. Son, D.-H. Kim, and Y.-J. Park, "Impedance matching considering cross coupling for wireless power transfer to multiple receivers," in 2013 IEEE Wireless Power Transfer (WPT). IEEE, May 2013.

[75] D. Ahn and S. Hong, "Effect of coupling between multiple transmitters or multiple receivers on wireless power transfer," IEEE Trans. Ind. Electron., vol. 60, no. 7, pp. 2602–2613, July 2013.

[76] W. Chen, Z. Bai, S. Rickers, G. H. Bruck, and P. Jung, "Transmitter with cooperative coils matrix for robust wireless power transfer system," in 2014 International Symposium on Electromagnetic Compatibility. IEEE, September 2014.

[77] D. Zhao, E. Ding, and X. Wang, "Multiple-input single-output wireless power transmission system for coal mine," TELKOMNIKA Indonesian Journal of Electrical Engineering, vol. 12, no. 6, June 2014.

[78] J. Zhang and F. Wang, "Efficiency analysis of multiple-transmitter wireless power transfer systems," International Journal of Antennas and Propagation, vol. 2018, pp. 1–11, July 2018.

[79] T. Arakawa, S. Goguri, J. V. Krogmeier, A. Kruger, D. J. Love, R. Mudumbai, and M. A. Swabey, "Optimizing wireless power transfer from multiple transmit coils," IEEE Access, vol. 6, pp. 23 828–23 838, 2018.

[80] H. D. Lang, A. Ludwig, and C. D. Sarris, "Convex optimization of wireless power transfer systems with multiple transmitters," IEEE Trans. Antennas Propag., vol. 62, no. 9, pp. 4623–4636, September 2014.

[81] H.-D. Lang and C. D. Sarris, "Semidefinite relaxation-based optimization of multiple-input wireless power transfer systems," IEEE Trans. Microw. Theory Techn., vol. 65, no. 11, pp. 4294–4306, November 2017.

[82] B. L. Cannon, J. F. Hoburg, D. D. Stancil, and S. C. Goldstein, "Magnetic resonant coupling as a potential means for wireless power transfer to multiple small receivers," IEEE Trans. Power Electron., vol. 24, no. 7, pp. 1819–1825, July 2009.

[83] J. Casanova, Z. N. Low, and J. Lin, "A loosely coupled planar wireless power system for multiple receivers," IEEE Trans. Ind. Electron., vol. 56, no. 8, pp. 3060–3068, August 2009.

[84] A. Kurs, R. Moffatt, and M. Soljačić, "Simultaneous mid-range power transfer to multiple devices," Appl. Phys. Lett., vol. 96, no. 4, p. 044102, January 2010.

[85] K. K. Ean, B. T. Chuan, T. Imura, and Y. Hori, "Impedance matching and power division algorithm considering cross coupling for wireless power transfer via magnetic resonance," in Intelec 2012. IEEE, September 2012.

[86] T. Zhang, M. Fu, C. Ma, and X. Zhu, "Optimal load analysis for a two-receiver wireless power transfer system," in 2014 IEEE Wireless Power Transfer Conference. IEEE, May 2014.

[87] J. Kim, D.-H. Kim, and Y.-J. Park, "Free-positioning wireless power transfer to multiple devices using a planar transmitting coil and switchable impedance matching networks," IEEE Trans. Microw. Theory Techn., vol. 64, no. 11, pp. 3714–3722, November 2016.

[88] Y.-J. Kim, D. Ha, W. J. Chappell, and P. P. Irazoqui, "Selective wireless power transfer for smart power distribution in a miniature-sized multiple-receiver system," IEEE Trans. Ind. Electron., vol. 63, no. 3, pp. 1853–1862, March 2016.

[89] H. Feng, T. Cai, S. Duan, J. Zhao, X. Zhang, and C. Chen, "An LCC-compensated resonant converter optimized for robust reaction to large coupling variation in dynamic wireless power transfer," IEEE Trans. Ind. Electron., vol. 63, no. 10, pp. 6591–6601, October 2016.

[90] K. Zhuo, B. Luo, Y. Zhang, and Y. Zuo, "Multiple receivers wireless power transfer systems using decoupling coils to eliminate cross-coupling and achieve selective target power distribution," IEICE Electron. Exp., vol. 16, no. 18, pp. 20 190 491–20 190 491, 2019.

[91] K. Lee and S. H. Chae, "Comparative analysis of frequency-selective wireless power transfer for multiple-rx systems," IEEE Trans. Power Electron., vol. 35, no. 5, pp. 5122–5131, May 2020.

[92] C. Zhong, B. Luo, F. Ning, and W. Liu, "Reactance compensation method to eliminate cross coupling for two-receiver wireless power transfer system," IEICE Electron. Exp., vol. 12, no. 7, 2015.

[93] M. Q. Nguyen, D. Plesa, S. Rao, and J.-C. Chiao, "A multi-input and multi-output wireless energy transfer system," in 2014 IEEE MTT-S International Microwave Symposium (IMS2014). IEEE, June 2014.

[94] J. Jadidian and D. Katabi, "Magnetic MIMO: How to charge your phone in your pocket," in Proceedings of the 20th annual international conference on Mobile computing and networking - MobiCom'14. ACM Press, 2014.

[95] D. Arnitz and M. S. Reynolds, "MIMO wireless power transfer for mobile devices," IEEE Pervasive Comput., vol. 15, no. 4, pp. 36–44, October 2016.

[96] S. Kim and L. Bomson, "Analysis of efficiencies for multiple-input multiple-output wireless power transfer systems," J. of Electromagn. Eng. Sci., vol. 16, no. 2, pp. 126–133, 2016.

[97] K. Wiedmann and T. Weber, "Optimizing the wireless power transfer over MIMO channels," Adv. Radio Sci., vol. 15, pp. 181–187, September 2017.

[98] G. Yang, M. R. V. Moghadam, and R. Zhang, "Magnetic MIMO signal processing and optimization for wireless power transfer," IEEE Trans. Signal Process., vol. 65, no. 11, pp. 2860–2874, June 2017.

[99] J.-S. Hong, Microstrip Filters for RF/Microwave Applications, 2nd ed. John Wiley & Sons, 2011, ch. 3, pp. 54–62.

[100] T. Imura and Y. Hori, "Maximizing air gap and efficiency of magnetic resonant coupling for wireless power transfer using equivalent circuit and neumann formula," IEEE Trans. Ind. Electron., vol. 58, no. 10, pp. 4746–4752, October 2011.

[101] S. Li, W. Li, J. Deng, T. D. Nguyen, and C. C. Mi, "A double-sided LCC compensation network and its tuning method for wireless power transfer," IEEE Trans. Veh. Technol., vol. 64, no. 6, pp. 2261–2273, June 2015.

[102] X. Liu, L. Clare, X. Yuan, C. Wang, and J. Liu, "A design method for making an LCC compensation two-coil wireless power transfer system more energy efficient than an SS counterpart," Energies, vol. 10, no. 9, p. 1346, September 2017.

[103] F. Lu, H. Zhang, H. Hofmann, W. Su, and C. C. Mi, "A dual-coupled LCC-compensated IPT system with a compact magnetic coupler," IEEE Trans. Power Electron., vol. 33, no. 7, pp. 6391–6402, July 2018.

[104] Y. Yao, Y. Wang, X. Liu, and D. Xu, "Analysis, design, and optimization of LC/S compensation topology with excellent load-independent voltage output for inductive power transfer," IEEE Trans. Transport. Electrific., vol. 4, no. 3, pp. 767–777, September 2018.

[105] Y. Li, Q. Xu, T. Lin, J. Hu, Z. He, and R. Mai, "Analysis and design of load-independent output current or output voltage of a three-coil wireless power transfer system," IEEE Trans. Transport. Electrific., vol. 4, no. 2, pp. 364–375, June 2018.

[106] V.-B. Vu, D.-H. Tran, and W. Choi, "Implementation of the constant current and constant voltage charge of inductive power transfer systems with

the double-sided LCC compensation topology for electric vehicle battery charge applications," IEEE Trans. Power Electron., vol. 33, no. 9, pp. 7398–7410, September 2018.

[107] X. Qu, H. Chu, S.-C. Wong, and C. K. Tse, "An IPT battery charger with near unity power factor and load-independent constant output combating design constraints of input voltage and transformer parameters," IEEE Transactions on Power Electronics, vol. 34, no. 8, pp. 7719–7727, August 2019.

[108] A. Ramezani, S. Farhangi, H. Iman-Eini, B. Farhangi, R. Rahimi, and G. R. Moradi, "Optimized LCC-series compensated resonant network for stationary wireless EV chargers," IEEE Transactions on Industrial Electronics, vol. 66, no. 4, pp. 2756–2765, April 2019.

[109] Y. Yao, Y. Wang, X. Liu, H. Cheng, M. Liu, and D. Xu, "Analysis, design, and implementation of a wireless power and data transmission system using capacitive coupling and double-sided LCC compensation topology," IEEE Trans. Ind. Appl., vol. 55, no. 1, pp. 541–551, January 2019.

[110] Q. Zhao, A. Wang, J. Liu, and X. Wang, "The load estimation and power tracking integrated control strategy for dual-sides controlled LCC compensated wireless charging system," IEEE Access, vol. 7, pp. 75 749–75 761, 2019.

[111] Y. Chen, N. Yang, Q. Li, Z. He, and R. Mai, "New parameter tuning method for LCC/LCC compensated IPT system with constant voltage output based on LC resonance principles," IET Power Electron., vol. 12, pp. 2466 – 2474, August 2019.

[112] L. Yang, X. Li, S. Liu, Z. Xu, and C. Cai, "Analysis and design of an LCCC/s compensated WPT system with constant output characteristics for battery charging applications," IEEE Journal of Emerging and Selected Topics in Power Electron., pp. 1–1, 2020.

[113] Y. Zhang, T. Lu, and Z. Zhao, "Reducing the impact of source internal resistance by source coil in resonant wireless power transfer," in 2014 IEEE Energy Conversion Congr. Expo. (ECCE). IEEE, September 2014.

[114] F. Zhang, S. A. Hackworth, W. Fu, and M. Sun, "The relay effect on wireless power transfer using witricity," in Digests of the 2010 14th Biennial IEEE Conference on Electromagnetic Field Computation. IEEE, May 2010.

[115] F. Zhang, S. A. Hackworth, W. Fu, C. Li, Z. Mao, and M. Sun, "Relay effect of wireless power transfer using strongly coupled magnetic resonances," IEEE Trans. Magn., vol. 47, no. 5, pp. 1478–1481, May 2011.

[116] C. K. Lee, W. X. Zhong, and S. Y. R. Hui, "Effects of magnetic coupling of nonadjacent resonators on wireless power domino-resonator systems," IEEE Trans. Power Electron., vol. 27, no. 4, pp. 1905–1916, April 2012.

[117] J.-H. Kim, B.-C. Park, and J.-H. Lee, "Accurate analysis method of wireless power transfer system with multiple relays," in 2013 Asia-Pacific Microw. Conf. Proc. (APMC). IEEE, November 2013.

[118] D. Ahn and S. Hong, "A study on magnetic field repeater in wireless power transfer," IEEE Trans. Ind. Electron., vol. 60, no. 1, pp. 360–371, January 2013.

[119] S. Y. R. Hui, W. Zhong, and C. K. Lee, "A critical review of recent progress in mid-range wireless power transfer," IEEE Trans. on Power Electron., vol. 29, no. 9, pp. 4500–4511, September 2014.

[120] M. Zarif, H. Aliabadi, and S. Khaleghi, "Analysis of relay effect on wireless power transfer," in Proceedings of the 12th International Conference on Informatics in Control, Automation and Robotics. SCITEPRESS - Science and and Technology Publications, 2015.

[121] W. Niu, J. Wang, J. Chu, and W. Gu, "Optimal single relay position of a 3-coil wireless power transfer system," The Journal of Engineering, vol. 2016, no. 7, pp. 249–252, July 2016.

[122] B.-H. Choi and J.-H. Lee, "Design of asymmetrical relay resonators for maximum efficiency of wireless power transfer," International Journal of Antennas and Propagation, vol. 2016, pp. 1–8, March 2016.

[123] E. Bou-Balust, R. Sedwick, P. Fisher, and E. Alarcon, "Multipath relaying effects in multiple-node resonant inductive coupling wireless power transfer," Wireless Power Transfer, vol. 3, no. 02, pp. 83–92, May 2016.

[124] Q. Zhao and A. Wang, "Optimization of multiresonant wireless power transfer network based on generalized coupled matrix," Math. Problems in Eng., vol. 2017, pp. 1–9, June 2017.

[125] J. Lee, K. Lee, and D.-H. Cho, "Stability improvement of transmission efficiency based on a relay resonator in a wireless power transfer system," IEEE Trans. Power Electron., vol. 32, no. 5, pp. 3297–3300, May 2017.

[126] W. Wang, X. Huang, J. Guo, H. Liu, C. Yan, and L. Tan, "Power stabilization based on efficiency optimization for WPT systems with single relay by frequency configuration and distribution design of receivers," IEEE Trans. Power Electron., vol. 32, no. 9, pp. 7011–7024, September 2017.

[127] C. Saha, I. Anya, C. Alexandru, and R. Jinks, "Wireless power transfer using relay resonators," Appl. Phys. Lett., vol. 112, no. 26, p. 263902, June 2018.

[128] Q. Wang and Y. Wang, "Power efficiency optimisation of a three-coil wireless power transfer using compensatory reactance," IET Power Electron., vol. 11, no. 13, pp. 2102–2108, November 2018.

[129] J. Lee and K. Lee, "Effects of number of relays on achievable efficiency of magnetic resonant wireless power transfer," IEEE Trans. Power Electron., vol. 35, no. 7, pp. 6697–6700, July 2020.

[130] Y. Ota, T. Takura, F. Sato, and H. Matsuki, "Wireless power transfer by low coupling electromagnetic induction - LC booster," in 2012 IEEE MTT-S Int. Microw. Workshop Series Innovative Wireless Power Transmission: Technol., Syst., and Appl. IEEE, May 2012.

[131] Y. Ota, N. Aruga, S. Miyahara, F. Sato, and H. Matsuki, "Method of wireless power transfer for high efficiency and high output stability," J. Magn. Soc. Jpn., vol. 39, no. 1, pp. 25–28, 2015.

[132] L. Sun, H. Tang, and S. Zhong, "Load-independent output voltage analysis of multiple-receiver wireless power transfer system," IEEE Antennas Wireless Propag. Lett., vol. 15, pp. 1238–1241, 2016.

[133] J. Kuang, B. Luo, Y. Zhang, Y. Hu, and Y. Wu, "Load-isolation wireless power transfer with k-inverter for multiple-receiver applications," IEEE Access, vol. 6, pp. 31 996–32 004, April 2018.

[134] K. Yamaguchi, T. Hirata, and I. Hodaka, "Using square wave input for wireless power transfer," Int. J. Elect. Comput. Eng. (IJECE), vol. 6, no. 1, p. 431, February 2016.

[135] A. Namin, E. Chaidee, T. Sriprom, and P. Bencha, "Performance of inductive wireless power transfer between using pure sine wave and square wave inverters," in 2018 IEEE Transport. Electrification Conf. Expo, Asia-Pacific (ITEC Asia-Pacific). IEEE, June 2018.

[136] M. Hardy, "An illuminating counterexample," Amer. Math. Monthly, August 2002.

[137] C. Cheng, W. Li, Z. Zhou, Z. Deng, and C. Mi, "A load-independent wireless power transfer system with multiple constant voltage outputs," IEEE Trans. Power Electron., vol. 35, no. 4, pp. 3328–3331, April 2020.

[138] C. Cheng, Z. Zhou, W. Li, J. Lu, Z. Deng, and C. C. Mi, "Long-distance wireless power transfer system powering multiple loads with constant voltage outputs using S-SP compensation," IET Power Electronics, vol. 13, no. 9, pp. 1729–1734, July 2020.

[139] K. Kusaka and J. ichi Itoh, "Development trends of inductive power transfer systems utilizing electromagnetic induction with focus on transmission frequency and transmission power," IEEJ J. Ind. Appl., vol. 6, no. 5, pp. 328–339, September 2017.

[140] W. Liu, K. T. Chau, C. H. T. Lee, C. Jiang, W. Han, and W. H. Lam, "Multi-frequency multi-power one-to-many wireless power transfer system," IEEE Trans. Magn., vol. 55, no. 7, pp. 1–9, July 2019.

[141] F. Liu, Y. Yang, Z. Ding, X. Chen, and R. M. Kennel, "A multifrequency superposition methodology to achieve high efficiency and targeted power distribution for a multiload MCR WPT system," IEEE Trans. Power Electron., vol. 33, no. 10, pp. 9005–9016, October 2018.

[142] Y. Huang, C. Liu, Y. Xiao, and S. Liu, "Separate power allocation and control method based on multiple power channels for wireless power transfer," IEEE Trans. Power Electron., vol. 35, no. 9, pp. 9046–9056, September 2020.

[143] F. Liu, Y. Yang, Z. Ding, X. Chen, and R. M. Kennel, "Eliminating cross interference between multiple receivers to achieve targeted power distribution for a multi-frequency multi-load MCR WPT system," IET Power Electron., vol. 11, no. 8, pp. 1321–1328, July 2018.

Appendix A

Mathematical Notation

$[\cdot]^{\mathrm{T}}$	the transpose of a vector or a matrix
$[\cdot]^{\mathrm{H}}$	the conjugate transpose of a vector or a matrix
$[\cdot]^{\text{-}1}$	the inverse of a matrix
$(\cdot)^*$	the conjugate of a complex number
$\lvert \cdot \rvert$	the absolute value of a complex number
$\mathrm{Re}\{\cdot\}$	the real part of a complex number
$\mathrm{Im}\{\cdot\}$	the imaginary part of a complex number
$j = \sqrt{-1}$	the unit imaginary number
boldface letters	a vector or matrix
$\boldsymbol{U}_N$	the identity matrix with N diagonal elements